THE CONTRIBUTION OF FUNCTIONAL BRAIN NETWORKS AND OSCILLATIONS TO THE DEVELOPMENT OF COGNITIVE CONTROL

by

Scott Allen Marek

BS, John Carroll University, 2012

Submitted to the Graduate Faculty of

The School of Medicine in partial fulfillment

of the requirements for the degree of

Doctor of Philosophy

University of Pittsburgh

2017

UNIVERSITY OF PITTSBURGH

SCHOOL OF MEDICINE

This dissertation was presented

by

Scott Allen Marek

It was defended on

April 3, 2017

and approved by

Julie A. Fiez, Professor, Psychology

Kirk I. Erickson, Associate Professor, Psychology

Peter J. Gianaros, Professor, Psychology

Avniel Singh Ghuman, Assistant Professor, Neurological Surgery

Timothy Verstynen, Assistant Professor, Psychology, Carnegie Mellon University

Dissertation Director: Beatriz Luna, Staunton Professor, Psychiatry & Psychology

THE CONTRIBUTION OF FUNCTIONAL BRAIN NETWORKS AND OSCILLATIONS TO THE DEVELOPMENT OF COGNITIVE CONTROL

Scott Allen Marek, PhD

University of Pittsburgh, 2017

Adolescence is a qualitatively unique period of development when cognitive control abilities are available but are unreliably engaged, which can lead to risk-taking behavior impacting survival. The specific neural mechanisms contributing to the maturation of cognitive control remain poorly understood. To address this issue, we employed functional magnetic resonance imaging (fMRI) and magnetoencephalography (MEG) to study brain networks and oscillations underlying cognitive control development in both the resting state and during a cognitive flexibility task. In the first study, we found that the organization of brain networks was established prior to adolescence. However, a network of brain regions anchored in the anterior cingulate cortex (ACC) and anterior insula (aIns) significantly increased its influence over other brain networks via increased network integration during the resting state, resulting in faster correct responses on a cognitive control task. In the second study, we leveraged increased temporal resolution using MEG to further probe resting state connectivity changes with age. We found similar medial prefrontal regions became less coupled in their interactions with the rest of the brain, specifically in the theta band (5-9 Hz oscillations), and were related to developmental decreases in

impulsivity. As such, these results suggest there are developmental increases in the flexibility of resting state connectivity, which may afford less effortful instantiation of cognitive control. The third study directly tested age-related changes in brain oscillations during a cognitive flexibility paradigm. We found evidence of strong induction of theta band oscillations in the ACC when task switching that scaled positively with average reaction time. Similar to our resting state MEG findings, we found that the prominence of ACC theta band rhythms decreased with development, suggesting that during cognitive flexibility, adolescents need to engage greater cognitive control to switch between cognitive demands compared to adults. Taken together, these results inform a model of adolescent development such that the specialization of medial prefrontal systems plays a primary role in developmental improvements in cognitive control as they strengthen their integration with other networks. Increased network integration affords these regions the ability to more flexibly engage other brain regions, supporting the maturation of cognitive control.

TABLE OF CONTENTS

LIST OF TABLES

LIST OF FIGURES

PREFACE

To my parents, Leonard and Karen Marek – Thank you for always keep me on the right path and providing the most stable and loving upbringing a child could ever ask for. You both were undoubtedly the most critical aspect of my personal development.

To my brother, Ryan Marek – You have always taken the responsibility of an older brother seriously. Thank you for paving the way for me, always wandering into uncharted water before me, despite your worrisome and overly cautious nature! Onward and upward!

To my girlfriend, Jusmita Saifullan – To say that your strength and resilient nature is inspirational is a vast understatement. A person of your character is rare, and I'm incredibly grateful that fate had us run into each other on a rainy January morning. Our future is brighter than a quasar, and I cannot wait to be alongside you making both of our dreams come true.

To my good friend Will Foran – Without you none of this work would have been possible. You've play a truly integral role in my development throughout graduate school, and always made sure I had enough junk food!

To my advisor, mentor, and Pittsburgh mom, Dr. Beatriz Luna – I came wandering into your lab not having the faintest idea of development; thank you for taking a chance on me. Your lab has been a blessing more so than you know, and I'll be forever grateful to you for getting my career as a scientist off the ground. We've undoubtedly accomplished some great science, and I look forward to continuing our collaboration long into the future.

1.0 INTRODUCTION

1.1 ADOLESCENT BRAIN DEVELOPMENT

Brain changes during adolescence are unique and critical for determining adaptive adult level control[1]. Decades of research support the idea that the adolescent brain is qualitatively and quantitatively different from either the child or adult brain. Gross brain morphology is in place by childhood; however, there are continued refinements in the form of synaptic pruning and increased myelination of major white matter tracts throughout adolescence and beyond[2–5]. By adolescence core brain processes are on line, supporting the ability to engage cognition at adult levels; however, performance in cognitive control tasks is not adult levels as adolescents engage these systems in an inconsistent manner. As such, by adolescence the ability to make complex decisions is available, but its lack of reliability may undermine goal directed behavior believed to underlie risk-taking behavior that has an impact on mortality[6]. Importantly, adolescence is a critical period of development in which many psychiatric disorders emerge[7], including schizophrenia, which has a strong link to deficiencies in neural oscillations related to cognitive control[8]. Therefore, characterizing the neural basis of normative development of brain networks and their oscillations is imperative for informing the neural basis concerning the emergence of psychiatric disorders.

1.2 IMMATURE COGNITIVE CONTROL SYSTEMS

Cognitive control refers to an emergent phenomenon characterized by the ability to voluntarily coordinate behavior within a noisy and variable environment to support goal-driven behavior[9]. Inhibitory control and working memory are key components of cognitive control. Importantly, these systems interact in a coordinated fashion during moment-to-moment cognition[10]. Inhibitory control describes the function of suppressing reflexive, goal-incompatible responses, while working memory refers to the active maintenance of information that guides goal-directed behavior. Critically, these components of cognitive control are available early in childhood[11]. Results reliably show that what continues to develop into adolescence is the rate at which accurate responses are made, decreases in reaction times, and decreases in the variability of reaction times[11,12]. Therefore, development is likely characterized by the refinements in the *interactions* between existing control systems, rather than the emergence of new networks. The neural basis for changes in aspects of cognitive control that support its reliable instantiation are not understood, limiting our ability to understand impaired development, such as in psychopathology.

fMRI studies have been inconclusive as to the mechanisms by which cognitive control refinements occur. This likely stems from the inherent inability of fMRI to speak directly to neural mechanisms. Developmental fMRI studies, which have primarily focused on lateral prefrontal cortex, have shown both increases and decreases in the blood-oxygen-level dependent (BOLD) signal between groups during control tasks, likely resulting from inhomogeneous tasks and different classification of age groups[13]. Here, we address these limitations by rigorously implementing rsfMRI connectivity and graph theory methods that overcome limitations in previous developmental studies. Furthermore, rather than studying activity within single regions

we probe changes in brain network function by using MEG as a complementary tool to fMRI, capitalizing on the excellent temporal resolution of MEG. This approach affords us the ability to probe connectivity and oscillatory mechanisms underlying cognitive control development at frequencies relevant to inter-regional communication at the timescales from which control constructs emerge (i.e., milliseconds). As such, the central aim of this dissertation is to directly address potential network and oscillatory mechanisms underlying the development of cognitive control through adolescence.

1.3 A NETWORK APRROACH TO BRAIN ANALYSES

In 1995, Biswal and colleagues noted that spontaneous BOLD oscillations in the ultra-slow frequency domain (0.01-0.10 Hz) were highly correlated in time between the left and right primary motor cortices while subjects were not engaged in any particular task[14]. Highly synchronized ultra-slow frequency oscillation between disparate regions of the brain have come to be termed resting-state networks. Since 1995, resting state BOLD activity has been used to determine networks of correlated BOLD oscillations, including sensory networks, such as the visual network, as well as cognitive networks, such as the cingulo-opercular and fronto-parietal control networks[15] and the brain's default mode network[16].

This conceptualization of brain functioning enabled the introduction of graph theoretical analyses to neuroscience, enabling neuroscientists to describe and quantify this high dimensional data, known as the human connectome[17]. As such, the brain can be conceptualized as a collection of brain regions (nodes) and their temporal correlation (links). Network approaches are a powerful way to understand brain functioning for several reasons. First, measuring the statistical

dependency between the oscillations of each region and every other region enables analysis of data across regional, network, and whole-brain scales. Next, these approaches provide a common framework for understanding and simplifying spatiotemporal aspects of whole-brain oscillations across conditions of rest and task.

Much like human social networks, the brain is organized into a small-world topology; that is, a high degree of clustering, with sparse connectivity to other clusters. The segregation of brain regions with strong internal correlations into a cluster is referred to as a *network*. The way in which all nodes in the brain cluster into segregated networks is referred to as network *organization*. Analytically, the clustering of nodes into networks is often accomplished via 'community detection' algorithms (e.g., see refs[18,19]). The networks resulting from these algorithms have proven to be highly reproducible across algorithms, parcellations, and scanning sites[20–22].

Some nodes within a network only engage in strong correlations within the network, while others exhibit strong correlations to nodes of other networks as well. These nodes are said to display a high level of network *integration*[23,24]. Nodes engaging in a high level of network integration are sometimes referred to as *hubs*. A similar network organization has been shown to be present in both the task state and resting state; however, patterns of coupling within and between networks are less static in non-random ways, such that they strongly predict patterns of co-activation across various task conditions[25].

1.4 FUNCTIONAL BRAIN NETWORK DEVELOPMENT

Functional networks are apparent by 2 years of age[26–29]. Small-worldness is present throughout childhood and adolescence, as in adulthood[30]. Within these small-world networks, the organization of hubs has been found to be different in infancy compared to adulthood shifting from predominance in sensory to association cortex[31,32]. By childhood, the organization, number, and connectivity of the hub architecture is at adult levels[30,33,34]. The relatively early stabilization of hub architecture suggests a foundational architecture in network connectivity that provides a backbone for network integration. A proxy of increased integration has been demonstrated in increased resting correlation strength between prefrontal hubs and *non-hubs* regions from childhood to adolescence when adult connectivity is mostly reached[30]. This period of integration parallels increases in white matter integrity of frontoparietal tracts[35], engagement of top-down networks supporting cognitive control[36], and performance in cognitive control tasks[11].

At the network level, cognitive control would be underlied by the effective integration of segregated networks supporting its components, such as those involved in inhibitory control, working memory, and performance monitoring. Initial studies investigating changes in segregation and integration found that children have a greater number of short-range connections and fewer long-range connections compared to adults, suggesting that with development there is a shift in predominance of local to distributed circuit engagement that may reflect increases in network integration[34,37–39]. These findings were subsequently undermined by the discovery that in-scanner head motion, which is greater in children than adults, resulted in spurious effects that biased short-range connections[40,41]. In our first study, we address this issue and resolve the ability to assess developmental changes while controlling for head motion.

Since this time, network integration has been defined by first identifying the network

organization of functional brain networks[42] and quantitatively defining integration based on network measures sensitive to network organization[24,43]. While this new approach has not been applied, based on the reliance of cognitive control on distributed circuitries that incorporate disparate specialized networks, the prediction is that with developmental changes, network organization would mature relatively early in development, while integration would continue to strengthen into adulthood when cognitive control is at its peak.

It is becoming increasingly apparent that brain networks deviate from this mostly static state over the course of a typical resting state acquisition (i.e., within minutes), though the degree to which this is the case is debated[44]. Regardless, recent work in fMRI has shown that resting state networks exhibit *increased* variability throughout development[45,46]. EEG studies further support this notion, noting that signal complexity increases throughout childhood and adolescence[47]. That said, the frequency spectra contributing to this finding remain unsolved. In Chapter 3, we will address this hole in the literature by analyzing the phase component of oscillations between large-scale networks. The ability for networks to integrate is an enduring aspect of network development, suggesting that communication across specialized networks may be a primary feature of age-related improvements in cognitive control. The studies within this dissertation will begin to uncover the mechanisms by which these network interactions contribute to refinements in cognitive control abilities.

1.5 BRAIN NETWORKS UNDELRYING COGNITIVE CONTROL

In 2003, Braver and colleagues used a mixed block-event related fMRI task switching paradigm to dissociate brain regions contributing to sustained cognitive control from those underlying

more transient cognitive control processes[48]. Results from this study concluded that the anterior prefrontal cortex is involved in sustained control, while the superior parietal lobes are involved in more transient control. Several years later, Dosenbach and colleagues used graph theoretical techniques introduced to neuroscience by Sporns and colleagues and found these regions are core nodes of two distinct networks operating in parallel[15,49]. Specifically, the anterior prefrontal cortex was a part of a broader network encompassing the anterior cingulate cortex, bilateral insula, and frontal operculum. This network of regions, coined the cingulo-opercular network, supports sustained cognitive control. Supporting transient aspects of cognitive control is the frontoparietal network, which includes the superior parietal lobes as core nodes of a broader network encompassing the dorsolateral prefrontal cortex, middle cingulate cortex, and inferior parietal lobes. One widely cited view of these networks is that they're involved with tasks that are involved in many forms of cognition, including language, reading, math, and working memory. Therefore, these control networks are thought to play a critical role in domain-general task set initiation and switching (frontoparietal network) and sustained control (cingulo-opercular network).

Around the same time, Seeley and colleagues discovered another cluster of brain regions involved in the interface between bottom-up and top-down processes[50]. This cluster, referred to as the salience network, comprised regions of the bilateral insula, anterior cingulate, dorsomedial nucleus of the thalamus, and several brainstem nuclei. Interestingly, these regions are some of the most common to appear in fMRI literature, ranging from tasks invoking cognitive control, as well as, those eliciting interceptive/autonomic responses, such as pain and empathy[51] (Craig 2009). Both the anterior cingulate and anterior insula are anatomical hubs in the brain, projecting to both frontal and parietal cortices and also displaying a high degree of connectivity between

themselves[52,53]. These three networks are central components of cognitive control, but need to operate while suppressing the default mode network which engages the medial anterior prefrontal cortex and posterior cingulate cortex, and supports a task-negative mind wandering state, rather than focused attention.

Functionally, the anterior cingulate and anterior insula play a critical role in cross-talk between functional brain networks. It has been shown that the anterior insula is a causal outflow hub, specifically acting as a 'switchboard' between functional networks, especially between the task-negative default mode network and task positive fronto-parietal network[54]. Developmentally, the strength of both structural and functional between network connections from the anterior insula to the default mode network and the fronto-parietal network was shown to be significantly stronger in adults compared to children, indicting the flexibility of insular functioning in task switching between a task positive and task negative state may improve throughout adolescence[55]. However, the mechanism linking control network development and adolescent improvements in cognitive control remain unclear.

1.6 OSCILLATIONS AND THEIR COMPONENTS: AMPLITUDE AND PHASE

Neural signals, whether measured directly or indirectly – as is the case in most human studies – are measured in the time domain. A measure of signal amplitude is obtained per unit of time. In fMRI, this time resolution is on the order of 1-3 seconds, while in MEG, this time resolution is on the order of milliseconds. Any time-varying signal, such as neural signals, that engages in periodic activity is *oscillatory*. Indeed, oscillations are an intrinsic property of populations of neurons[56]. To study a signal's oscillatory components in greater details, the time-varying signal

can be decomposed into its frequency components (units = Hz) via frequency decomposition techniques (e.g., fast-Fourier transform) and/or time/frequency decomposition techniques (e.g., Morlet wavelets). The resulting oscillations filtered into a specific frequency or frequency range can then be described in terms of signal *amplitude* and *phase.*

The strength of a neural oscillation at a given frequency is reflected in the *amplitude* of the oscillation, defined as the amount of deviation away from a baseline. Squaring this term results in the total amount of *power* for that oscillation. Stronger oscillations result in a greater deviation away from baseline (i.e., greater amplitude/power). The *phase* of an oscillation refers to the angle of the sinusoidal function of that oscillation (Figure 1). The phase angle within a group of neurons has been shown to affect the likelihood of spike output from a sending group of neurons and sensitivity of input in a receiving group[57].

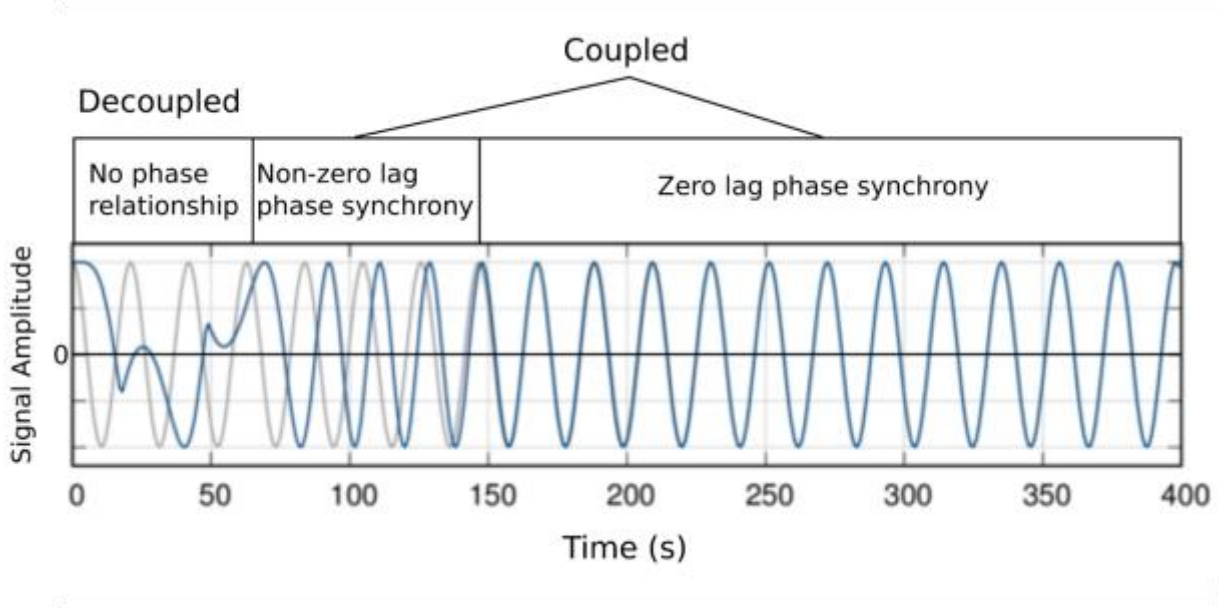

Figure 1. Oscillatory components: amplitude and phase

The level of phase synchrony between two regions can be measured using a phase-locking value (PLV)[58]. PLV measures the *variability* in the phase of the oscillations of two brain

regions over time. PLV ranges from 0 to 1, representing a random phase relationship and fixed phase relationship, respectively. Regional interactions exhibiting a high PLV indicate a relatively low level of variability, while interactions exhibiting a low PLV indicate a relatively high level of variability[58].

Oscillations in the beta/gamma (14-80Hz) band have been shown to play a critical role in enabling local neuronal synchronization, while alpha/theta (4-14Hz) band oscillations have been shown to be critical for long-distance integration[59,60]. Specifically, long-range frontoparietal interactions during working memory retention and mental imagery evolved most strongly in the theta and alpha (4-14Hz) frequency range[61,62]. As such, cortical oscillations could play a central role in synaptic pruning, supporting the temporal coordination and specification of local and long-distance connectivity[63]. Indeed, evidence has begun to emerge from electroencephalographic literature that the precision of temporal coordination, as measured by the co-fluctuation of the phase of neural populations, continues to increase throughout childhood and adolescence across several frequency bands, including theta-, beta-, and gamma-bands while subjects are engaged in a task[64]. However, it is still unknown how phase relationships between brain networks develop at rest when oscillations are not locked to an external cue. In sum, at the core of cognition is a dynamic communication structure enabling rapid, coordinated interactions between disparate regions of the brain. Viewed in this way, networks and their oscillations provide a valuable avenue for the assessment of normative brain development[65].

1.7 MECHANISMS UNDERLYING IMPROVEMENTS IN COGNITIVE CONTROL: A MODEL

Recent evidence supports the notion that the integration of existing large-scale brain networks subserving cognitive processes underlies mature cognitive control. For example, integration between the cingulo-opercular (CO) network, which subserves task-set maintenance, and the fronto-parietal (FP) network, which underlies trial-by-trial updating, increases with working memory demands[66]. Furthermore, performance in adolescence is associated with greater interactions between these cognitive control networks and the default mode network[67,68].

We recently proposed a novel model of a network-based mechanism for improved cognitive control abilities throughout development[69]. We postulate that underlying the maturation of cognitive control is the strengthening of the dynamic interaction of neural systems supporting cognitive control including: working memory, inhibitory control, and performance monitoring. This model of control shares features with a recently proposed model of cognitive control, relying on context-dependent, cross-component interactions[70]. The components of cognitive control (inhibitory control, performance monitoring, and working memory) are composed of both distinct and overlapping brain regions (Figure 2). Indeed, these three components compliment one another and rarely is one used but not the others[71]. Distinct regions within each component represent those that have greater segregation predominantly participating in a specific component of cognitive control. In contrast, other regions that overlap across components play a more integrative role, allowing for more flexible and coordinated activity between components. Each pairwise relation between regions carries some connectivity weight (representing the degree of correlation), which is modulated by the current task state. Developmentally, with experience, successful interactions (i.e. connectivity patterns that

facilitate goal achievement) would be reinforced, while connections leading to unsuccessful or inefficient outcomes would be pruned leading to specialization within and between network connectivity in adulthood. During a *task-state*, this maturation would result in decreases in the variability of performance, while an increase in variability would be expected in the *resting-sate*, supporting increased flexibility. Over development, experience would strengthen connectivity patterns between components that would support timely and flexible engagement of cognitive control[45,72,73].

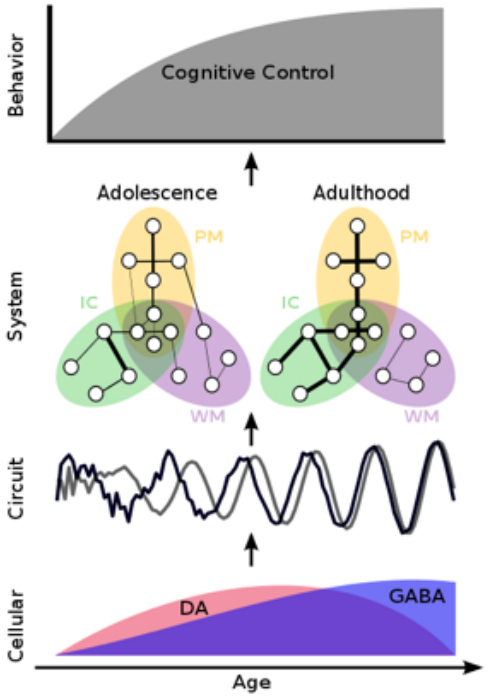

Figure 2. A model of the maturation of cognitive control.

At the **cellular** level, DA (red) and GABA (blue) systems undergo dynamic changes throughout adolescence. We propose that maturational neurotransmitter changes during adolescence lead to increased signal-to-noise, power, and synchrony in the cortex at the circuit level when control systems are engaged during a task. These changes in maybe unique in cortical regions underlying cognitive control. These **circuit level** changes lead to **systems-level** alterations of distributed connectivity patterns depicted for inhibitory control (PM = performance monitoring; IC = inhibitory control; WM = working memory). Circles represent brain regions, and lines between them indicate a pair-wise connection. Line thickness represents connection strength. Circles within overlapping networks, represent highly integrative regions. Connections that lead to successful performance are strengthened by adulthood, while connections that do not, are weakened and/or pruned. Taken together, these developmental changes, occurring across multiple levels of brain function, contribute to mature cognitive control **behavior**.

1.8 DEVELOPMENT OF TASK SWITCHING

Switching between components of cognitive control is a central feature of the model explained above. Two types of flexibility associated with task switching have been previously defined: instructed flexibility and adaptive flexibility. Instructed flexibility involves subjects adapting their behavior based on changing task rules, while adaptive flexibility requires subjects to infer rules based on feedback, as in the Wisconsin card-sorting task. Here, our paradigm focuses on instructed, cue-based flexibility. The neural and behavioral cost of switching has been shown to be greater in adolescence than in adulthood. Behaviorally, though more pronounced in children, adolescents incur a greater switch cost (i.e., increased reaction times when comparing switch trials within a block to non-switch trials within the same switch block[74] than adults), indicating immaturities in temporal aspects of component interactions. To determine the neural correlates of these behavioral changes with age, Rubia and colleagues implemented fMRI and a response-switching paradigm in adolescence (10-17yrs) and adults (20-43yrs) in which subjects were presented with a grid divided into four squares, with either a vertical or horizontal bidirectional arrow in the middle of the grid[75]. Trials began with a red dot appearing in one of the four quadrants. When the bidirectional arrow was vertical, subjects had to determine whether the dot was in the top or bottom of the grid. Conversely, when the arrow was horizontal, subjects were instructed to indicate whether the dot was on the left or right side of the screen. When contrasting switch to non-switch trials, these researchers found areas of the inferior frontal, posterior parietal, and anterior cingulate cortices were significantly more active (as measured with BOLD) in adults compared to adolescents. Similar regions were shown to display this same developmental profile in a subsequent study[76].

1.9 SUMMARY AND OVERVIEW

Adolescence is a significant period of cognitive development characterized by the specialization of interacting brain systems. The oscillatory network mechanisms underlying the reliable engagement of cognitive control remain elusive. This proposal aims to elucidate the spatiotemporal large-scale network mechanisms contributing to more reliable, adult-like engagement of cognitive control.

In Chapter 2, we characterize the *spatial* aspects of large-scale network topology contributing to the developmental improvements in cognitive control, specifically network organization and network integration. Chapter 3 seeks to understand the role of neural oscillations resting-state network development and how these dynamics relate to cognitive control development. Lastly, in Chapter 4 we analyze the role of oscillations in the developmental improvements in cognitive control, specifically the ability to rapidly switch brain states to meet current cognitive demands. To this end, we have developed a novel cognitive control task, requiring subjects to switch between more automatic and inhibitory control processes. Together, the experiments contained within these aims will allow us to better understand the spatiotemporal network and oscillatory mechanisms underlying the remarkable improvement in cognitive abilities from adolescence to adulthood.

2.0 THE CONTRIBUTION OF NETWORK ORGANIZATION AND INTEGRATION TO THE DEVELOPMENT OF COGNITIVE CONTROL

2.1 BACKGROUND

Cognitive control is the ability to execute voluntary, goal-directed behavior[77–79]. It requires flexible and adaptive coordination of core executive systems that are supported by integration among by widely distributed, specialized brain circuitries[10]. The core components of cognitive control are available early in development[80]. However, in adolescence cognitive control abilities become significantly more reliable and flexible, as response accuracy and speed stabilize in adulthood[81]. These developmental gains in information processing occur in parallel with brain maturational events, including synaptic pruning[82] and myelination[83], which predominantly enhance collaboration among brain systems[84]. The nature of the interaction between brain network maturation and cognitive development during adolescence is not well understood[7], limiting our ability to understand the neural basis of psychopathology that emerges at this time, many of which are characterized by deficits in cognitive control[85].

Characterizing functional brain network interactions during the resting state (i.e., while the subject is not engaged in any particular task) has become a valuable emerging approach for investigating the brain basis of cognitive development. Studies using this approach have revealed roles for these networks in supporting cognitive control[10,15]. Approximately 20 functional

networks have been identified in the functional connectome[86], including sensorimotor networks, such as the somatomotor (SM) and visual networks; cognitive networks, such as the fronto-parietal (FP) and cingulo-opercular/salience (CO/Salience) networks; and a task-negative default mode (DM) network [21]. Each functional network operates as a module within the full connectome. Networks are demarcated by dense internal connectivity[18,87], defining a foundational organization for the functional brain. Thus, network *organization* refers to the network affiliation of each region of the connectome. Initial studies characterizing age-related changes in functional network organization suggested that the organization of these networks continued to change into adulthood[88], such that development proceeded from short-distance anatomical networks in infancy and childhood, to long-range, widely distributed networks in adulthood[39,88–90]. However, age-related differences in head motion artifacts may have confounded the connectivity distance findings[40,41,91]. Advances in data processing methods[40,41,91], and recent findings suggest that foundational aspects of functional network *organization* are established early in development, while processes related to network *integration* continue to mature into adulthood[92]. Network *integration* refers to the level of functional coupling between networks, measured by participation coefficient (PC), a graph theoretical construct[23]. PC is a particularly useful construct to measure network integration, given its sensitivity to between-network connectivity, while maintaining robustness to the total number of connections (degree). Degree-based measures of integration have been shown to be dependent on the size (number of nodes) in a network and therefore can skew results towards a greater number of hubs within larger networks, such as the default mode network[24]. Participation coefficient is normalized by the degree of the node. As a result, increases in participation coefficient are driven by increases in the number of between-network connections.

Properties of network organization and integration could parallel cognitive development, which is characterized by enhanced adaptive and flexible integration of mature core control components. Thus, in the present study, we sought to identify whether age-related changes in functional networks are determined by changes in network *organization* and/or network *integration* and whether these changes are related to developmental improvements in cognitive control. We applied graph theory[93,94] to a rich developmental resting-state functional magnetic resonance imaging (RS-fMRI) dataset obtained in 10-26 year olds who also performed the antisaccade task, a robust developmental measure of cognitive control.

Given that core cognitive components are on-line by childhood and that the ability to adaptively and flexibly engage these components improves into adulthood[95–99], we hypothesized that network *organization*, which supports component processes, would not change with age, but that network connectivity *strength* and *integration*, which both support interaction between components, would strengthen with age. In turn, we hypothesized increased control network integration would predict age-related improvements in cognitive control as measured by the antisaccade task.

2.2 METHODS

2.2.1 Subjects

One hundred ninety-five subjects aged 10 – 26 years participated in this study (Table 1 in section 2.3.1). Written informed consent was obtained from every subject and minors did sign assents. A phone screen questionnaire was used to assess medical history and history of psychiatric

disorders. As determined through the interview process, neither subjects nor their 1st degree relatives included in this study currently or previously had any neurological disease, brain injury, or diagnosed psychiatric illness. Substance use was assessed using the drug use and history questionnaire. Subjects included in this study were free from substance use/abuse. A post-scan questionnaire was used to inquire if subjects had fallen asleep. Sixteen subjects reported periods when they may have briefly drifted into sleep but none reported sleeping throughout the entire resting state scan. Data from three subjects were discarded due to excessive head motion. Therefore, we report data from 192 subjects. While age was considered as a continuous variable, some analyses considered developmental stages by binning ages after first sorting individual subjects by age, similar to methods used in the past to characterize changes in childhood (n=41 10-12 year olds), early (n=41 13-15 year olds) and late adolescence (n=53 16-19 year olds), and adulthood (n=57 20-26 year olds).

2.2.2 Task Design

The antisaccade task was performed by subjects outside of the MR scanner on a separate day from the MR visit. For a full description of the antisaccade task used, see[100]. Briefly, neutral trials were extracted from an incentivized antisaccade task, consisting of reward, loss, and neutral trials. There were a total of 40 of each trial type. Each neutral trial began with a white central fixation, which then turned red for 1.5 sec, prompting subjects to prepare a response. Next, a peripheral stimulus (yellow dot at approximately 0.5 degree/visual angle) appeared at an unpredictable location on the horizontal meridian (± 4 and 8 degrees/visual angle) for 1.5 sec. Subjects were instructed to inhibit making a saccade towards the stimulus, and instead to saccade to the mirror location of the stimulus. Eye movement data were scored on-line using interfaced

E-Prime (Psychology Software Tools, Inc., Pittsburgh, PA) and ASL (Applied Science Laboratories, Bedford, MA) eye tracking software. A script detected if at any time during the first 1000 ms a subject made a saccade to the stimulus or if no eye movement was generated. An auditory tone (1163 Hz) was played for 400 ms if the subject made a saccade to the stimulus. If the subject made a correct saccade a "cha-ching" sound (1516 Hz) was presented for 400ms. Correct responses were defined as those in which the first eye movement in the saccade was directed toward the mirror location at a velocity greater than or equal to 30°/s[101] and extended beyond a 2.5° /visual angle from the central fixation. A response was considered incorrect when the first saccade was directed towards the target beyond a 2.5° /visual angle from central fixation, but were subsequently directed to the hemifield opposite the target, similar to previously published work[100].

2.2.3 Eye Tracking

In addition to the on-line scoring, eye data were scored offline by a technician for various saccade metrics, including correct trials and errors, as well as saccade latency, using ILAB software[101] and an in-house scoring suite written in MATLAB (Math Works, Inc., Natic, MA). A correct antisaccade response was one in which the first saccade following stimulus onset was towards the mirror location of the stimulus and extended beyond a 2.5 degrees/visual angle central fixation zone. Errors were defined as occurring when the first saccade following stimulus onset was directed towards the stimulus and extended beyond central fixation.

2.2.4 MR Data Acquisition

Data were acquired using a 12-channel Siemens 3T Tim Trio at the University of Pittsburgh Medical Center Magnetic Resonance Research Center. The resting-state scan was acquired at the end of the scanning session and was always at the same time of acquisition for all subjects. For each subject, we collected 300 seconds (200 TRs) of resting-state data. Structural images were acquired using a sagittal magnetization-prepared rapid gradient-echo sequence (repetition time [TR] = 1570 ms, echo time [TE] = 3.04 ms, flip angle = 8°, inversion time [TI] = 800 ms, voxel size = 0.78125 × 0.78125 × 1 mm). Functional images were acquired using an echo-planar sequence sensitive to BOLD contrast (T_2*; TR = 1.5 s, TE = 29 ms, flip angle = 70°, voxel size = 3.125 × 3.125 mm in-plane resolution, 29 contiguous 4-mm axial slices). During the resting-state scan, subjects were asked to close their eyes and relax, but not fall asleep.

2.2.5 RS-fMRI Preprocessing

Functional images were preprocessed using AFNI[102] and Freesurfer[103]. Standard preprocessing steps were completed, including: (1) normalization based on global mode, (2) wavelet despiking[104], (3) simultaneous multiple regression of nuisance variables from BOLD data and bandpass filtering[41] at 0.009 Hz < f > 0.08, and (4) spatial smoothing using a 6 mm full-width at half-maximum Gaussian blur. Given the Power parcellation used within this study models regions of interest as 10mm spheres, we decided to use smoothing to increases SNR. The canonical networks derived from this parcellation have been shown to not be influenced by spatial smoothing[21]. Freesurfer was used to segment gray matter, white matter, and ventricular voxels. Nuisance regressors included ventricular signal averaged from ventricular regions of

interest (ROIs), six head realignment parameters obtained by rigid body head motion correction, and the derivatives of these signal and parameters. In addition to wavelet despiking, we removed any remaining high motion volumes via a scrubbing procedure[40,91]. For the original 195 subjects, we calculated two quality control measures with respect to head motion, volume-to-volume frame displacement (FD) and the RMS derivative of fMRI time series (DVARS). We censored and removed volumes in individual subjects that had an FD > 0.5 mm and DVARS > 5, as well as the frame preceding the motion artifact and the two subsequent frames. FD is calculated on the original motion time series (i.e., before motion correction with wavelet despiking). On the other hand, DVARS is calculated after motion correction with wavelet despiking. Large DVARS values after wavelet despiking would indicate motion/artifact-related noise in the global signal (i.e., brain-wide change from one volume to the next) still remained after despiking, which we did not observe (Table 1: note DVARS after wavelet despiking is considerably lower in all 4 groups than DVARS calculated prior to wavelet despiking). Because we collected 300 seconds of data, subjects were dropped entirely if > 20% of their volumes were removed, leaving the minimum amount of rest data for any subject 240 seconds. This procedure resulted in the removal of three subjects from further analyses. Of the remaining 192 subjects, only four did not contain a full 300 seconds of data.

2.2.6 Functional Network Parcellation

For each subject, nodes (n=264) were defined from the functional parcellation derived by Power and colleagues[21]. Coordinates were derived through fc-Mapping[105,106] and a meta-analytic procedure[21], covering major brain systems involved in both tasks and rest. All ROIs were modeled as 10mm diameter spheres around a center coordinate. For each subject, the time series

of voxels within each ROI were averaged and then correlated to produce a 264x264 correlation matrix for each subject. Any comparisons made between correlations were transformed to z values using Fisher z(r) transformation, and then reconverted to Pearson r values for reporting and visualization.

2.2.7 Individual and Group Correlation Matrices

Network-level age-related changes were assessed using individual correlation matrices. For all other RS-fMRI analyses, age was treated as a categorical variable to assess stage-like developmental changes in graph metrics and changes in the distribution of connections between children (aged 10-12), early adolescents (aged 13-15), old adolescents (aged 16-19), and adults (aged 20-26). Notably, no standard for binning age groups over adolescence currently exists, though binning roughly follows Luna and colleagues[11]. Since short-distance correlations (Euclidean distance < 20mm) can arise from artifacts[40], these connections were not included in tests for age-dependent significant strength changes in connectivity.

2.2.8 Network Detection and Comparison

Since there is no ideal, biologically salient threshold that definitively defines functional networks, we explored a range of network densities from 1-25% to avoid any thresholding bias. Results involving participation coefficient at the group level reflect values that are averaged across all network densities to remove any bias of a single threshold. For a representative network assignment, we chose a network density of 10%, since this threshold results in meaningful network organization (i.e., 5 networks), while maintaining full connectedness.

Importantly, we did not impose network assignments according to[21], since that would erode the ability to make conclusions concerning developmental changes in network organization.

To define and examine the developmental trajectory of functional network organization, we partitioned the full connectome of 264 ROIs into functional networks using Newman's Q-metric coupled with an efficient optimization approach proposed by Blondel et al.[18,19,107].This method has been verified to be one of the best-performing community detection algorithms of undirected networks[108]. Furthermore, unlike recent community detection approaches, Newman's algorithm does not include a gamma parameter for the biasing of larger vs. smaller modules. Therefore, the only input to the algorithm was the adjacency matrices. We then calculated normalized mutual information (NMI) to determine the level of similarity between network assignments across age groups, with values closer to 0 indicating dissimilar network assignments and values closer to 1 indicating similar assignment. We permuted the labels of individual matrices between contrasts 1000 times to generate a null distribution of NMI values for each contrast. Matrices between groups were randomly shuffled and partitioned into functional networks, and NMI was calculated. Upon the finding that the observed NMI values fell within one standard deviation of the mean of the null distribution, we executed a leave one out cross validation to generate a distribution of observed NMI values for the following analysis. Because conventional significance testing does not allow stating evidence in favor of null findings, we implemented a Bayes factor alternative[109] to compare the observed NMI distribution with the null distribution. Values greater than 1 indicate the likelihood of stable functional network organization is 'n' times more likely than the likelihood of developmental changes in functional network organization.

2.2.9 Connectivity Strength Changes during Adolescence

A general concept in the development of functional networks is that they develop from "local to distributed"[88]. To test this hypothesis, given methodological improvements for head motion and a denser, more representative functional network[21], we contrasted connectivity values from averaged weighted matrices in children versus adults for each ROI-ROI pair. Euclidean distance was also calculated for each pairwise relation. We then performed a simple linear regression with distance as a predictor of change in connectivity strength between the children and adult matrices.

We also addressed changes in connectivity strength as a function of within- and between-network interactions. First, within each group-averaged matrix, we averaged all within-network pairwise relations and all between-network pairwise relations, separately. We then performed a two-tailed t-test for each consecutive age contrast. We then wanted to test for significant increases or decreases in connectivity with respect to specific network interactions. To this end, within each group-averaged matrix, the average connectivity strength was calculated for each network. We then tested each combination of within-network (e.g., DM/DM network) and between-network (e.g., DM/FP network) interactions to determine significant increases or decreases in connectivity strength between consecutive age groups. For each comparison, we ran a two-tailed t-test to determine significance (Bonferroni corrected for multiple comparisons).

2.2.10 Developmental Changes in Participation Coefficient at the Network Level

For each subject, we partitioned the full network into sub-networks imposing the community assignments from the adult group in the analysis outlined above, and subsequently calculated

participation coefficient for every node within each group. Participation coefficient (PC) is a graph measure quantifying the degree to which a node engages in inter-network communication[23,24]. Higher PC indicates more distributed between network connectivity, while a PC of 0 signifies a node's links are completely within its home network (within network). Nodal participation coefficients were then averaged within each network and were tested for significant age-related effects using linear and inverse models.

2.2.11 Long-Term Fluctuation in Network-level Participation Coefficient

To determine any long-term fluctuations in participation coefficient that may not be captured at the individual subject data, we calculated average subject correlation matrices using a moving average approach, used previously in functional brain network data[88] and commonly used in economics research. Averaged group matrices were formed using a moving average of age-ordered subjects (e.g., group1: subjects 1-30, group2: subjects 2-31, … group163: subjects 163-192), thus generating 163 groups of 30 subjects in each group. Each group matrix was then parcellated according to the adult network assignment and PC was calculated for each ROI within each group. For each group, the PC for ROIs within a network were averaged and plotted as a function of age.

2.2.12 Relating Changes in Integration to the Development of Inhibitory Control

To test the hypothesis that the relationship between age and performance (accuracy and RT) on the antisaccade task is moderated by integration of the CO/Salience network with other functional networks, a hierarchical multiple regression analysis was conducted separately for

accuracy and reaction time. If a significant interaction was observed, age groups were binned into the four age groups previously defined and a median split of the averaged participation coefficient within the CO/Salience network was conducted. Within each bin, we tested for significant differences in RT using a t-test between high and low PC groups and corrected for multiple comparisons using the Bonferroni method.

2.2.13 Identifying Specific Nodes Increasing in Participation Coefficient

We sought to discover brain regions that significantly increased in the ability to integrate information from widespread functional networks using graph theory. PC was calculated for each node within each categorical age group. Importantly, the degree, or number of links a node has, was not considered as a metric for integration since network measures that are degree-based have recently been called into question in Pearson correlation RS-fMRI networks[24]. PC for each node was contrasted between each set of chronological age groups (children vs. early adolescents, early adolescents vs. late adolescents, and late adolescents vs. adult) and between adults and children by subtracting the younger group's PCs from the older group's PCs resulting in four total contrasts. Permutation tests were conducted on each node to test nodes for significant changes in PC. To generate a null distribution of PCs for each node, subject labels were randomized within groups 1000 times and PC was calculated for every node in each run. Contrasts between age groups were then generated by subtracting the PCs for each node for the younger group from the older group. This process was repeated for each age contrast. Significant increase or decrease in participation coefficient for a node was Bonferroni corrected for multiple comparisons.

2.2.14 Age-related Changes in the Distribution of Regional Participation Coefficient

Within each group, and for each node that significantly increased in participation coefficient, we calculated the degree of the ROI to each network, including its 'home' network, and then contrasted these values for consecutive age groups for comparison. The degree of a node is determined by the number of links a node has. This approach allowed us to contrast the distribution of links to each network between consecutive age groups (i.e., within-network vs. between-network connectivity). This approach affords the ability to characterize the driving factor(s) behind the observed significant increases in PC.

2.2.15 Computations and Visualizations

AFNI[102] and Freesurfer[103] were used to process MRI images. We used the Brain Connectivity Toolbox[94] in MATLAB (The Mathworks, Natick, MA) for network computations and statistical testing. For brain visualizations, we used the BrainNet Viewer[110].

2.3 RESULTS

2.3.1 Development of Functional Network Organization

We used a previously defined functional connectome parcellation of 264 functional regions of interest (ROIs) across cortical, subcortical, and cerebellar structures[21] in a sample of 192 individuals, aged 10-26 years old (Table 1). For each subject, we correlated the time series of

each ROI with that of every other ROI. We then formed group matrices by averaging each subject's connectivity matrix within categorical age groups (10-12; 13-15; 16-19; and 20-26 year olds) (Figure 3A). For each group, we partitioned the full functional connectome into modules using Newman's Q-metric coupled with an efficient optimization approach[18,19,107] across network densities ranging from the top 1% to 25% of pair-wise correlations in terms of correlation strength. Notably, Newman's Q-algorithm returns modules of densely interconnected nodes. We interpret these modules as being functionally connected collections of brain regions sub-serving common functions and therefore refer to them as functional brain networks. The representative network partition of the full connectome was thresholded at a density of 10% (Figure 3A) to partition the network into a meaningful structure while maintaining high connectedness, which would be limited with lower thresholds. This approach identified more comprehensive networks compared with those incorporating lower thresholds[21], such that a single network encompassed the cingulo-opercular, subcortical, and salience networks. We refer to this network, which includes regions critical to cognitive control, as the CO/Salience network.

Group	n	Age Mean (SD)	IQ Mean (SD)	Race	Mean FD	Mean DVARS [a]	Mean DVARS [b]
Child	41(20F)	11.55 (0.82)	112.10 (13.17)	28(68%) white	0.64*	26.72	2.59
Early Adolescence	41(18F)	14.54 (0.91)	110.17 (10.94)	30(73%) white	0.20	21.97	2.17
Late Adolescence	53(28F)	17.89 (0.92)	112.51 (12.01)	44(83%) white	0.22	24.84	1.60
Adult	57(30F)	22.38 (1.83)	116.84 (13.18)	40(70%) white	0.18	22.97	2.43

Table 1. Demographics

[a] DVARS calculated prior to wavelet despiking

[b] DVARS calculated on motion time series after wavelet despiking. Large decreases indicate wavelet despiking was effective in mitigating head motion confounds.

* Mean FD was significantly greater in the child group compared to each other age group ($p < 0.05$, Tukey's HSD corrected for multiple comparisons). A one-way analysis of variance (ANOVA) was conducted between groups for mean DVARS *before* wavelet despiking (Mean DVARS [a]) and again between groups *after* wavelet despiking (Mean DVARS [b]), with no significant differences observed in either test ($p > 0.05$). Note FD is calculated prior to our motion correction procedure while the final DVARS values (Mean DVARs **[b]**) are calculated after our motion correction procedure.

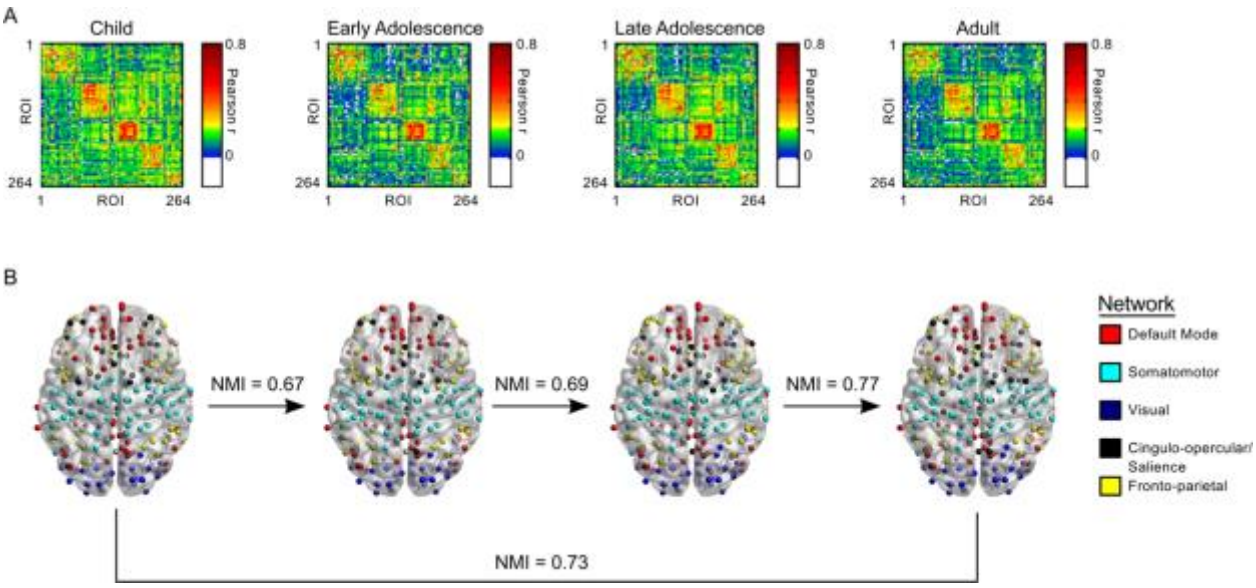

Figure 3. Development of network organization.

(A) Group averaged correlation matrices organized according to network affiliation. ROI order is consistent across all 4 groups. (B) Regions of interest imposed on a semitransparent brain Normalized mutual information (NMI) is a measure of similarity between two sets of data. Here, NMI refers to the comparison between two sets of network affiliation vector between each consecutive age group and between children and adults.

We tested changes in network organization using normalized mutual information (NMI), which measures the mutual dependence of two variables (i.e., how much information in variable one is also contained in variable two). NMI values range from 0 to 1. A value of 0 indicates no mutual dependence (no shared information), while a value of 1 indicates complete dependency (completely shared information). We calculated NMI for networks between consecutive age groups and between children and adults (Figure 3B). We used a random permutation test to compare observed NMI values to a null distribution of 1000 NMI values. For the adult vs. child

contrast, observed NMI = 0.73 (null M = 0.68, null SD = 0.07); between children and early adolescents, NMI = 0.67 (null M = 0.73, null SD = 0.08); between early adolescents and late adolescents, NMI = 0.69 (null M = 0.76, null SD = 0.06); and between late adolescents and adults, NMI = 0.77 (M = 0.70, SD = 0.06) (Figure 4). Importantly, all observed NMI values fell maximally just over one standard deviation of the null mean, indicating no significant differences in network organization from late childhood into adulthood. To provide statistical evidence for findings reflecting stable network organization, we took a Bayesian approach, weighting evidence in favor of the null hypothesis (stable network organization) versus the evidence for the alternative hypothesis (dynamic network organization)[109]. First, we generated a distribution of observed NMI values by performing a leave one out cross validation. We removed one subject from each group for any given contrast and calculated NMI on the remaining group-averaged thresholded matrices. Then, we compared the resulting distribution to the previously generated null distribution for each contrast by calculating the Jeffreys-Zellner-Siow (JZS) Bayes factor[109]. Values greater than 1 provide evidence supporting the null hypothesis, while values between 0 and 1 provide support for the alternative hypothesis. With respect to the null hypothesis of stable developmental network organization, values ranging from 1 to 2 indicate anecdotal evidence and from 3 to 10, substantial evidence. For children vs. early adolescents, JZS Bayes factor = 3.82; for early adolescents vs. late adolescents, JZS Bayes factor = 2.49; for late adolescents vs. adults, JZS Bayes factor = 5.34, and for children vs. adults, JZS Bayes factor = 8.01. These results indicate substantial evidence in favor of stable network organization throughout late childhood, adolescence, and adulthood. Importantly, these results were robust across network densities; thus, our results were not due to our choice of representational network density (Appendix A.2, Table 4).

In addition to group-averaged matrices, we also calculated NMI between modules defined on the basis of individual subject data and the group-averaged adult module assignments to provide an analysis of subject variability. No significant differences were observed between groups, as any potential between-group variability was found to be smaller than that of within-group variability (Appendix A.2; Figure 26).

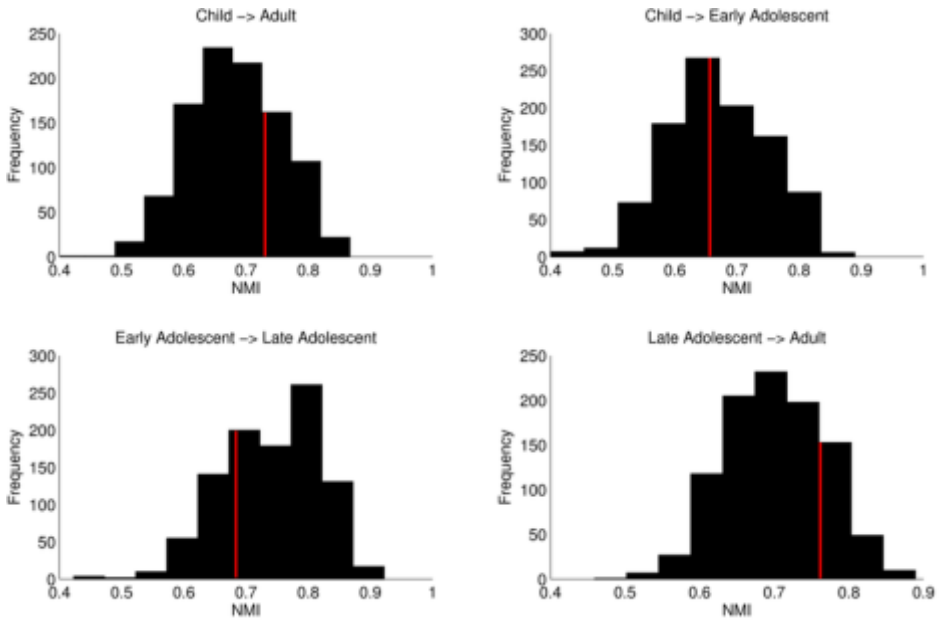

Figure 4. Comparison of NMI to a null distribution

Red lines denote the observed value for NMI. This value was plotted against a null distribution for each subsequent age group comparison and between children and adults. For each comparison, observed values fell within one standard deviation of the null distribution, indicating a lack of evidence for significant differences between module assignments between age groups (i.e., no change in network organization). Importantly, this effect was not restricted to the network density represented here (Appendix A.2, Table 4).

2.3.2 Connectivity Strength Changes during Adolescence

Given that network *organization* is on-line by childhood and remains stable throughout this developmental period, it likely does not account for cognitive changes during adolescence. Hence, we investigated developmental changes in network connectivity strength *within* networks (reflecting the integrity of specialized networks) and *between* networks (reflecting the integration of information processing across functional domains). First, we partitioned each group-averaged matrix into networks according to the adult network assignment. Consecutive age group comparisons of within- and between-network connectivity were conducted using a two-tailed t-test that was Bonferroni corrected for multiple comparisons ($p < 0.01$).

Age-related changes in connectivity strength were unique to developmental stages. From childhood (10-12 years) to early adolescence (13-15 years), there was a global decrease in network connectivity strength for both within-network and between-network connectivity (Figure 5A) ($p < 0.05$, corrected). From early adolescence (13-15 years) to late adolescence (16-20 years) within-network connectivity remained stable while between-network connectivity increased across networks, with the exception of DM/FP network connectivity, which remained stable (Figure 5B). Lastly, from late adolescence (16-19 years) to adulthood (20-26 years), within-network connectivity strength again decreased, while between-network connectivity continued to increase (Figure 5A, 5B). These results indicate that the transition to adult-level network connectivity is characterized by a shift from predominance of within-network connectivity to reliance on between-network connectivity. Together, these results suggest that increased collaborative brain function may underlie improvements in cognitive control.

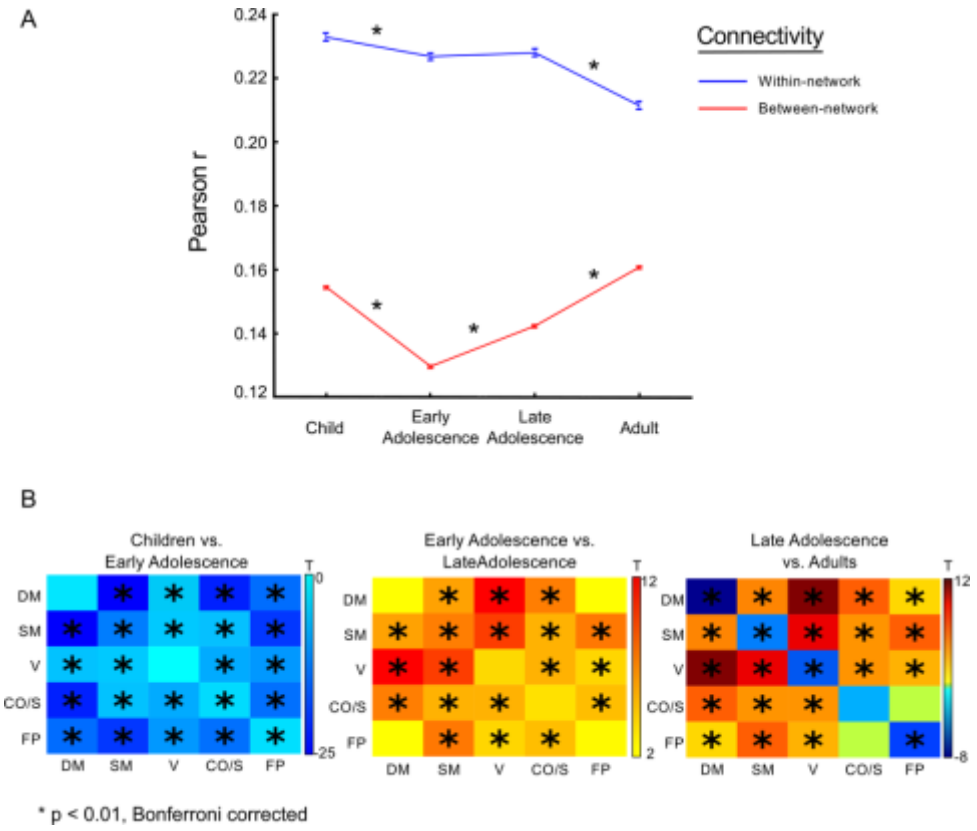

Figure 5. Connectivity strength changes as a function of network organization

Connectivity strength changes through development as a function of network organization. (A) Connectivity strength changes as a function of within- and between-network connectivity. Asterisks denote significant differences between groups ($p < 0.05$, corrected) (B) Each cell represents the t-statistic resulting from a t-test of connectivity strength between each network contrast. The diagonal represents within-network comparisons (e.g., DM-DM network connectivity strength differences between groups), while off-diagonal elements are between-network comparisons (e.g., DM network and CO/Salience network). Therefore, matrices are symmetric. Asterisks denote significant differences between groups ($p < 0.01$, corrected).

2.3.3 No Changes in Distance-dependent Connectivity through Adolescence

Next, we examined the presence of distance related changes with development[39,88,90]. In the present study, age-related change in connectivity strength between ROI pairs was assessed by subtracting each pairwise relation of averaged child connectivity matrix from the averaged adult connectivity matrix. We also calculated Euclidean distance for each pairwise relation and regressed the change in connectivity strength against Euclidean distance (Figure 6B). Results showed that Euclidean distance accounted for a non-significant amount of the variance in change in connectivity with age ($R^2 = 0.002$, $p > 0.05$), indicating distance alone does not play a significant role in connectivity *strength* changes from childhood to adulthood[39,88,90]. We also contrasted the distributions of the top 100 increasing and decreasing connections in terms of connectivity strength between children and adults and found no significant differences ($p = 0.33$; Figure 6A).

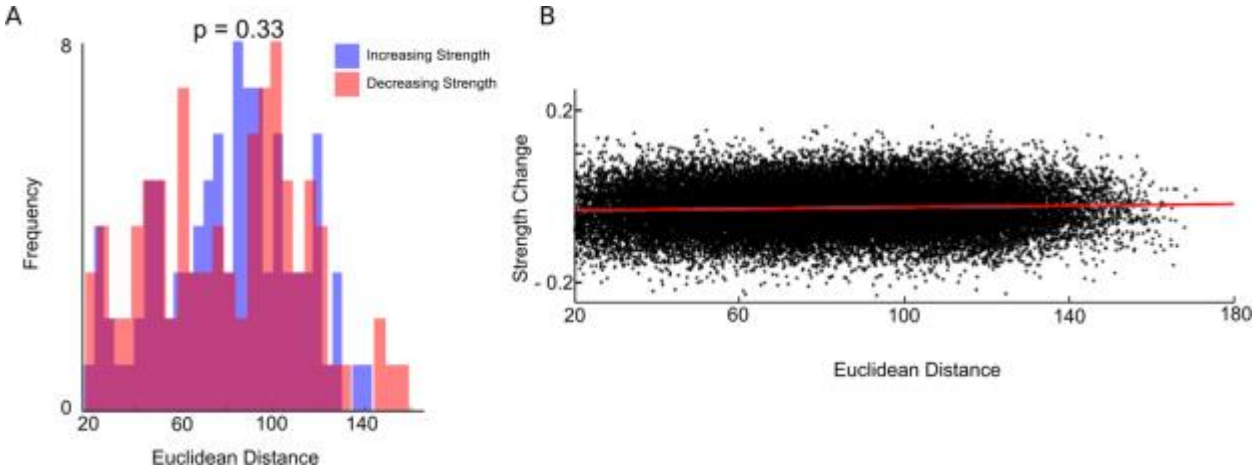

Figure 6. Developmental changes in connectivity strength are not a function of distance.

(A) Distance distributions of significantly increasing connections (blue) and significantly decreasing connections (red) between the child and adult group. No significant difference was found between the two distributions, indicating a lack of evidence for distance-dependent effects on change in connectivity strength ($p = 0.33$). (B) Each point represents a pairwise relationship between two regions of interest. Data values represent the difference by subtracting the averaged child matrix from the averaged adult matrix, plotted as a function of the Euclidean distance between regions of interest. No significant relationship was found between changes in correlation strength and distance ($p > 0.05$).

2.3.4 Developmental Trajectories of Network-level Integration

In addition to characterizing age-related changes in the strength of connectivity both as a function of network organization and as a function of distance, we also aimed to quantitatively characterize the *distribution* of these between-network interactions using graph theory. Brain regions (nodes) within networks may either contain connections (links) solely to nodes within

the same network or may also contain between-network links. A node that has distributed links across multiple networks can be regarded as a highly integrated region (Figure 7A). Here, we operationally define *integration* as the level to which a region contains distributed links from its 'home' network to a foreign network. Participation coefficient (PC) is a graph theoretical construct that is used to calculate integration between brain networks[23]. PC refers to the level to which a node establishes links to foreign networks, with values ranging from 0 to 1. Nodes that link solely to other nodes within their 'home' network would have a PC of 0, while nodes with many distributed between-network links would have a PC closer to 1. Delineating the level of integration using a node's PC extends beyond defining the degree centrality (i.e., number of links) of a node, to defining the relative importance of those links with other networks[87].

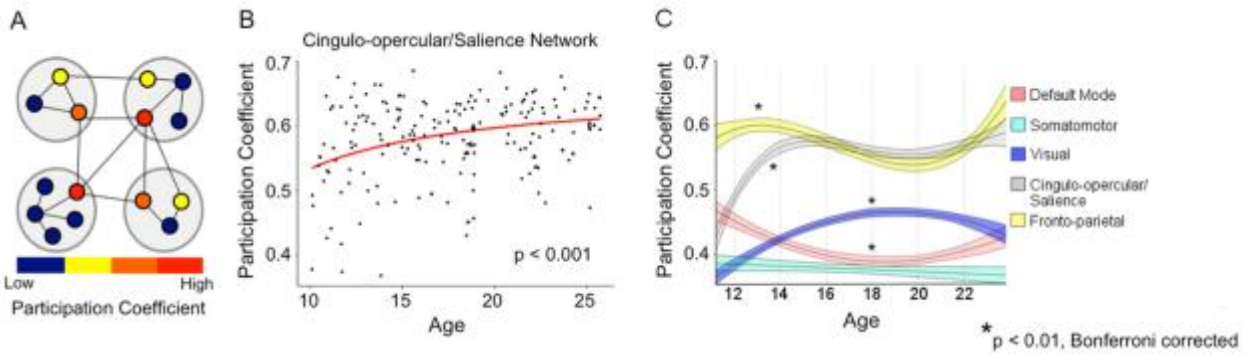

Figure 7. Development of network integration.

Development of network integration (A) Model network with four communities (larger gray circles) to illustrate participation coefficient (PC). Nodes (smaller colored circles) that are warmer colors have a larger PC due to the existence of distributed links to other networks, representing network *integration*. (B) The CO/Salience network significantly increased in PC, and thus integration, through adolescence ($p < 0.001$). No other network demonstrated any significant relationship with age in individual subjects ($p > .05$). (C) Development of long-term fluctuations in participation coefficient by network after smoothing data. The centerline of each curve represents the mean. Upper and lower bounds represent the 95% confidence interval. Asterisks denote statistically significant results from the regression analysis.

To analyze developmental trajectories of integration at the network level, we calculated PC for every node within individual subject matrices at each network density. As an important aside, to remove the arbitrary bias in thresholding, all subsequent calculations involving PC are represented as the mean value across the range of network densities. Though we chose this method, PC values at a range of network densities are highly correlated with the mean value across thresholds (Appendix A.2; Figure 27). PC across all nodes is significantly positively correlated with the PC of all nodes at each network density. If our results were only driven by a

specific threshold (e.g., 5%), but not others (e.g., 20%), a significant relationship between mean PC and the specific threshold driving the effect (5% in this example) would exist, but would not exist in others (20% in this example). This provides evidence that PC is robust to any biases that could be introduced by thresholding.

For each subject, nodes were grouped according to the network to which they were assigned in the adult group. Then, we calculated the mean PC value for each network and tested each network for significant age-related effects on individual subjects, fitting both linear and inverse regression models, which are known to best fit this period of development [11]. The choice of superior model fit was made quantitatively, using Akaike information criterion (AIC). The PC of the CO/Salience network significantly increased over the age range studied ($R^2 = 0.11$, $t = 4.76$, $p < 0.001$) (Figure 7B) optimally fit with an inverse model. No other network displayed age-related changes in PC for either linear or inverse models ($p > 0.05$). The purported role of the CO/Salience network is the maintenance of cognitive control. Thus, increased integration of the CO/Salience network with other brain networks may underlie improvements in cognitive control performance during adolescence. We tested this hypothesis by investigating associations between network integration and behavioral performance in the antisaccade task.

To identify any long-term fluctuations in PC that may not be captured at the individual subject level, we sorted individual subject matrices by age and then calculated average subject correlation matrices using a moving average approach. After calculating PC for each region within each moving average group, we computed the mean PC within each network. We then fit linear, inverse, quadratic, and cubic regression models to the data, with the best fit model defined as the one with the lowest AIC (Figure 7C). The best fit model for the CO/Salience network was an inverse fit ($R^2 = 0.59$, $p < 0.05$), showing an increase in PC from late childhood through ~14

years of age, followed by relative stability (Figure 7C, black curve). The quadratic model best fit age-related changes in the DM network ($R^2 = 0.28$, $p < 0.05$), which decreased in PC throughout adolescence, but increased slightly into early adulthood (Figure 7C, red curve). A quadratic model best fit the visual network ($R^2 = 0.51$, $p < 0.05$), with peak levels of integration occurring late in adolescence (Figure 7C, blue curve). A cubic model best fit the FP network ($R^2 = 0.29$, $p < 0.05$), where PC increased from late childhood through ~14 years of age before declining from ~14 to 20 years, and then increasing again throughout early adulthood (Figure 7C, yellow curve). Lastly, the SM network remained relatively stable throughout development ($R^2 = 0.01$, $p > 0.05$) (Figure 7C, cyan curve). The fact that no other network demonstrated significant age-related effects in the individual subjects analysis compared to the moving average approach suggests the lack of differences is likely to due a high amount of individual subject variability.

2.3.5 Cingulo-Opercular/Salience Network Integration Moderates the Relationship between Age and Antisaccade Latency

The antisaccade task is a particular robust test of inhibitory control that reliably shows sensitivity to cognitive development through adolescence as accuracy and reaction times (RT) during successful response inhibition improves through adolescence[111–113]. First, we tested the effect of age on accuracy and RT separately, with age modeled as both a linear and an inverse function. As is typical for the adolescent age range[11], all regression models involving age were best fit by an inverse model, as determined by lower AIC, compared to linear models. Similar to previous studies[111–117], we found developmental increases in the accuracy of correct inhibitory response ($R^2 = 0.14$, $t = 5.55$, $p < 0.001$) and decreases in RT through the adolescent period ($R^2 = 0.14$, $t = -5.51$, $p < 0.001$) (Figure 8A, 8B).

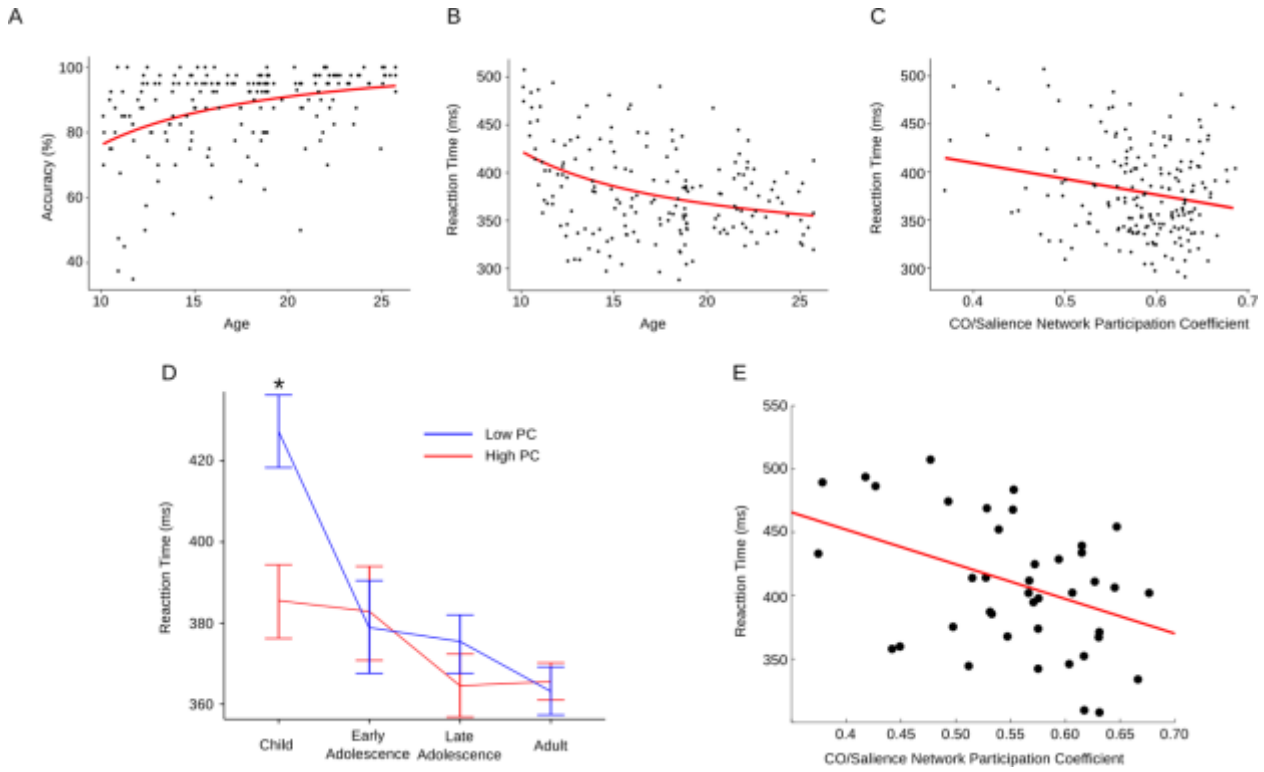

Figure 8. Relationship between increased cingulo-opercular/salience network integration and cognitive control

Performance on the antisaccade task improves throughout adolescence, evidenced by increased accuracy (A) and decreased reaction time (B). As integration of the CO/Salience network increase, reaction times significantly decrease (C). (D) Results from the moderation analysis. CO/Salience integration significantly moderated the effect between age and antisaccade reaction time, such that less CO/Salience integration was predictive of longer reaction times, while higher CO/Salience integration led to significantly faster reaction times ($p < .01$). Note that this effect only occurred during late childhood, indicating earlier maturation of the CO/Salience network is critical for achieving adult-like behavior earlier in development. (E) Reaction time as a function of CO/Salience network integration in the child group.

Next, we tested the association between PC of the CO/Salience network (i.e., CO/Salience network integration) and antisaccade accuracy and RT, controlling for age. Results showed no association between CO/Salience network PC and accuracy ($p > 0.05$). However, as CO/Salience network PC increased, RT to correct inhibitory responses decreased ($R^2 = 0.11$, $t = -2.22$, $p = 0.02$) (Figure 8C), suggesting that greater CO/Salience network integration supports age-related improvements in timely successful inhibitory control. Notably, no other network displayed a significant relationship between PC and accuracy or RT (all $p > 0.05$). While it may be surprising that FP did not associate with antisaccade latency, exerting sustained control within an inhibitory state may play a critical role in the time to initiate a correct response. The CO/Saliency network exhibited a robust increase in integration to the SM network (Appendix A, Table 5), potentially facilitating more reliable control signals to the SM network for motor output. Conversely, the frontoparietal network has been shown to support transient control, rather than sustained control. Antisaccade accuracy may be underlied by the within-network interactions of control networks rather than integration between networks. Indeed, antisaccade accuracy has been associated with DLPFC and FEF interactions, both within the frontoparietal network[118].

Given the relationship between age and both antisaccade performance and CO/Salience network PC, we assessed whether CO/Salience network PC moderates the relationship between correct antisaccade RT and age. To test this, we ran two moderation analyses, one including CO/Salience network PC as a moderator of age and antisaccade accuracy and a second including CO/Salience network PC as a moderator of age and antisaccade RT. In each model, both regressors were centered prior to model fitting. CO/Salience network PC did not significantly moderate the relationship between age and accuracy ($p > 0.05$). However, CO/Salience network

PC did moderate the relationship between age and correct antisaccade RT ($R^2 = 0.16$, $t = -3.28$, $p < 0.001$). To identify when in development this interaction was most prominent, we investigated effects on RT within age groups by performing a median split of CO/Salience network PC (Figure 8D). We observed a significant difference in individual subjects within the child group (10-12 years) between RTs of subjects with high vs. low CO/Salience network PC. Lower CO/Salience network PC resulted in longer RTs, while higher CO/Salience network PC resulted in shorter RTs ($t = 2.07$ $p = 0.04$, Bonferroni corrected). When we extracted the data for each subject, the results showed that as PC increased, antisaccade RT decreased ($R^2 = 0.19$, $t = -2.94$, $p < 0.01$) (Figure 8E).

2.3.6 Developmental Patterns of Regional Integration

Given the finding of changes in network integration with age, we were interested in probing specific regional contributions to increased network integration. In order to identify the contribution of regions of interest (ROIs) to age-related differences in network integrations, which is overlooked when averaging at the network level, we tested each ROI in the network for significant increases in PC across age groups. Specifically, we permuted the connectome 1000 times between consecutive age groups to generate a null distribution of PC for each brain region. The resulting null distributions were normally distributed. Here, we report significant regional increases in PC in a stage-like manner throughout development (Figure 9).

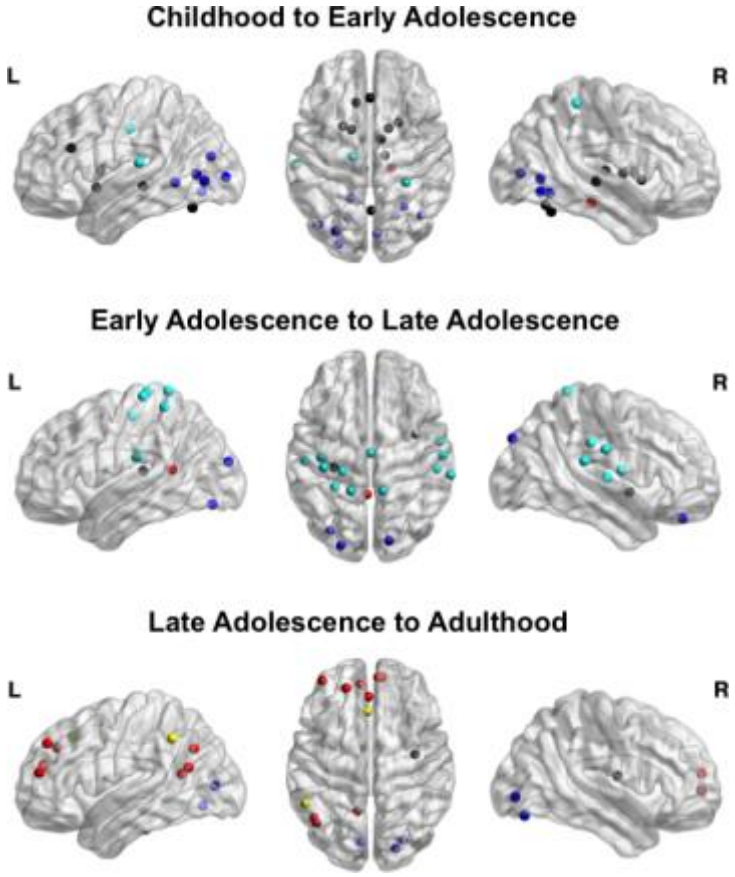

Figure 9. Regional increases in participation coefficient.

Node color represents network affiliation. In the transition from childhood to adolescence, most regional increases were localized to the CO/Salience network, corroborating network-level findings. During adolescence, regional increases were mostly within the SM network, while regions within the DM network and FP network increased in integration from late adolescence into early adulthood.

2.3.6.1 Childhood to Early Adolescence

From childhood to early adolescence, 26 ROIs demonstrated significant increases in PC (Figure 9; Appendix A.2, Table 5). Of those, two were in the DM network, three were in the SM network, 10 were in the visual network, 11 were in the CO/Salience network, and zero were in

the FP network. The significant increases in PC for ROIs within the SM network were mainly driven by increased degree (i.e., number of links) to the visual, CO/Salience, and FP networks, with a concomitant decrease in degree within the SM network. Within the visual network, ROIs that significantly increased in PC also increased in degree to the DM, SM, and FP networks. ROIs within the CO/Salience network showed an increase in degree with the SM, visual, and FP networks, and a decrease in degree within the CO/Salience network. Importantly, many regions within the CO/Salience network that significantly increased in PC were anatomically located in the dorsal anterior cingulate (dACC), anterior insula (aIns), and striatum, including bilateral putamen and globus pallidus.

2.3.6.2 Early Adolescence to Late Adolescence

Twenty regions significantly increased in PC from early adolescence to late adolescence (Figure 9; Appendix A.2, Table 5). Of those, two were in the DM network, 14 were in the SM network, three were in the visual network, one was in the CO/Salience network, and zero were in the FP network. Within the DM network, the posterior cingulate cortex showed a decrease in degree with the DM and visual networks, but an increase in degree to the CO/Salience network. Within the SM network, ROIs increased in both within- and between-network degree, especially to the FP, visual, and CO/Salience networks. The only region within the CO/Salience network that significantly increased in PC was the right posterior insula. This region demonstrated increased degree within network and between all networks. Three ROIs within the VN increased significantly in PC: the left middle occipital gyrus, right cuneus, and left fusiform gyrus. All three regions increased in degree to the DM, SM, and FP networks.

2.3.6.3 Late Adolescence to Adulthood

Seventeen ROIs significantly increased in PC from late adolescence into adulthood (Figure 9; Appendix A.2, Table 5). Of those, nine were in the DM network, one was in the SM network, four were in the visual network, one was in the CO/Salience network, and two were in the FP network. Profiles of change in degree were variable for regions within the DM network. The left superior frontal gyrus, left temporal-parietal junction (TPJ), and left fusiform all decreased in within-network degree, while the left angular gyrus, left posterior cingulate, and right medial frontal gyrus (MFG) all increased in within-network degree. The regions that increased in within-network degree also had increases in degree with other networks. The left TPJ, left angular gyrus, and bilateral MFG increased in degree to the FP network. Interestingly, many DM network regions, including the bilateral MFG, also had increased degree to the CO/Salience network. With the exception of the right lingual gyrus, the regions within the visual network that significantly increased in PC showed decreased within-network degree and increased between-network degree to each of the four other networks. For the first time throughout development, nodes within the FP network significantly increased in PC, namely the left inferior parietal lobe (IPL) and left dorsolateral prefrontal cortex (dlPFC). Both regions decreased in within-network degree and increased in between-network degree with the DM network. Additionally, the left dlPFC also decreased in degree to the CO/Salience network.

2.4 INTERIM DISCUSSION

We sought to characterize the development through adolescence of functional brain network organization, connectivity strength, and integration. Furthermore, we tested the relationship

between network integration and developmental improvements in inhibitory control. Our results provide evidence that: (1) network organization is stable by late childhood; (2) connectivity strength changes with development, reflecting concurrent decreases in within-network connectivity and increases in between-network connectivity; (3) anatomical distance does not account for age-related changes in connectivity strength through adolescence; (4) increased integration of the CO/Salience network throughout the adolescent period and; (5) CO/Salience network PC moderates the relationship between age and antisaccade reaction time, such that higher PC, and thus integration, of this network contributes to faster RTs on the antisaccade task. These findings suggest that foundational aspects of functional network architecture, specifically network *organization*, are established early in development, while the processes underlying network *integration* continue to mature into adolescence[92]. This process reflects the way cognitive control develops, as characterized by more adaptive and flexible interactions of earlier maturing core components.

2.4.1 Developmental Stability in Functional Brain Network Organization

Within the human functional connectome, densely interconnected brain regions are organized into well-defined functional networks, subserving sensory, motor, and cognitive functions. Our findings indicate that this network organization is stable between 10 and 26 years of age, countering earlier findings that suggested developmental changes in network organization reflect a shift from localized to distributed organization, which may have been confounded by head motion artifact[40,88,91,119,120]. The current study applied a wide array of advanced preprocessing steps to limit head motion artifact, including wavelet despiking[104], simultaneous bandpass filtering the time series data and nuisance regressors[41], as well as scrubbing[40]. These results

suggest that, after controlling for head motion, there are no changes in network organization from late childhood to adulthood.

Previous studies found that many aspects of human functional network topology remain stable throughout adolescence, including small-worldness[88,89,121], global efficiency, and hub organization[92]. Combining these findings with our results showing the stability of network organization, we see strong evidence that the large-scale organization of functional networks is stable by late childhood, possibly even earlier. Despite the fact the brain undergoes continual structural maturation of both gray and white matter[3,4,83,122], key fundamental properties of large-scale functional circuitry, including organization, are stable throughout late childhood to adulthood. While non-significant age-related changes to network organization cannot be concluded through inferential statistics, Bayesian inference via JZS Bayes factors allowed us to test the likelihood of the null vs. the alternative hypothesis[109]. Using this method, we confirmed the finding that network organization does not change significantly with age.

2.4.2 Age-related Changes in Connectivity Strength

Our results show age-related changes in connectivity strength. Within-network connectivity strength decreased with age, suggesting that maturity results in network refinements akin to pruning unnecessary connections, which improves signal transmission within networks. On the other hand, we found that between-network connectivity strength decreased into early adolescence and subsequently increased into adulthood, ultimately enhancing the ability for different networks to collaborate. Interestingly, adolescence demarcated the period when between-network connectivity began to increase, perhaps reflecting a qualitative shift in network interactions towards collaborative network functioning. These changes were sensitive to network

organization, not solely by the distance between connections, as initial studies had suggested[39,88,90,123]. These results are not surprising given our implementation of recent advances in head motion control that minimized its confounds on age differences in connection strength as a function of distance[40,91]. Distance-related changes in connectivity strength by age have been found after controlling for head motion, albeit with a weaker effect than previously reported, in a sample that included children younger than those in the current sample (8 vs. 10 years of age)[123]. Decreasing short-range connectivity and increasing long-range connectivity may be specific to an earlier developmental stage, when greater changes in white matter connectivity are occurring[83]. These results suggest that the adolescent transition to maturity is a period of refinements in connectivity within stable networks and concomitant increases in connectivity across widely distributed circuitry.

2.4.3 Increased Integration of the Cingulo-opercular/Salience Network

While between-network connectivity increased with age, the distribution of links (i.e., integration) among networks remained stable for most networks studied. This suggests that the framework for network integration is available by childhood, with continued increases in the strength of these established between-network links. An exception, however, was the CO/Salience network, which displayed age-related changes in integration with other networks, as assessed by participation coefficient. The CO/Salience network is involved in maintaining a task set, saliency, and configuring sensory information, cognitive state, and motor output[15,124]. The continued enhancement of CO/Salience network integration follows what is known about the development of cognitive control. Core cognitive control abilities are present early in development, but the consistent successful implementation of control continues to improve into

adulthood. This developmental pattern has been found for a wide range of cognitive control tasks, such as the antisaccade, go-no-go, and stroop tasks[13,99]. Our findings of stable network organization, coupled with increased integration, are consistent with these behavioral findings, suggesting that the underlying architecture supporting mature brain functioning is present early in development, with refinements continuing into adolescence.

Developmental differences in integration patterns at the regional scale within the CO/Salience network corroborated the network-level findings. From childhood into early adolescence, specific regions that drove increased integration of the CO/Salience network included the right aIns, bilateral dACC, anterior and mediodorsal nuclei of the thalamus, and putamen. Both the aIns and dACC are extensively anatomically connected to many major brain networks across cortical and subcortical regions[52,125]. Together these regions drive a control network guiding mental activity and behavior through an interaction of cognitive, affective, and homeostatic functions[51,124,126,127]. We observed an increase in the number of links between the CO/Salience network and the SM network from every region that became more integrated within the CO/Salience network, enabling more rapid access from this control system to the motor system to guide goal-directed behavior[127]. Due to its role in detecting salient stimuli and acting as a switch between large-scale networks[86], the aIns may play a particularly important role in normative development, supporting enhanced integration of brain processes. In line with this, there is evidence that abnormal engagement of the aIns and dACC may underlie neurodevelopmental disorders, such as autism[123,127–129].

Many of the regions within the CO/Salience network that significantly increased in integrative properties were subcortical, including the putamen and thalamus. These regions show larger changes than cortical areas with respect to fractional anisotropy in white matter, increasing

30% to 50% from childhood into early adulthood[130] and also show a protracted neurophysiological development[131]. This parallels our findings of increased integration of these subcortical structures with cortical networks. Given that adolescence is a period of enhanced sensation seeking[11,86], the steep increase in the integrated nature of these regions with other brain networks during early adolescence suggests a mechanism by which motivational systems are reconfigured with more cognitive, sensory, and affective systems[132].

2.4.4 Cingulo-opercular/Salience Network Integration Moderates Age-related Improvements in Inhibitory Control

In agreement with an extensive literature[99,113], we found age-related decreases in reaction times of correct inhibitory responses. Our network analyses indicated that increased CO/Salience network integration predicted faster RTs on the antisaccade task, underscoring the importance of the CO/Salience network integrating with other networks, subserving cognitive control. Importantly, we found that CO/Salience network integration moderated decreases in antisaccade latency as a function of age. This moderation was significant in the transition from late childhood to early adolescence, when (at both the network and the regional scale) the CO/Salience network became significantly more integrated with other functional networks. Together, these results indicate that development brings greater integration between the CO/Salience network, supporting sustained cognitive control[15], and regions that underlie action such as the SM network, resulting in the ability to generate quicker execution of correct cognitive control signals[133].

2.4.5 The Role of Resting-state Coupling in Network Integration

Although intrinsic, spontaneous coupling between regions at frequencies <0.1 Hz has been studied for over 20 years, the neural substrate and the meaning of the slow frequency signal remains unclear[134,135], though functional networks observed using fMRI have also been identified using magnetoencephalography[136]. Many ROI-ROI pairs demonstrate high correlations between their time courses despite a lack of monosynaptic connections[137,138]. Though the functional purpose of spontaneous slow frequency BOLD oscillations is not known, a range of possibilities exist. Resting-state functional networks may be groups of regions that often co-activate in task-based settings, reflecting a history of co-activation[15,139,140]. This interpretation is supported by studies finding strong resting-state correlations, despite the lack of a direct anatomical connections. However the existence of strong functional connectivity in the absence of direct anatomical connections allows for other alternatives, including the notion that resting-state networks are constantly sampling a possibility of configurations, constrained by anatomy, to make predictions about optimal network configurations for a given input[135]. Furthermore, over long timescales, such as in this study, resting-state functional brain networks are dependent on anatomical connectivity; however, at shorter timescales, numerous configurations are possible[141]. That said, changes in the framework of integration within the functional connectome during adolescence may reflect differences in the pattern in which information is shared across distributed neural networks. Specifically, from a graph theoretic view, the regions that significantly increased in participation coefficient are areas that integrate across multiple functional networks to a greater extent. Importantly, the role these brain regions play in integrating information may reflect a particular vulnerability for the emergence of

psychopathology, which emerges during adolescence - a time when the brain is reorganizing the way it shares and processes information across these networks.

2.4.6 Limitations

This study was not without limitations. The sample was cross-sectional, undermining our ability to analyze subject-specific growth trajectories. We are also limited by some inherent limitations to fMRI, including residual head motion, though we took multiple processing steps towards mitigating these effects including wavelet despiking, simultaneous bandpass filtering of the time series and nuisance regressors, and scrubbing. Additionally, five minutes of resting-state data is considered a minimum requirement for analyses of resting-state fMRI data, with recent pushes for longer acquisitions[138,142]. That said, relatively short resting state acquisitions in fMRI are susceptible to reliability issues, as it has been shown that the stability of resting state correlations requires upwards of 15+ minutes. However, longer acquisitions may lead to even greater differences between age groups in head motion. Furthermore, our study contained a relatively large sample size, which helps to assuage acquisition length issues. Lastly, because PC was averaged over all nodes within a network, it is possible that some single brain regions could be driving this effect more than others. That said, we still found CO/Salience network increases in integration with age that moderated the relationship between cognitive control performance and age. This finding stresses the importance of network integration for adult-like cognitive control performance, rather than the maturation of any singular brain region. Future studies could aim to elucidate specific brain regions driving cognitive control maturation via integration.

2.4.7 Summary

These results provide evidence that the period of childhood through adulthood is characterized by increased integration of widely distributed, but stable, networks. As such, a critical component underlying the adolescent transition to adult-level execution of control is the refinement and strengthening of integration between existing specialized networks. In particular, the CO/Salience network continues to increase its integration, and thus influence, on other networks, providing a mechanism for developmental improvements in cognitive control. These findings support a novel two-stage model of adolescent brain development in which network organization stabilizes prior to adolescence, while the integration of information across widely distributed circuitry increases in the transition from adolescence to adulthood.

3.0 OSCILLATIONS, NETWORKS, AND THEIR RELATIONSHIP WITH THE DEVELOPMENT OF IMPULSE CONTROL

3.1 BACKGROUND

The transition from adolescence to adulthood is characterized by significant enhancements in brain function, supporting increased cognitive control and normative decreases in impulsivity[69,143]. Developmental task fMRI studies indicate that core regions supporting cognitive control (e.g., anterior cingulate cortex (ACC)) are engaged in adolescence during cognitive tasks, but their blood oxygen-level-dependent (BOLD) signal activation[144,145] and connectivity with other brain regions continues to mature into adulthood[92,146,147]. As such, brain systems supporting cognitive control are present prior to adolescence; however, the successful instantiation of cognitive control continues to improve[13]. As we demonstrated in the previous chapter, developmental resting state fMRI studies analyzing whole brain connectivity patterns parallel this principle, such that the intrinsic organization of functionally connected networks is apparent by childhood[123,147,148], while integration (between-network functional connectivity) continues to refine well into late adolescence and early adulthood, supporting improvements in cognitive control[147]. However, due to the lack of temporal specificity of the BOLD fMRI response, the oscillatory properties and frequency specificity of age-related changes in functional

connectivity remain poorly understood, limiting a mechanistic understanding of neurocognitive development.

Electrophysiological (EEG/MEG) studies have begun to offer insight into development changes in cortical oscillations. The majority of research concerning electrophysiological maturation across development has used electroencephalography (EEG), finding age-related decreases in total power (total amount of activity across broadband frequencies)[149] and absolute power in each frequency band[149–152]. Additional work has shown there is a redistribution of power from lower to higher frequency bands, with frontal regions reaching adult levels of power after more posterior sensorimotor regions[149,150,153]. Similar posterior-to-anterior gradients have been observed using EEG measures of coherence, an index of regional coupling including both phase and amplitude components[154]. Interestingly, the curvilinear decreases in slow-wave power (i.e., 0.5 – 7 Hz) are highly correlated with gray matter volume decreases during adolescence [155]. Although these studies have begun highlighting developmental trajectories of neural oscillations, the poor spatial specificity of EEG has limited our understanding of the interactions between specific brain regions and their role in large-scale functional networks supporting cognitive control development.

We seek to bridge this gap in the literature, linking the age-related changes in brain network oscillations to the development of cognitive control. In a sample of 68 adolescents and young adults (aged 14-31 years), we employed magnetoencephalography (MEG) to explore intrinsic properties related to oscillatory developmental within and between cortical networks. Specifically, within frequency intervals related to inter-areal neural interactions (1-49 Hz)[58,156], we examined functional coupling of well-defined brain networks using the phase locking value (PLV). Unlike correlation or coherence measures, the PLV permits the separation between the

phase and amplitude components between two oscillators, enhancing the ability to speak to the variance in coupling between two brain regions during the resting state[157].

Using this approach, we demonstrate age-related increases in functional decoupling of theta band oscillations during adolescence, which followed a robust posterior-anterior gradient, with the greatest age-related changes in frontal regions, especially along the midline. Using a priori network membership, we show the greatest developmental theta band decoupling occurred in higher-order cognitive networks, relative to sensorimotor networks. Finally, we demonstrate that decoupling of theta band oscillations between orbitofrontal cortex and the anterior temporal lobe mediates self-reported impulsivity, a developmentally sensitive measure of adolescent cognitive control. Together, these findings provide new insights into an oscillatory mechanism underlying developmental improvements in control-related behavior.

3.2 METHODS

3.2.1 Subjects

Of the 81 adolescents and adults we recruited for this study, we include data from 68 subjects, ranging in age from 14-31 years (M = 22.51, SD = 5.55). Thirteen subjects were dropped due to unavailable ECG and/or EOG data. None of the subjects, nor their first degree relatives, currently or previously had a psychiatric or neurological disorder. All participants gave written informed consent, and the University of Pittsburgh Institutional Review Board approved the study. Subjects were compensated monetarily for their participation in the study.

3.2.2 Structural MRI Acquisition

For each subject, we acquired a structural MRI to co-register MEG data for analyses in source space. Data from the 68 remaining subjects were pooled from 2 separate protocols within the lab and thus had slightly different structural MR sequences. Importantly, the slight differences in acquisition would not affect subsequent processing steps. For the first 28 subjects from the first protocol, structural images were acquired using a sagittal magnetization-prepared rapid gradient-echo sequence (repetition time [TR] = 2100 ms, echo time [TE] = 3.43 ms, flip angle = 8°, inversion time [TI] = 1050 ms, voxel size = 1mm isotropic). For the 40 subjects included in the second protocol, structural images were acquired using a sagittal magnetization-prepared rapid gradient-echo sequence (repetition time [TR] = 2200 ms, echo time [TE] = 3.58 ms, flip angle = 9°, inversion time [TI] = 1000 ms, voxel size = 1mm isotropic).

3.2.3 MEG Acquisition

MEG data were acquired using an Elekta Neuromag Vectorview MEG system (Elekta Oy) comprising 306 sensors arranged in triplets of two orthogonal planar gradiometers and one magnetometer, distributed to 102 locations. The MEG scanner was located inside a three-layer magnetically shielded room within the University of Pittsburgh Medical Center. The data were acquired continuously with a sampling rate of 1000 Hz. Head position relative to the MEG sensors was measured continuously throughout the recording period to allow off-line head movement correction. Two bipolar electrode pairs were used to record vertical and horizontal electro-oculogram (EOG) signals to monitor eye movement.

3.2.4 MEG Data Processing

For artifact removal, we first manually visually inspected every channel across the resting-state run for noisy or flat channels and squid jumps. MEG data were then preprocessed off-line using the temporal signal space separation (tSSS) method (10 second correlation window, 0.98 correlation limit), which uses spatial and temporal features to separate signals into components generated within the MEG helmet and components from outside the helmet, which must be artifactual[158,159]. This method greatly increases the signal-to-noise ratio (SNR) of the resulting data[160]. tSSS also performs head movement compensation by aligning sensor level data to a common reference[161]. This head motion correction procedure also provides estimates of head motion relative to sensor coordinates that we subsequently used for head motion estimates for each subject. Lastly, the raw time series data were down-sampled to from 1000Hz to 250 Hz.

An independent component analysis (ICA) approach was used to automatically detect and attenuate heartbeat, eye blink, and eye movement artifacts. ICA was performed on each channel using the Infomax algorithm, with the number of components selected to account for 95% of the variance. The Pearson correlation of the components and the ECG or EOG channel is used to identify artifactual sources through an iterative thresholding method (as implemented in MNE Python) and subsequently manually inspected. After removal of the artifactual sources, the data was reconstructed from the remaining components.

MEG sensor data were then projected from the sensors on to the cortical surface to estimate source activities, using the minimum-norm estimates (MNE) procedure. First, the geometry of each participant's cortical surface was reconstructed from the respective structural MR images using FreeSurfer[162,163]. The solution space for the source estimation was then constrained to the gray/white matter boundary by placing 5,124 dipoles per hemisphere. A

forward solution for the constructed source space was calculated using a single compartment boundary-element model. The noise covariance matrix was calculated from a two-minute empty room scan, in which we acquired data with no subject present. The noise covariance matrix and the forward solution were then combined to create a linear inverse operator to project the resting-state MEG sensor data to the cortical surface. We then warped individual subject data from native space to FreeSurfer average space to facilitate the interpretation of specific regions and networks.

3.2.5 Regions of Interest (ROIs)

We extracted the time series of resting-state MEG data from a recent parcellation of 333 ROIs covering the entire cortical surface[20]. This atlas was chosen because it comprises major cortical functional networks, including control networks, sensorimotor networks, and the default mode network and covers the entire cortical surface. These networks are known to have protracted developmental trajectories in the resting-state fMRI literature[30,147] and are thus candidates for developmental changes at the faster timescales, of which MEG is sensitive.

3.2.6 Measure of Neural Coupling: The Phase-locking Value (PLV)

For each pair-wise relation between ROIs for each subject, a PLV was calculated for each frequency of interest (1-49Hz in 1Hz intervals). Phase-locking is a measure of the propensity for two signals to maintain a constant phase separation with each other (i.e., synchrony). Therefore, the PLV provides a measure of temporal variability between two MEG signals[58]. To calculate the PLV at each frequency, two time series are spectrally decomposed at a given frequency, resulting

in a phase estimate at each time point. A single time-averaged PLV can then be computed by averaging all of the phase-locking values, ranging from 0 to 1, representing a random phase relationship and fixed phase relationship (synchrony), respectively. Here, we binned the data into 100 three second chunks and obtained one PLV across the time windows using multitapers. The PLV was calculated for each ROI pair, resulting in 55,278 PLVs for each frequency and for each subject.

3.2.7 Determining Age-related Changes in Coupling

After ROI x ROI PLV individual subject matrices were calculated at each frequency, individual subject matrices were concatenated forming a 333 x 333 x 49 x 68 4-D matrix. First, we asked if there were developmental changes in PLV across a broadband frequency range (1-49 Hz). To this end, we averaged the 4D matrix along the first 2 dimensions of the upper triangle, resulting in a single PLV value at each frequency for each subject. A linear mixed effects model with maximum likelihood estimation was used to examine main effects and interactions predicting PLV. Age and frequency were entered as fixed effects and random intercepts were estimated for each subject. Significance values for fixed effects were obtained through a likelihood ratio test between models with and without the effects in question (chi-square test). To test individual frequencies for PLV ~ Age effects, we regressed PLV against age within each frequency bin and corrected for multiple comparisons using false discovery rate[164].

3.2.8 Posterior-to-anterior Gradient of Decoupling across Development

Once we determined the frequency range of global decreases in phase locking (5-9 Hz), we sought to determine the specific regions in which phase locking was significantly decreasing. To this end, we ran linear regression models to determine the rate of change in PLV within the 5-9 Hz theta band as a function of age, controlling for potential confounds, including motion, power, and distance (see below). This resulted in a 333 x 333 matrix of beta weights from the age regressor, representing the rate of change in phase-locking for every ROI pair. To obtain a summary statistic for each ROI, we summed down each column of the matrix, resulting in 333 summed beta weights, which we use to characterize the summed rate of change with age for every ROI across the cortical surface. This process was repeated across frequencies of interest (1-49 Hz) by averaging across frequencies in 5 Hz bins (i.e., 1-5 Hz, 6-10 Hz, … , 46-49 Hz).

We were interested in general trends across the cortical surface. To this extent, we calculated the center of mass for every ROI to obtain a center coordinate and to also get a measure of Euclidean distance between each ROI pair. We the regressed the y-coordinate of the ROI onto the summed beta weights for each ROI, controlling for average distance between ROIs and ROI surface area. This process was also repeated across 5 Hz frequencies bins in the range of 1-49 Hz to determine the specificity of the posterior-to-anterior gradient in the theta-band.

3.2.9 Specific ROI Interactions Driving Regional Changes in PLV

Next, we wanted to identify any trends in specific ROI pairs driving regional decreases in phase-locking. First, we sorted ROIs according to the magnitude of the summed beta weights. We then further probed the top 5% of these ROIs (n = 16), which represents the 16 ROIs undergoing the

greatest amount of developmental decrease in phase-locking. Of those 16 ROIs, we further thresholded each ROIs specific interactions with other ROIs to maintain only the top 5% of each ROIs pairwise beta weight (n = 16 pairwise interactions for each of the 16 ROIs), resulting in a total of 256 pairwise beta weights demonstrating the greatest rate of ROI-ROI decrease in phase-locking.

3.2.10 Control for Power

We wanted to ensure any age-related changes we observed in PLV were not due to changes in the total amount of activity (power) in an area within any given frequency band. First, we extracted a power estimate for each ROI. Specifically, we extracted the time series ('mean flip' in MNE Python) of each ROI and calculated power at each frequency in the interval from 1-49 Hz. We then extracted relative power in the 5-9 Hz frequency band within subjects by taking the mean power within this frequency range for each ROI and dividing by broadband total power (1-49 Hz) for each ROI. For each ROI within each subject, this procedure resulted in relative theta band power. We then averaged across subjects to obtain a mean normalized theta band power for each ROI. This value was then plotted against each ROIs y-coordinate to determine the posterior-to-anterior gradient in power across the cortex. Because a significant posterior-to-anterior gradient in power was observed, we included as nuisance regressors the power of each ROI, the interaction between each ROI pair, the log-transformed power of each ROI, and the log-transformed interaction term of each ROI pair into the age models for each ROI pair. Additionally, we regressed power into age to demonstrate there were no significant differences in theta band power across this age range.

3.2.11 Head Movement Correction

During MaxFilter preprocessing, continuous head position estimates are calculated and any large or sudden head movements are recorded. While MaxFilter performs head movement correction by aligning sensor data to a common reference, it does not account for artifacts generated by head movements, and we wanted to ensure any effects were not a result of head motion artifacts. After extracting the estimated movements from the MaxFilter output, we used the translation vector and rotation matrix for the head position relative to the sensor array (obtained from co-registration) to calculate a three-dimensional head movement vector relative to each sensor at each time point. The norm of this movement vector was averaged across sensors to obtain a single measure of head motion. This motion estimate for each subject was included as a nuisance regressor in all regression models involving the analysis of age-related changes in PLV.

3.2.12 Relationship between Impulsivity and Theta-band Phase Locking

Prior to the neuroimaging visit (M = 43.61 days, SD = 43.33 days), a sub-sample of participants (n = 62) completed the UPPS-P Impulsive Behavior Scale[165], either in an online screening (n = 28) or a separate behavioral visit (n = 34). In the current analysis, total impulsivity scores were estimated according to procedures outlined by[165]. We then regressed age onto this total impulsivity score and observed a significant negative linear relationship between total impulsivity and age (see Results).

First, individual subject matrices were submitted to the network-based statistic[166] and a t-test was run between adolescents and adults to extract a cluster of regions with a significant decrease in PLV with age. We then performed the network-based statistic on the relationship

between impulsivity and PLV, controlling for age. A total of three connections met this criterion and were subsequently submitted for a mediation analysis.

To examine whether differences in PLV may account for age-related differences in impulsivity, mediation analysis was performed on PLV values within connections that had significant associations with 1) age and 2) impulsivity (while controlling for age), as defined above. Significance values for indirect effects were obtained using 5,000 draws in a bootstrap procedure[167].

3.3 RESULTS

3.3.1 Developmental Differences in Global Cortical Phase Locking

In order to probe developmental changes in cognitive processes, we used a previously defined functional parcellation established from resting-state functional magnetic resonance imaging (rs-fMRI)[20] to segregate the cortical surface into 333 regions of interest (ROIs) in a sample of 68 individuals aged 14-31 years (see Figure 10 for a workflow overview). For each ROI pair at each frequency (1-49 Hz, 1 Hz intervals), we calculated a phase-locking value (PLV) to determine the degree of coupling between the phases of the oscillations between two ROIs, resulting in 49 ROI x ROI PLV matrices for each subject.

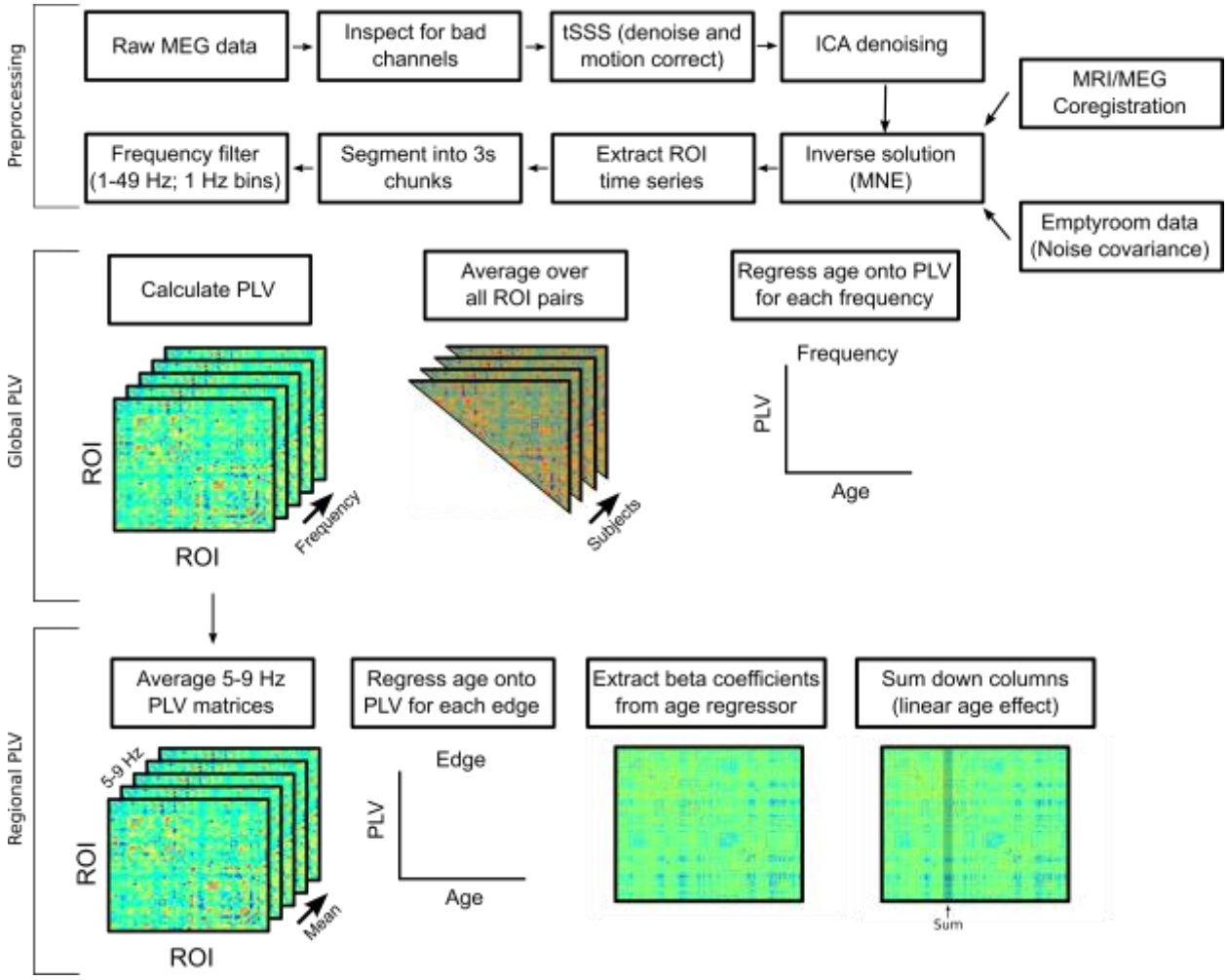

Figure 10. Workflow schematic

First, we averaged the PLV matrices at each frequency across both ROI dimensions for each frequency and subject. This resulted in one global cortical PLV for each frequency, for each subject. There was no significant main effect of age predicting PLV (B= -0.0004, t = -1.255, $\chi 2(1)= 1.576$, $p = .209$). However, there was a significant age by frequency interaction predicting PLV ($\chi 2(48)= 125.56$, $p < 0.001$). A significant negative relationship between global PLV and age at each frequency interval between 5-9 Hz (all $p < 0.05$, FDR corrected) emerged, suggesting

an overall oscillatory activity becomes more decoupled at rest within the theta band (Figure 11). No other frequency intervals showed a significant age-related change in PLV.

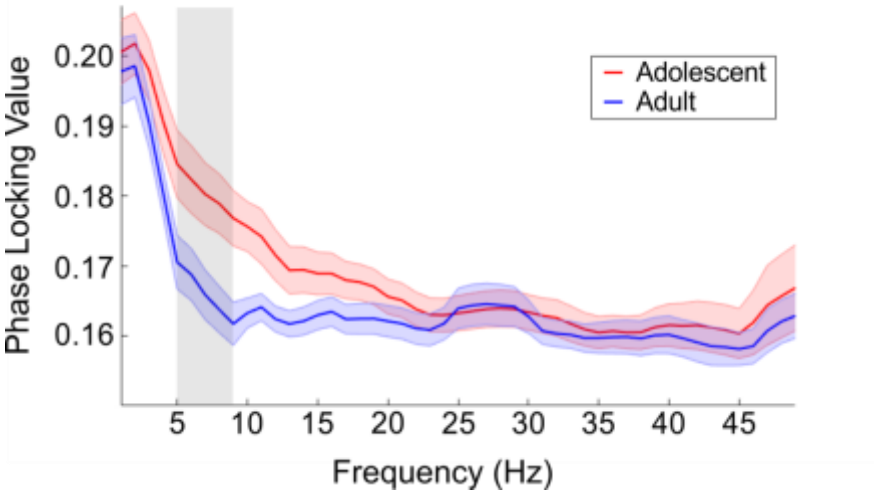

Figure 11. Theta-band phase-locking decreases across development.

Across most frequency bands, adolescents displayed similar resting-state phase-locking to adults. However, in the 5-9 Hz frequency band, there was a significant linear decrease in phase-locking throughout development (gray highlighted region; $p < 0.05$, FDR corrected). Decoupling of oscillations at slow frequencies, which enhances integration of widely distributed circuitry, may play a significant role in brain development throughout adolescence. Data displayed categorically. Error bars represent standard error of the mean.

3.3.2 Regional Changes in PLV

To determine the anatomical locus of PLV decreases with age in the theta band, we averaged each individual subject's PLV matrices in the 5-9 Hz frequency interval. Next, we regressed age onto each ROI pair's PLV, controlling for motion and power (see Methods), and extracted the

beta weight for age from each model. This resulted in a pairwise matrix of beta values, representing the rate of change across development in theta band PLV for each ROI pair.

We examined whether age-related changes in PLV followed a topographic gradient across the cortex, we obtained a summary rate of change for each ROI by summing down the columns of the beta matrix and regressed each ROIs summed beta weight against its x-coordinate (in MNI coordinate space) in each hemisphere and y-coordinate separately, controlling for average distance from each ROI to every other ROI and ROI surface area. In the lateral-to-medial gradient, we observed a significant negative relationship between the summed beta weights and the x-coordinate in the left hemisphere ($t = -6.97$, $p = 8.44*10^{-11}$), but only a trend in the right hemisphere ($t = 2.01$ $p = 0.05$), indicating phase-locking decreased more rapidly with age along the medial wall. We also observed a significant negative relationship between the summed beta weights and the y-coordinate ($t = -13.19$, $p = 3.68*10^{-32}$), indicating a strong posterior-to-anterior gradient of PLV change, such that frontal regions experienced greater decreases in PLV (i.e., more decoupling) with age than posterior regions (Figure 12). Regions undergoing the greatest decrease in PLV (top 5%) over development in rank order listed in Table 2. In sum, the greatest rate of decrease in PLV occurred in frontal regions, especially along the medial wall.

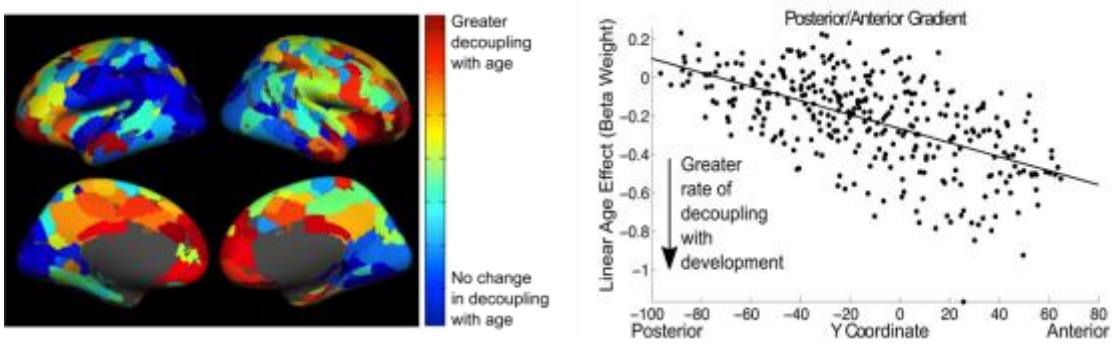

Figure 12. Regional decrease in phase locking in the theta band.

There was a posterior-to-anterior gradient in the decrease in phase-locking throughout adolescence evident across parietal, temporal, and frontal regions, with relatively greater age-related decreases in frontal regions and along the medial wall.

X	Y	Z	Label	Network
-22.87	30.04	-17.67	Middle Frontal Gyrus	Default
35.67	36.83	-11.64	Middle Frontal Gyrus	Default
31.88	14.36	-30.62	Superior Temporal Gyrus	Default
22.60	31.59	-18.07	Middle Frontal Gyrus	Default
3.92	20.38	-21.68	Orbitofrontal Gyrus	Default
2.74	38.45	-18.07	Orbitofrontal Gyrus	Default
-11.93	24.61	-18.61	Medial Frontal Gyrus	Default
37.93	6.63	-39.65	Middle Temporal Gyrus	Default
41.73	49.58	-7.32	Middle Frontal Gyrus	Frontoparietal
45.60	28.86	-7.42	Inferior Frontal Gyrus	Frontoparietal
39.61	47.59	8.39	Middle Frontal Gyrus	Frontoparietal
-7.24	33.40	23.28	Anterior Cingulate Cortex	Salience
30.20	18.99	-16.89	Inferior Frontal Gyrus	Ventral Attention
12.40	25.56	-24.03	Orbitofrontal Gyrus	None
25.06	7.74	-16.41	Subcallosal Gyrus	None
51.90	-10.20	-35.81	Inferior Temporal Gyrus	None

Table 2. Regions displaying the greatest decreases in theta band PLV during adolescence

3.3.3 Greatest Rate of Change in PLV is Specific to the Theta Band and to the Resting state

To explore developmental changes in the posterior-to-anterior gradient of other frequency bands, for each subject, we binned the data in intervals of 5 Hz by averaging PLV matrices accordingly (1-5 Hz, 6-10 Hz, … , 46-49 Hz). Beta weight matrices were generated for each frequency bin (see Methods), summed, and regressed against the ROI's y-coordinate. We then extracted the beta weight from the y-coordinate regressor in each regression model and plotted this as a function of frequency, demonstrating the greatest posterior-to-anterior age effect was at ~6-10 Hz (Figure 13).

To assess the specificity of our findings to the resting-state, rather than a task-state, activity we analyzed data from the maintenance period of a working memory paradigm in a subset of our sample (n = 28; details of task method and results in Appendix A.3 & A.4). After extracting pairwise PLVs for each subject and frequency band within the band of interest (5-9 Hz), we averaged across frequency bands, resulting in one theta-band phase-locking matrix per subject. Paralleling the resting-state analysis, we regressed age on each pairwise PLV across subjects, controlling for subject head motion. We extracted the beta weight from the age regressor, resulting in a beta weight matrix, representing linear effects of age on changes in PLV during working memory maintenance. To test for a posterior-to-anterior effect as was observed during the resting-state, we summed down the columns and regressed the ROI's y-coordinate on this summed linear age effect. We did not observe a posterior-to-anterior gradient during this task state (t = -0.02, p = 0.98). However, we did observe the posterior-to-anterior gradient in this subset of subjects (t = -9.31, $p < 10^{-17}$) during rest. These findings suggest that the strong decreases in theta band phase-locking in frontal regions likely is specific to the resting-state.

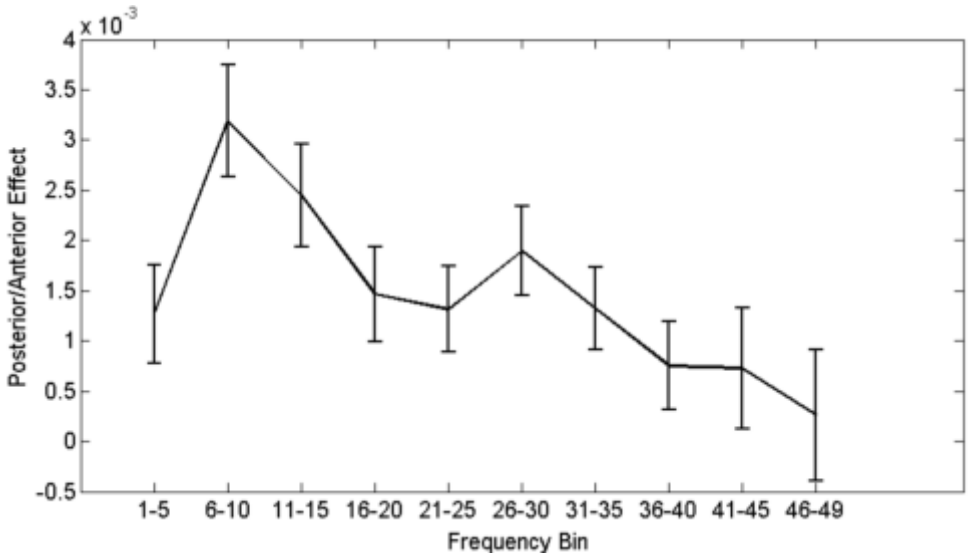

Figure 13. Band specific posterior-to-anterior gradients.

After binning phase-locking matrices into 5 Hz bins, we found the greatest posterior-to-anterior gradient developmental effect was in the theta band. Error bars represent 95% confidence intervals.

3.3.4 Network-level Changes in PLV

In addition to specific regional changes in PLV we aimed to characterize developmental changes in PLV as a function of networks rather than regions [20]. For each network combination (e.g., DMN-DMN, DMN-FP, etc.) we obtained the mean beta weight of the linear effect of age on PLV for all ROIs of the networks being compared. The resulting heat map is shown in Figure 14A. We then performed a one-way analysis of variance (ANOVA) to quantitatively assess whether some networks experienced a greater rate of change in PLV with age compared to others. Here, we submitted averaged beta weights of within-network interactions (e.g., default mode to default mode) to the ANOVA. As determined by the ANOVA test, there was a significant difference in the average beta weight for age effects at the network level ($F_{(12,320)}$ =

9.57, $p = 10^{-16}$). A subsequent post hoc analysis revealed the negative linear age effect was greatest for the salience network compared to any other network, with the exception of the cingulo-parietal network ($p < 0.05$) (Figure 14B).

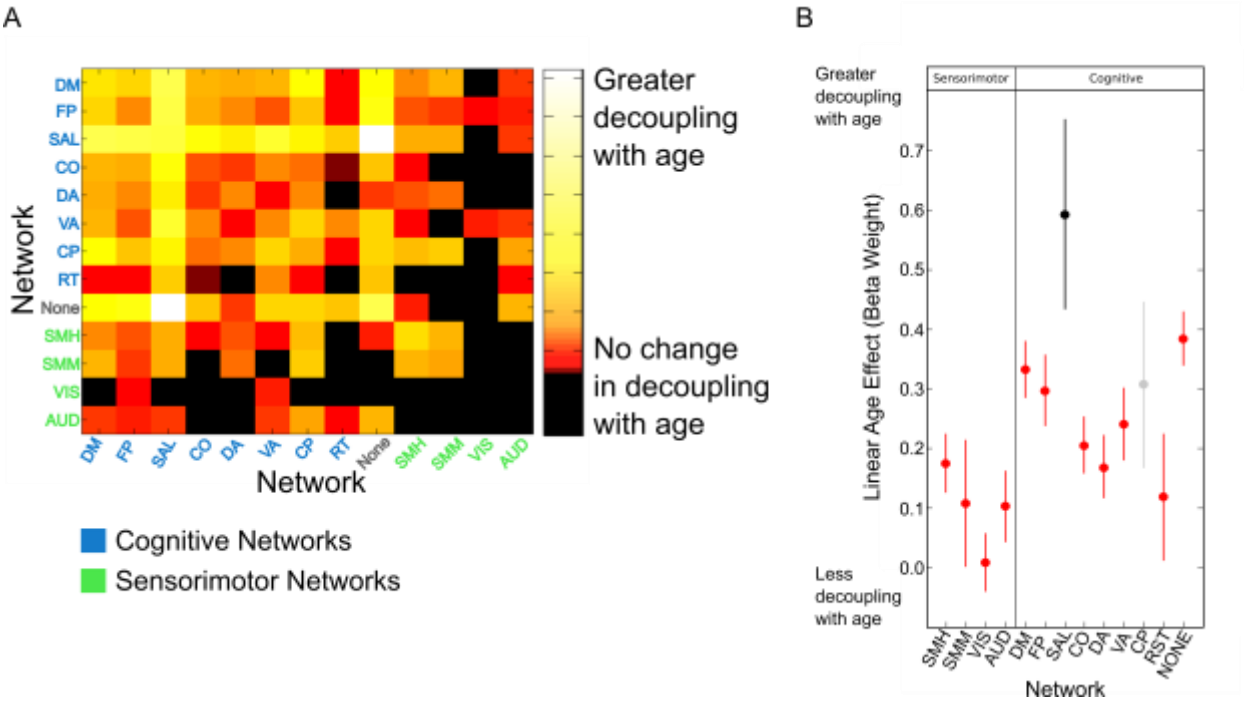

Figure 14. Network changes in phase-locking.

(A) Age-related decreases in phase-locking tended to be within and between cognitive networks (e.g., default mode, frontoparietal, and salience), while within and between-network oscillations involving sensorimotor networks remained relatively stable. (B) Age-related increases in theta-band decoupling were greater in cognitive networks than in sensorimotor networks ($p = 10^{-9}$). Oscillations in the salience network became significantly more decoupled compared to any other cognitive or sensorimotor network, with the exception of the cingulo-parietal network (all $p <$ 0.05, corrected) SMH = somatomotor hand; SMM = somatomotor mouth; VIS = visual; AUD = auditory; DM = default mode; FP = frontoparietal; SAL = salience; CO = cingulo-opercular; DA = dorsal attention; VA = ventral attention; CP = cingulo-parietal; RST = retrosplenial temporal; NONE = none (limbic according to ref[22]).

3.3.5 Pairwise Decreases in Phase Locking

After determining the gradient and locus of decreased phase coupling from adolescence to adulthood, we analyzed specific ROI pairs driving this decrease. Specifically, we aimed to determine the specific pairwise interactions that contributed to the greatest rate of theta band decoupling. We first identified the top 5% of ROIs that showed the greatest rate of theta band decoupling (developmental hubs) from the regional analysis. From those ROIs, we extracted the top 5% of negative beta weights and plotted the connections, with ROIs grouped by networks (Figure 15), as assigned by[20]. All ROIs from the regional analysis were within higher-order cognitive networks, with eight belonging to the default mode network, three belonging to the fronto-parietal network, one belonging to the salience network, one belonging to the ventral attention network, and three belonging to an undefined network, though all regions were within anterior portions of the frontal lobe and are considered part of the limbic network in other parcellations (e.g., ref [22]). With the exception of two links, all links from these developmental hubs were to regions of other cognitive networks, indicating that pairwise decreases in theta band coupling are largely specific to cognitive networks.

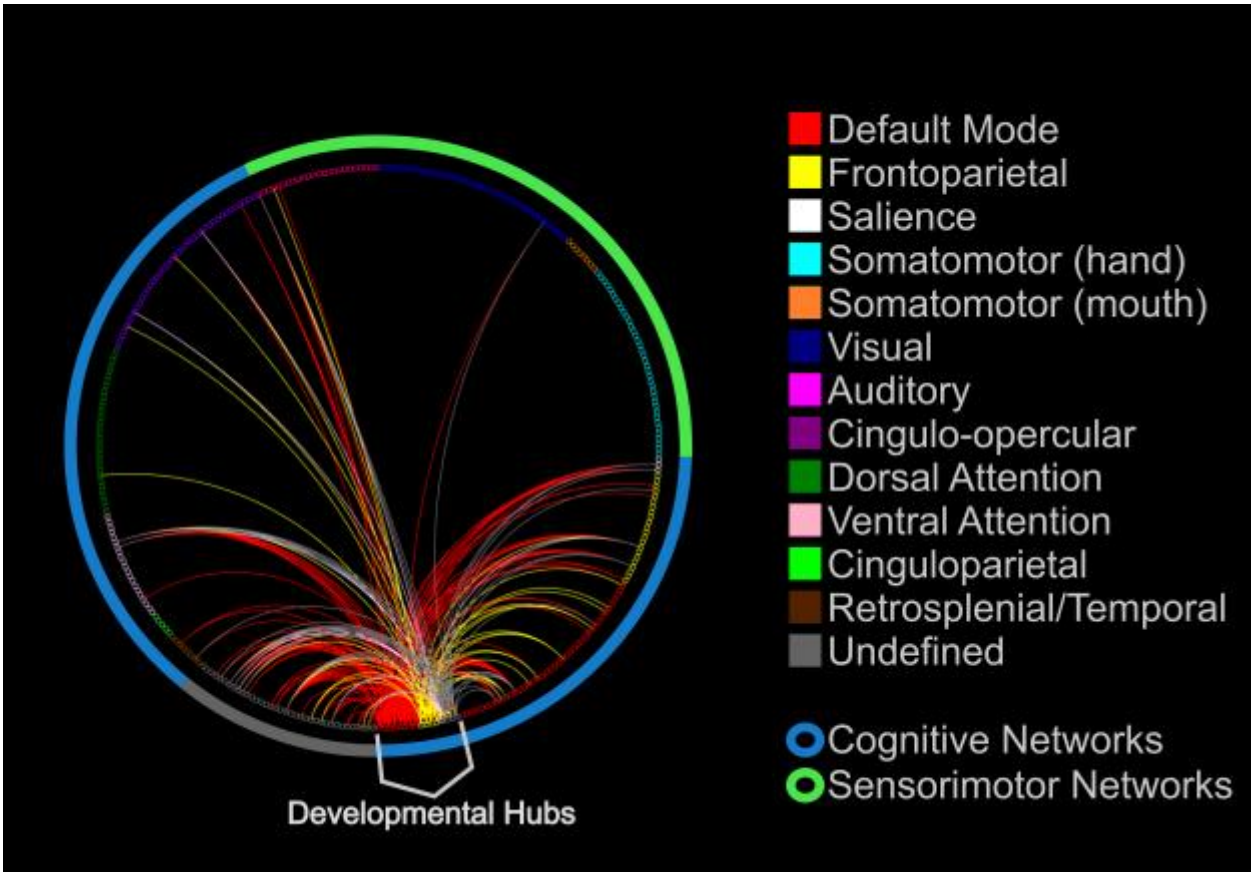

Figure 15. Pairwise increase in resting-state decoupling.

Pairwise increases in decoupling between the top 5% of brain regions that showed age-related increases in decoupling (developmental hubs) and their respective top 5% pairwise interactions. Regions (little circles) are colored by the network to which they are affiliated. Link color represents the network affiliation to which the developmental hub belonged. The most significant pairwise increases occurred between regions of the default mode, frontoparietal, and salience networks to other cognitive networks.

3.3.6 PLV Mediation of Age and Impulsivity

We have demonstrated a strong decrease in theta band phase locking, most strongly in frontal midline regions. Given the role of anterior prefrontal cortex and anterior temporal lobes in impulse control[168] and the role of theta oscillations in cognitive control[169], we sought to determine whether decreases in frontal theta PLV mediated the relationship between impulsivity and age. Mediation analysis was performed on PLV values within connections that had significant associations with 1) age (path A) and 2) impulsivity (while controlling for age; path B). Impulsivity, as measured by the UPPS-P, was negatively associated with age (β = -.333 , t = -2.74, p = . 008), such that the oldest subjects reported the lowest levels of impulsivity (path C). To obtain a cluster of regions that significantly decreased in PLV as a function of age (path A), we submitted the individual subject matrices to the network-based statistic. A cluster composed of 49 regions with 122 links survived the permutation test (1000 samples). Similarly, we performed a median split on impulsivity to break the sample into a high impulsivity group and a low impulsivity group. Individual subject PLV matrices were once again submitted to the network-based statistic, controlling for age to determine whether PLV predicted impulsivity (path B). A cluster composed of 13 regions with 14 links survived the permutation test (1000 samples). Of the 14 links, three link were also significant in path A (i.e., PLV ~ Age). These three links comprising five distinct regions were submitted to three separate mediation analyses. The fist link (L_1) was between the left superior frontal gyrus (MNI coordinates: -15.05, 64.73, 13.29) and the right inferior frontal gyrus (MNI coordinates: 25.07, 7.38, -16.41); the second link (L_2) was between the left temporal gyrus (MNI coordinates: -50.60, 9.26, -18.71) and right medial frontal gyrus (MNI coordinates: 12.40, 25.55, -16.38); and the third link (L_3) was between

the left middle temporal gyrus (MNI coordinates: -44.87, 7.38, -34.85) and the right medial frontal gyrus (MNI coordinates: 12.40, 25.55, -16.38).

Mediation analyses conducted on each ROI pair separately revealed that partialing out the variance each of the three ROI pairs significantly attenuated the relationship between age and impulsivity (indirect pathway [path a*b], L_1: β = -0.133 , 95% CI, -0.244, -0.017, p = .03; L_2: β = -0.154 , 95% CI, -0.322, -0.023, p = .02; L_3: β = -0.130, 95% CI, -0.251, -0.036, p = .003). For statistics on individual paths, see Figure 16B. These findings suggest the observed relationship between age and impulsivity is, in part, accounted for by the decoupling of theta oscillations during the resting-state between prefrontal cortex and the anterior temporal lobe.

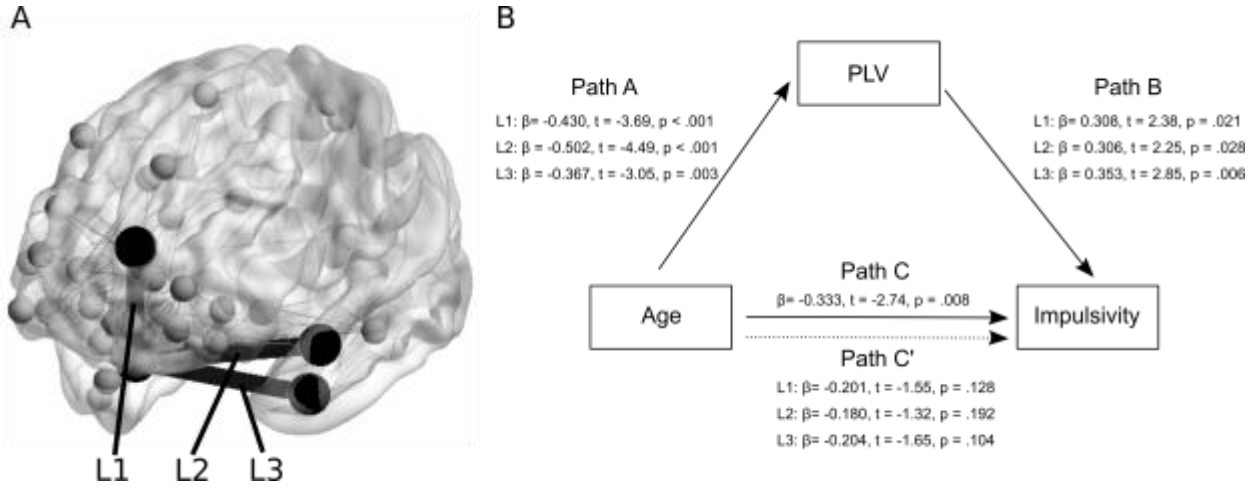

Figure 16. Orbitofrontal/anterior temporal theta-band phase-locking mediates the relationship between age and impulsivity.

(A) Anatomical location of mediation effect. Black nodes and link represent interactions mediating the relationship between age and impulsivity. Gray nodes and links represent a cluster of regions and their interactions for which a significant relationship between age and PLV existed. (B) Mediation model including statistics for specific paths. Note PLV of these three interactions fully mediated the relationship between age and impulsivity (difference in p-values between path C and paths in C'.

3.4 INTERIM DISCUSSION

Interactions between functional brain networks demonstrate a protracted development well into adolescence and early adulthood[92,147,148]. Likewise, electrophysiological studies have reported neural oscillations continue to mature throughout adolescence (for a review, see[170]). We sought to bridge these two avenues of research to characterize the developmental trajectory of resting-

state network oscillations at fast timescales utilizing the excellent temporal resolution of MEG. Furthermore, we aimed to anchor developmental changes in resting-state oscillations to maturation of control abilities that occur during adolescence. We found an increase in theta-band decoupling that was stronger in frontal and midline regions, especially in higher-order cognitive networks. In parallel, many of the strongest pairwise increase in resting-state theta decoupling occurred between regions affiliated with the default mode, fronto-parietal, and salience networks. Furthermore, theta-band coupling between anterior frontal and temporal lobe regions mediated the relationship between age and impulsivity, providing an oscillatory mechanism for decreased impulsivity throughout development.

Similar to early electrophysiological work using EEG to study coherence between cortical lobes[171], we found a protracted development of frontal lobe interactions. In particular, the salience network, comprised of the anterior cingulate and anterior insula. Both of these regions are anatomical and functional hubs of the cortex[52,172], with anatomical connections to several major brain systems. It has been proposed that midline frontal theta may act to entrain disparate neural systems when cognitive control is needed[169]. Here, we extend this idea in the resting-state, such that an increase in frontal theta decoupling may be an intrinsic marker for an increased ability for these regions to variably interact with disparate brain systems, enhancing the brain's flexibility of cognitive systems throughout development during the resting-state.

A network of regions in orbitofrontal and anterior temporal lobes also displayed a high rate of theta-band decoupling with development. Furthermore, interactions between this network and the salience network had the greatest rate of theta-band decoupling of any within- or between-network comparison (Figure 14a). Regions belonging to this network are often prescribed a role in impulse control and when lesioned, lead to greater impulsivity[173,174]. Here,

we showed evidence that several interactions between orbitofrontal and anterior temporal regions mediated the relationship between age and impulsivity. Theta-band oscillations may be the mechanism by which these regions communicate to execute impulse control, given the role of theta oscillations in control abilities[169]. Lending support to this theory, theta-band activity tends to flow from frontal regions to more posterior regions[175]. Though we cannot speak to the direction of information flow here, given the drastic increases in cognitive control abilities from adolescence to adulthood and role of frontal theta in this domain, further research should probe directly the relationship between frontal theta and increases in cognitive performance throughout development.

Developmental decreases in phase-locking may be conceptualized as increases in noise. An increase in noise during the idle resting-state may be beneficial to the brain in the form of stochastic resonance and/or neural flexibility[176]. If the brain were to maintain one rigid configuration of interactions during rest, the flexibility required to create complex thought or initiate a rapid response to exogenously driven input would be hampered. Indeed, a prominent theory on the nature of resting-state is the sampling of multiple network configurations along an anatomical backbone[135,141]. If this is the case, brain networks require flexibility in the form of imperfectly coupled oscillators to maintain dynamics in networks. Evidence is accumulating more rapidly supporting the notion that the brain engages in multiple states (i.e., nonrandom and significantly differing network configurations)[177,178], even as fast as once every 100-200 ms[179]. Additionally, several studies have found evidence for increased cortical variability throughout development[45,176,180]. Our findings here support these fMRI-based findings in that decreased phase-locking may represent an overall increase in variability[58,181,182], though decoupling of oscillators may also be due to an overall increase in signal complexity.

Developmental changes in phase-locking should be largely unaffected by power within the same frequency band (but see ref [183]). To assuage any concerns regarding potential artifactual effects of power, we first demonstrated that power in the 5-9 Hz frequency band did not change with age. Additionally, to control for relative theta power in our regression models of PLV and age, we included the power of each ROI and the interaction between each ROI pair as nuisance regressors.

Our results provide electrophysiological evidence that decreases in theta-band coupling between higher-order networks underlies the transition from adolescence to adulthood. Furthermore, we provide a mechanism that contributes to decreases in impulsivity throughout adolescence. In the next chapter, we will probe frontal theta rhythms as a mechanism by which cognitive control, specifically cognitive flexibility, refines to adult levels.

4.0 DEVELOPMENT OF COGNITIVE FLEXIBILITY

4.1 BACKGROUND

Thus far, resting-state analyses have demonstrated a critical role for the anterior cingulate and insular cortices – core nodes of the cingulo-opercular/salience control network – in the developmental enhancements in control processes, including inhibitory control and impulsivity. In this chapter, we aim to directly test the function of these regions and broader control networks during cognitive flexibility, which is known to have a protracted development[184]. Cognitive flexibility refers to the ability of an organism to effectively switch between multiple goal states quickly and accurately. As such, cognitive flexibility is a core function of cognitive control[185]. Humans have the unique ability to rapidly and flexibly alternate between tasks requiring the instantiation of very different rule sets[10], often signaled by a single cue externally driven cue, referred to here as exogenously-driven task switching. This form of cognitive flexibility hinges on a readiness to redirect attention away from old rule sets and orient attention to novel events.

Cognitive flexibility as measured using task switching paradigms is driven by a core of 'flexible hubs' (i.e., DLPFC and IPL) that comprise the canonical fronto-parietal network[10,186,187]. In addition to fronto-parietal regions, the ACC plays a central role in task switching. An extensive body of ERP, EEG, and MEG literature has consistently found a robust P3-like component in fronto-parietal regions in response to cue-based task switching[188,189],

indicating an increase in activity several hundred millisecond after a subject has been cued to switch rule sets. Both task switching and novelty detection have been shown to elicit the P3 response in humans[190], likely due to the fact they both present a realization for the need to instantiate control[133,169] requiring conflict to be resolved[191] (i.e., an instance of cognitive flexibility). In all these tasks, a common spectral signature resides in the theta band (4-8 Hz) oscillations within the ACC and has been shown to be phase locked to the onset of the cue stimulus[192]. However, whether the ACC is functioning to solely resolve conflict and/or is playing a role in task switching reaction time directly remains debated[193–195].

The purpose of this section is to better understand temporal and frequency components underlying successful implementation of task switching processes as well as their developmental trajectories through adolescence. For the following reasons, we hypothesize age-related decreases in theta power during preparation to successfully switch between tasks. First, cognitive flexibility improves with development, indicating that when young subjects generate a correct response it would require greater effort, and thus greater need for cognitive control. Given theta band power scales with conflict resolution[169], we expected adolescents would require greater theta band power to generate a correct response to conflict. Second, our MEG resting state results indicated age related decreases in ACC coupling reflecting a possible enhancement in the ability for control processing regions to flexibly adapt to changing demands. Lastly, the cingulum is one of the last major white matter tracts to fully mature[83]. Within increased myelination into adulthood, we reasoned this greater structural integration may afford the ACC the ability to instantiate a weaker signal to produce the same correct response with age. Additionally, given recent models of the interplay between ACC and regulatory regions within

the fronto-parietal network[169,196,197], we predicted beta/gamma oscillatory power in the DLPFC would scale linearly with trial-to-trial fluctuations in RT on switch trials.

4.2 METHODS

4.2.1 Subjects

Sixty-five subjects participated in our MEG study. Of those, eight subjects had poor EOG/ECG recordings, not allowing us to remove heartbeat and/or eye blink artifacts. An additional three subjects had > 2 cm head displacement and were thus discarded. Four subjects did not return for an MRI and thus did not have a structural MRI to which we could co-register the MEG data. Three subjects did not have > 15 switch trials and were thus not included in the final analysis. This left us with a total of 47 subjects for further analyses. Based on a questionnaire, none of the subjects, nor their first degree relatives, currently or previously had a psychiatric or neurological disorder. All participants gave written informed consent, and the University of Pittsburgh Institutional Review Board approved the study. Subjects were compensated monetarily for their participation in the study.

4.2.2 Task Design

In the Multi-Source Interference Task (MSIT; See Figure 17), subjects place their index, middle, and ring fingers on the buttons that correspond respectively to the numbers 1, 2, and 3. Trials begin with a colored crosshair cue (see paragraph below) presented for 500 ms, followed by a

horizontal display of three numbers (e.g., 1 0 0). Subjects are instructed to push the button of the finger corresponding to the *unmatched* number (1-index; 2-middle, 3-ring finger; correct answer = index finger above) as quickly and accurately as possible. Subjects fixate a gray crosshair until the beginning of the next trial (200 – 1300 ms). Trials last 2000 ms.

The color of the crosshair cue at trial onset determines the trial type of which there are three: *congruent* (green crosshair), which is used elicit a motor response with a minimal 'cognitive' response; *incongruent* (red crosshair), in which finger-to-number incongruence elicits inhibitory processes; and *working memory* (blue crosshair). Congruent trials present unmatched stimuli corresponding to the congruent finger mapping (e.g., 1 0 0). Incongruent trials present an *unmatched* number in a different location from the finger stimulus pair and flanked by two other non-zero numbers (e.g., 2 2 1). Because the unmatched number is located in a position incongruent with respect to the finger corresponding to it, finger-to-number incongruence is induced.

The task is grouped into two main blocks – a pure block (PB), where subjects are presented the trial type with its corresponding crosshair color (e.g., all congruent trials cued by a green colored crosshair) and a mix block (MB), where cue colors change in a pseudorandom fashion. Each pure block consists of 35 trials, while each switch block consists of 60 trials with an average of 11 switch trials. Each block is separated by 60 seconds. Block order is randomized to control for any possible learning effects across blocks. For the remainder of this chapter, our analyses will focus on *incongruent* trials only. Our rationale for this was twofold: (1) effects of task switching (i.e., switch cost: switch trial performance – MB non-switch trial performance) were only present in switching to *incongruent* trials (see section 4.3.1), reflecting the notion that resources are only allocated for switching into a state eliciting to need for more control (i.e., one

requiring response inhibition); (2) We wanted to isolate processes related to switching into this state, rather than an easier task state (i.e., switching into congruent trials). Switching into a congruent or working memory trial from and incongruent trial set offloads resources related to response inhibition, making the switch to these trials a relatively easier process by which more automatic number-to-finger mapping ensues.

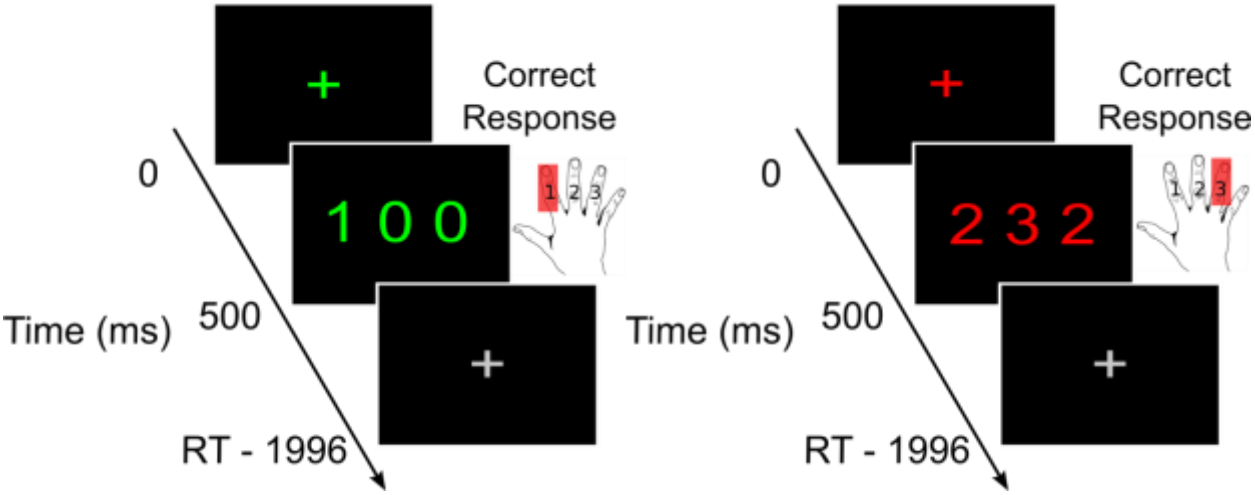

Figure 17. MEG switch task design

4.2.3 Structural MR Acquisition

For each subject, we acquired a structural MRI to co-register MEG data for analyses in source space. Structural images were acquired using a sagittal magnetization-prepared rapid gradient-echo sequence (repetition time [TR] = 2200 ms, echo time [TE] = 3.58 ms, flip angle = 9°, inversion time [TI] = 1000 ms, voxel size = 1mm isotropic).

4.2.4 MEG Acquisition

MEG data were acquired using an Elekta Neuromag Vectorview MEG system (Elekta Oy) comprising 306 sensors arranged in triplets of two orthogonal planar gradiometers and one magnetometer, distributed to 102 locations. The MEG scanner was located inside a three-layer magnetically shielded room within the University of Pittsburgh Medical Center. The data were acquired continuously with a sampling rate of 1000 Hz. Head position relative to the MEG sensors was measured continuously throughout the recording period to allow off-line head movement correction. Two bipolar electrode pairs were used to record vertical and horizontal electro-oculogram (EOG) signals to monitor eye movement.

4.2.5 MEG Data Processing

For artifact removal, we first manually visually inspected every channel across all nine runs for noisy or flat channels and squid jumps. MEG data were then preprocessed off-line using the temporal signal space separation (tSSS) method as detailed in section 3.2.4. Lastly, the raw time series data were down-sampled to from 1000Hz to 250 Hz and concatenate across runs for artifact identification and removal. Subjects who had total head displacement > 2 cm were excluded from further analyses (n=3).

Next we imported the structural MR data into Brainstorm[198], defining 15,000 vertices (dipoles), representing the cortical envelope. We first defined the nasion point and left and right preauricular points. We then implemented an affine transformation to the MNI coordinate system. Using the three fiducial points, we co-registered the MEG data in sensor space with

individual subject anatomy. We further refined this registration iteratively using digitized head points obtained during MEG data acquisition.

Next, the raw MEG time series were imported into Brainstorm. First, we imported a list of bad channels for each subject, removing these channels from inclusion in further analysis. We then removed 60Hz line noise using a notch filter. Using the EOG and ECG channels, we identified heart beat and eye blink events automatically, with subsequent manual inspection to ensure events were properly identified. These events were used in the removal of artefactual components using the signal-space projection (SSP) approach as implemented in Brainstorm. Once these artifacts were removed, we manually inspected the data once more for any additional noisy segments of data to ensure any segments not corrected by the above automated methods were removed from further analyses.

4.2.6 MEG Deconvolution

To isolate neural responses related to task switching from the motor components of the task (i.e., the button press), we developed a deconvolution approach similar to those used in BOLD fMRI activation studies. From each subject's concatenated data file, we estimated the time course of activity at the sensor level using a finite impulse response regression (FIR) model. FIR design matrices were constructed manually and applied to the sensor time series using in-house Matlab code. Sensors and events labeled as 'bad' (in addition to 1000ms around these noisy segments) were excluded from the model. Additionally, we only considered correct trials. We were interested in modeling the trial onset (0ms) up to one sample before the subsequent trial (1996ms, total of 499 samples), while removing activity related to the button push. Button pushes were modeled over a duration consisting of -1000ms to 3600ms (1151 samples) around

the button push event. These parameters were chosen manually after iteratively inspecting the data for a relaxation to baseline of motor-related activity. We modeled a total of 9 unique trial events (3 trial types: congruent, incongruent, working memory; each consisting of switch trials, non-switch trials within a mix block, and pure block trials) in addition to the button push. Signal drift was modeled as an 8th order Legendre polynomial time series. After deconvolution, data were baselined using the mean of 12 samples after cue onset (48ms), given this interval of time is well below the amount of time a neural response be elicited in primary visual cortex. As an important aside, our task design did not include jitter between trials, as this deconvolution step was not anticipated during task design. Due to natural jitter in reaction times, we were able to isolate the motor response using a window longer than a trial duration (2000ms); however, we could only model a given trial as far as the duration of the trial due to a lack of jitter between subsequent trial onsets. That said, deconvolution allows us to conclude with certainty that the effects we observe in both the time and frequency domain are locked to the trial onset, rather than having mixed contributions from different trial events or any other ongoing background oscillations.

4.2.7 Head Model, Inverse Model, and Warping

At this step, we did not constrain the orientation of our dipoles, resulting in 3 vectors of data (x,y,z) for each dipole, totaling 45,000 dipoles (3 orthogonal orientations * 15,000 vertices). We used overlapping spheres as magnetic fields are far less sensitive to heterogeneity of tissue in the brain, skull and scalp than are the scalp potentials measured in EEG. This locally-fitted spheres approach achieves reasonable accuracy relative to more complex BEM-based methods[199,200]. A data covariance matrix was calculated over all trials and combined with the individual subject

head model to a create a linearly constrained minimum variance (LCMV) beamformer[201], projecting MEG sensor-level time courses to the cortical surface. Our choice in a LCMV beamformer over MNE was made after comparing inverse models from averaged deconvolved button presses in primary motor cortex and noting more focal activation using LCMV beamformer. Because we were interested in comparing task switching effects between subjects, we warped individual vertex time series to MNI space by taking the norm of the x,y, and z direction dipoles within each vertex and subtracting off a baseline period of 50ms, starting at cue onset.

4.2.8 Regions of Interest

Subjects included in the MEG analysis completed the task in an fMRI scanner on a separate day. To avoid any issues of circularity when discerning task effects in the MEG data, we defined regions of interest using fMRI. Individual subject BOLD data were preprocessed and deconvolved to separate switch from non-switch trials. We then built a contrast of switch – non-switch trials and subsequently averaged across all subjects to obtain an average map for which activity was significantly greater for switch trials than non-switch trials (cluster extent > 50 voxels). Using this approach, we found a total of 11 ROIs that displayed greater activity during switch trials, relative to non-switch trials, including bilateral dorsolateral prefrontal cortex (DLPFC), bilaterial inferior parietal lobe (IPL), bilateral superior parietal lobe (SPL), bilateral anterior insula (aIns), anterior cingulate cortex (ACC), posterior cingulate cortex (PCC), and middle cingulate cortex (MCC). These MNI coordinates were subsequently used as centers of

mass for MEG ROIs (Table 3). For the MEG data, these center coordinate were then grown to include ~100 vertices per ROI.

ROI Label	X	Y	Z
Right IPL	42	-48	51
Left IPL	-41	-38	48
Left DLPFC	-47	16	29
PCC	0	-42	24
MidCingulate	0	-23	45
Right aIns	38	20	4
Left aIns	-35	19	4
Left SPL	-35	-61	50
Right SPL	38	-62	51
Right DLPFC	47	15	30
ACC	0	25	20

Table 3. ROI MNI coordinates

4.2.9 Average Time Courses

Our first objective was to obtain an average of activity within each ROI related to task switching. First, we calculated the average time course of activity across all subjects for switch and non-switch trials, separately. This resulted in an average time course of activity for each vertex across the cortical surface for switch and non-switch trials. We then extracted the time series of activity for each ROI as defined above while aligning the sign of the current fluctuations across the

vertices. Next, we contrasted switch vs. non-switch trials by subtracting single-subject averaged non-switch trials from averaged switch trials for each ROI and subsequently averaging these differences across subjects. This procedure resulted in difference time courses for each ROI. To test for significant difference between task conditions at each time point, we created a sampling distribution by permuting the condition labels (switch, non-switch) and computing a one-sample t-test at each time point (H_A: switch > non-switch) for each ROI separately. This resulted in a t-statistic at each time point for every ROI.

4.2.10 Frequency Components of Task Switching

We obtained an estimate of power at each frequency in the interval from 1-50 Hz for each ROI. To this end, we executed a fast Fourier transform (FFT) using the full trial length (cue onset at 0ms – 1996ms post cue onset) data from the individual subject switch and non-switch trials separately. We then subtracted the resulting power spectrum densities of non-switch trials from switch trials and removed the mean offset, given switch trials in general were found to have greater power across all frequencies. We then performed a one-tailed one-sample student's t-test to test each positive deviation from zero in the difference of switch vs. non-switch conditions.

4.2.11 Time/Frequency decomposition

After observing significant effects within specific frequency bands (i.e., theta and alpha, 4-14 Hz) across many ROIs, we next wanted to determine the approximate time interval in which the power in these frequency bands significantly increased. To decompose the data its frequency components across time, we convolved ROI time-domain data with a series of complex Morlet

wavelets in a frequency interval of 3-50 Hz, using a 3-cycle wavelet. Wavelets have high frequency resolution at lower frequencies, but the temporal resolution is poor. However, the poor temporal resolution is not a limitation here, given the deconvolution step outlined above in **section 4.2.6**. We can be confident that any fluctuations in activity in the time domain are well localized in time (4ms) and are locked to the trial onset. Similarly, any oscillations we observe would also be locked to the trial onset. Altogether, at the relative low frequencies that we are interested in, with relative good precision, we can determine the frequency and timing of switch effects.

4.2.12 Brain regions predicting trial-to-trial differences in reaction time

Next, we aimed to determine brain regions that demonstrated a significant trial-level relationship with RT. Moreover, we wanted to isolate brain regions that exhibited this relationship in switch trials significantly more than non-switch trials. To this end, we categorized RTs into a fast and slow group via median split and re-deconvolved MEG sensor level data, resulting in patterns of brain activity corresponding to fast and slow reaction times. This procedure was executed for both switch and non-switch trials and projected into source space at the individual subject level and warped to MNI space. We then subtracted source level beamformer estimates of slow RT trials from fast RT trials, resulting in a contrast map of activity. This was done for both switch and non-switch trials separately, resulting in a contrast for both switch and non-switch trials. Because we were interested in brain regions exhibiting a significantly relationship with RT in switch trials extending beyond regions generally related to RT (regions exhibiting a significant relationship with RT in non-switch trials), we subtracted the non-switch contrast at every time step from the switch contrast and tested for significant differences at each time step using a one-

sample paired t-test. We considered a brain/RT relationship significant only if an ROI difference time course was significantly positively related to RT for two contiguous time samples (H_A: $difference_{tn\&tn+1} > 0$).

After observing that several regions significantly predicted trial-to-trial fluctuations in RT in switch trails vs. non-switch trials at specific time intervals, we wanted to determine the frequency component(s) underlying these differences. As was done earlier, the data was decomposed into its frequency components with a series of complex Morlet wavelets in a frequency interval of 3-50 Hz, using a 3-cycle wavelet. We did this in individual subject space on source level data. Here, we were building contrasts of contrast; thus, rather than calculating power across time, we calculated amplitude across time to retain the sign of the signal prior to contrasting. As was done in the time domain, the resulting time-frequency matrices for trials with slower RTs were subtracted from trials with faster RTs for switch and non-switch trials separately. This resulted in averaged contrast RT matrices for switch and non-switch trials. We then computed the differences between switch and non-switch trials and tested the differences for significance against 0 using a one-tailed one-sample student's t-test.

4.2.13 Relationship between power, age, and average reaction time

Next, we sought to determine the developmental trajectory of oscillations underlying task switching. For each frequency in the interval from 3-50 Hz (1 Hz bins), we regressed age onto average power for each brain regions for switch and non-switch conditions separately. From there, we were interested in probing brain/behavior relationships within the frequency bands demonstrating a significant relationship with age. To that end, the relationship between power and average RT was determined by regressing subject's average regional power onto their

average RTs, controlling for age. In the first step of this analysis, we binned and averaged oscillations into their canonical frequency bands (theta: 3-7 Hz; low alpha 8-10 Hz; high alpha: 11-14 Hz; low beta: 15-22 Hz; high beta: 23-30 Hz; gamma: 30-50 Hz). If we observed both a relationship between frequency and age and between frequency and RT controlling for age, we ran a linear mixed effects model, testing the interaction of oscillatory power and age on average RTs.

4.3 RESULTS

4.3.1 Behavior

In general, subjects performed worse on *incongruent* switch trials compared to *incongruent* non-switch trails. Specifically, accuracy (% correct) on switch trials (M = 84.74, SD = 15.73) was significantly worse (t = -2.14, p = 0.03) than non-switch trials (M = 90.30, SD = 10.67). Additionally, reaction times (ms) on switch trials (M = 828, SD = 112) was significantly longer (t = 2.33, p = 0.02) than non-switch trials (M = 777, SD = 90). Developmentally, there was a negative trend level relationship between accuracy and age on switch trials (r = 0.28, p = 0.07); however, we did not find evidence for a relationship between age and average response time on switch trials (r = 0.04, p = 0.75). No differences in accuracy (t = -0.57, p = 0.57) or reaction times (t = 1.33, p = 0.18) were observed in the comparison of congruent switch vs. non-switch trials. There were also no differences in accuracy (t = 0.93, p = 0.35) or reaction times (t = -0.21, p = 0.83) for *working memory* switch vs. non-switch trials. For reasons listed in section 4.2.2, as well as these behavioral findings, the remainder of this chapter will focus on *incongruent* trials.

4.3.2 Regional effects of task switching

First, we wanted to ensure regions that showed significantly more activation for switch compared to non-switch trials from the mix block (correct trials only) in the fMRI data also demonstrated significantly more activation in the MEG data. Because we were interested in switch effects, we contrasted the total activity for each ROI in an interval spanning 100-800 ms post cue presentation (trial onset). This window was chosen to isolate the effects that would be due solely to task switching. In conjunction with the fMRI data, all ROIs in the MEG data demonstrated significantly more activity in switch vs. non-switch trials (all $t > 3.42$, $p < 0.05$, FDR corrected; Figure 18A, 18B). Generally, most ROIs displayed significantly greater activity in switch vs. non-switch, with the greatest differences occurring in an interval from 100-800 ms. To probe these effects further, we ran a permutation test to compare switch vs. non-switch activity at every time step within this same time interval (Figure 18C).

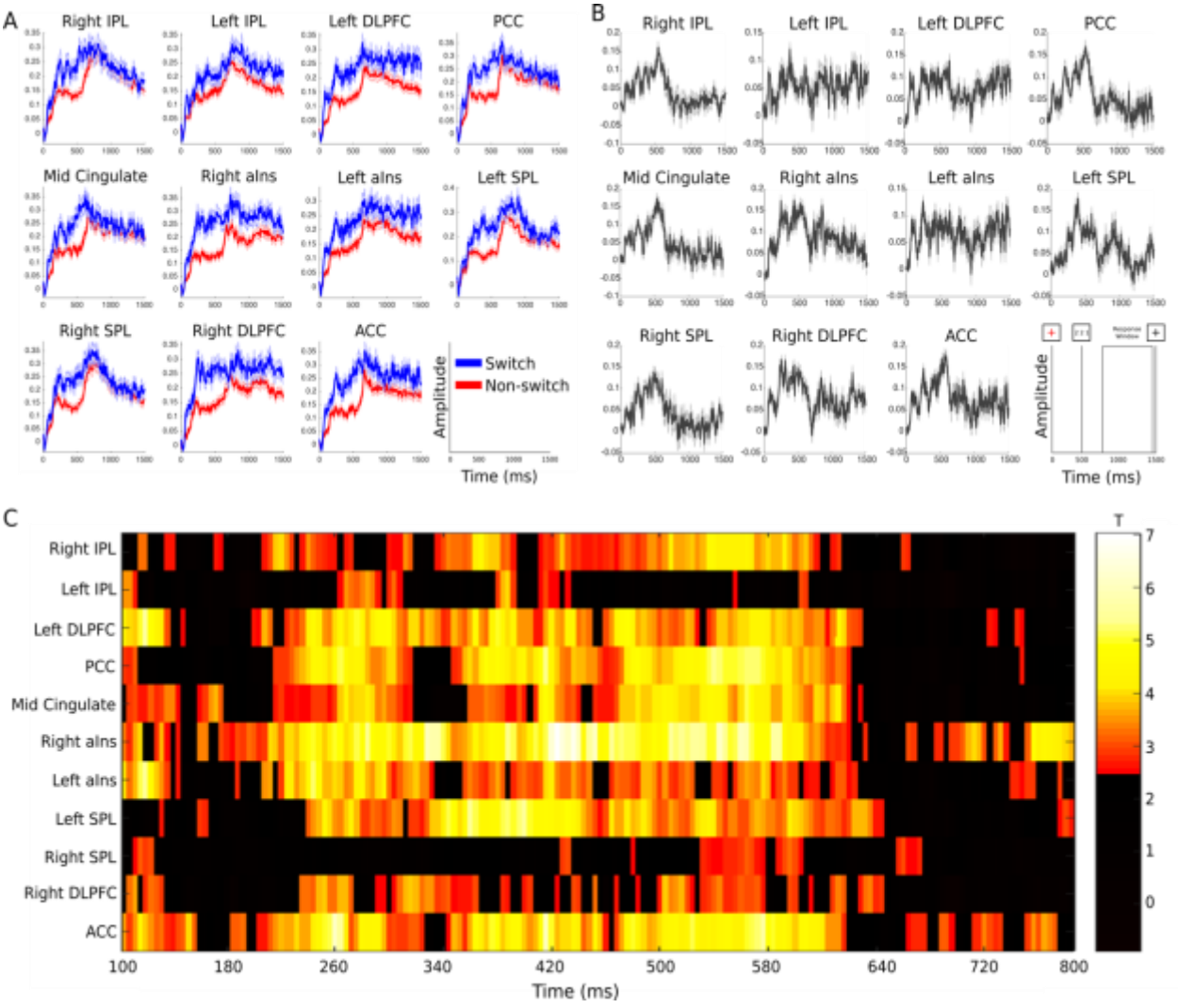

Figure 18. Spatiotemporal effects of task switching.

(A) Average time courses of switch and non-switch trials separately. (B) Average difference time courses between switch and non-switch trials. Schematic of trial events are depicted in the bottom right panel. (C) Resulting t-statistics of one-tailed permutation paired t-test and each time step.

4.3.3 Frequency Components

We found a significant condition (switch vs. non-switch) by frequency interaction for each ROI (all $p < 0.05$, FDR corrected; Figure 19A). To determine the loci of the interaction, we computed the difference in the power spectrum densities for each ROI and further subtracted to mean difference between the two to observe effects beyond the general increase in power in switch trials (Figure 19B). In general, there is commonly increased activity in theta – beta bands during tasks requiring cognitive control. We subtracted the main difference off to isolate effects of task switching over and above this general increase in slower wave power. Significance was determined as a t-statistic greater than 2.75, corresponding to $p < 0.05$, FDR corrected across ROIs. In general, there were increases in theta band power in switch trials compared to non-switch trials in bilateral DLPFC, bilateral insula, and along the cingulate, including separate regions in the anterior, mid, and posterior cingulate cortices. Additionally, there were increases in alpha band power in more posterior regions, such as bilateral IPL and SPL and the PCC. The bilateral DLPFC and MCC also showed significantly greater increases in alpha band power in the switch vs. non-switch condition.

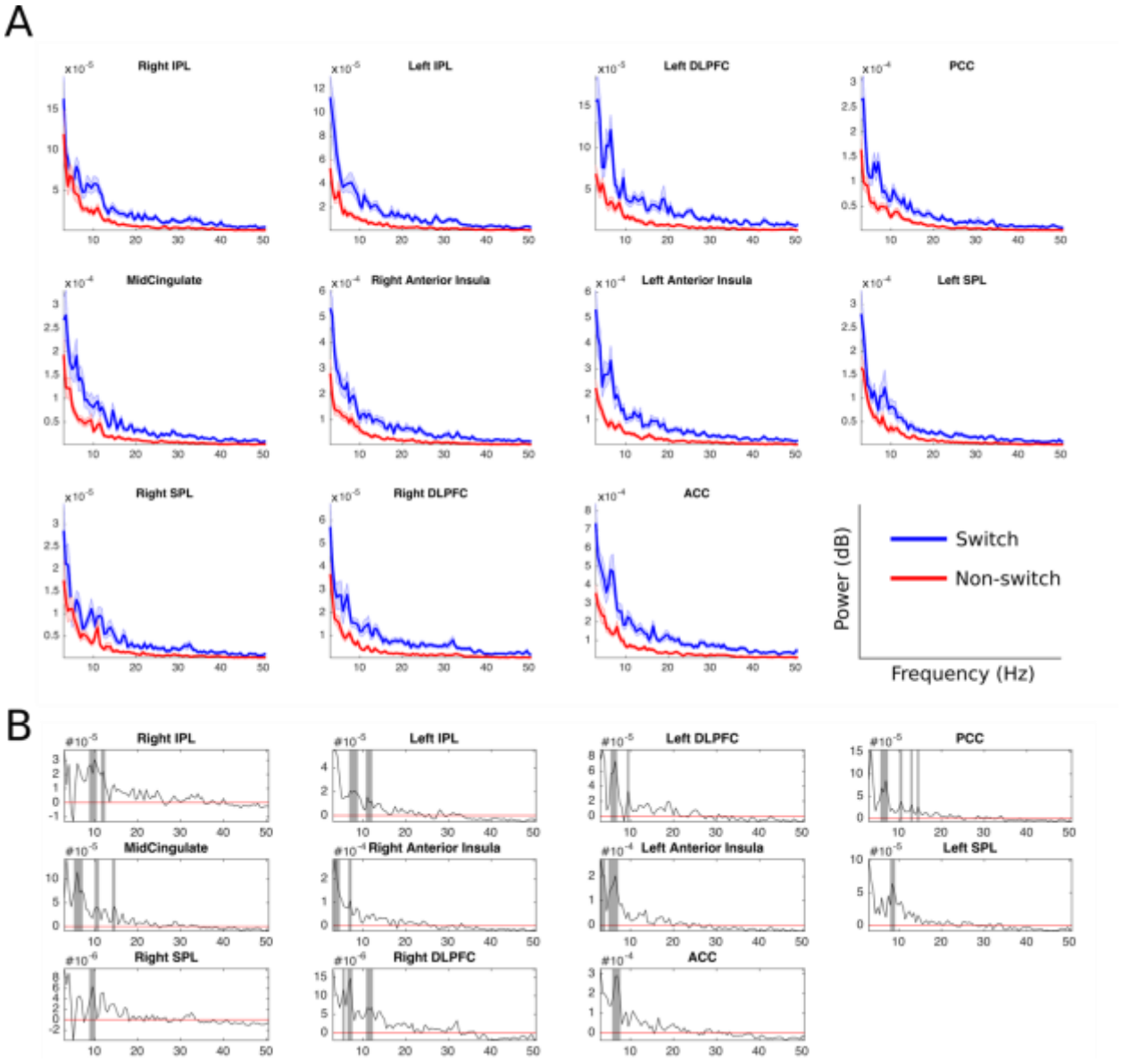

Figure 19. Frequency components of task switching.

(A) Average power spectra for switch and non-switch trials. Note overall greater activity across all frequency bands (B) Difference in power across frequencies in switch vs. non-switch conditions. Red line denotes equal amounts in power in both conditions. Deviations above zero and within gray shaded bars indicate significantly greater power in at a given frequency for switch compared to non-switch ($p < 0.05$, corrected).

4.3.4 Temporal specificity of increases in power during task switching

Next, we aimed to determine the locus of time in which these increases in power occurred during task switching. For each subject, we decomposed the time series of activity of switch and non-switch trials separately into their frequency components across the duration of the trial. We then contrasted the average of switch vs. non-switch conditions and subtracted the mean difference of the two conditions. The first observable increases in theta power across several ROIs, including the ACC, began shortly after the cue presentation (within 200 ms) signaling the need to switch (Figure 20). The bilateral DLPFC, ACC, and left IPL all showed two dissociable peaks in theta band activity during task switching, occurring shortly after cue presentation (~200 ms) and again after the mean of the button pushes (~1400 ms). Furthermore, because our deconvolution procedure accounts for any trial-to-trial differences in the time courses of activity that would arise trivially from temporal shifts of motor preparation and execution signals, the observed differences here correspond to those changes in MEG signal amplitude that are associated with task switching processes.

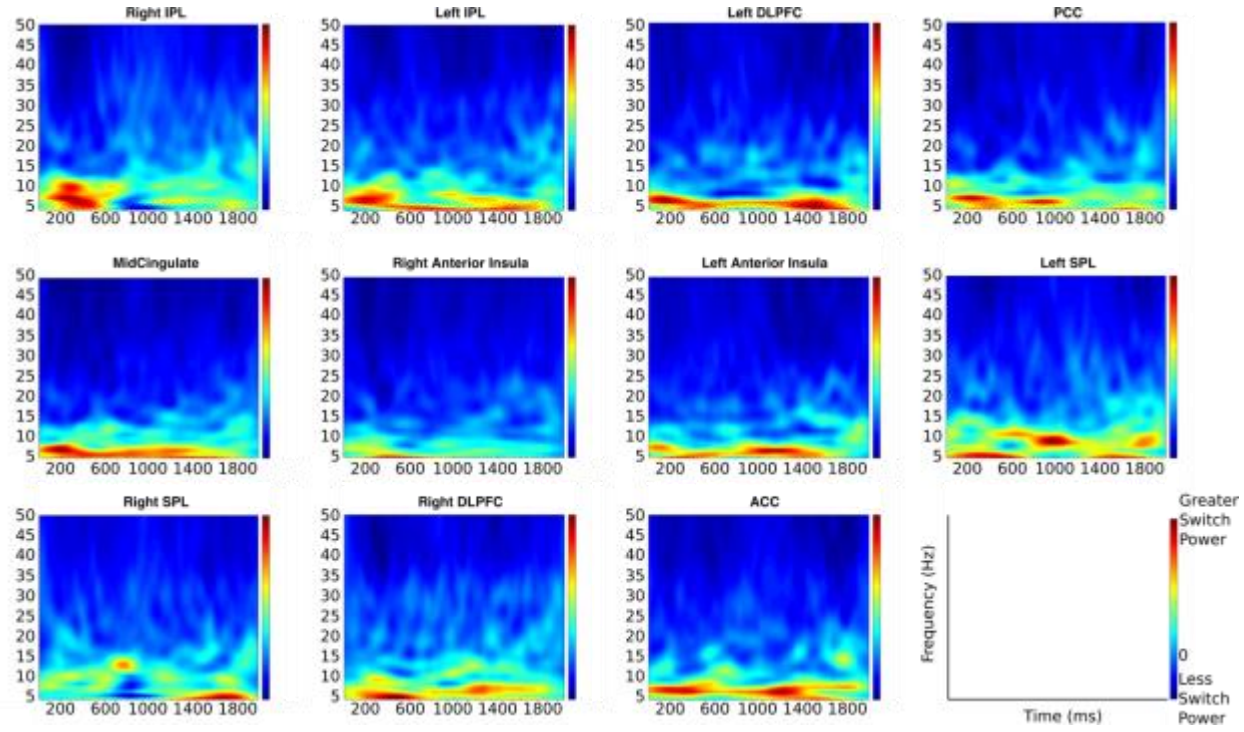

Figure 20. Time/Frequency decomposition of switch vs. non-switch contrast.

4.3.5 Regional contributions to trial-to-trial fluctuations in reaction time during task switching

In the context of task switching, trial-to-trial behavioral variability can be conceived of as resulting from two distinct classes of neural variability. The first class of behavior-relevant neural variability is that which affects the processes supporting the performance requirements of a particular rule set. For instance, in the *congruent* task condition, variability in behavioral performance could be produced by trial-to-trial fluctuations in the activity of neurons within brain areas that support perceptual or decision making processes; for *incongruent* trials, neural variability affecting response inhibition processes may additionally affect behavioral performance. Importantly, this kind of neural variability can, in principle, influence behavioral

variability regardless of whether a trial occurs within a switching or non-switching context. The second class of neural variability is that which impacts neural processes related to either the act of switching into a particular rule set or maintaining an appropriate state of readiness in anticipation of switching rule states. This kind of neural variability will influence behavioral performance either during trials that that constitute a switch event –e.g. an *incongruent* trial immediately following any trials that occur within the context of a switch block. The goal for the next series of analyses is to isolate the neural sources of behavioral variability that are specific to task switching processes and to determine when they occur within the time course of task-related neural events.

To dissociate the contributions to trial-to-trial differences in RT from task switching-related neural variability and neural variability specifically related to the demands of response inhibition, we separately estimated time courses of activity for the trials with the fastest and slowest RTs (defined by median split) within *incongruent-switch* and *incongruent-non-switch* trials. Contrasting fast and slow RT time courses within each condition reveals the regions and times at which trial-to-trial fluctuations in neural activity are associated with variations in behavioral performance. To determine the regions whose contributions to RT variability were specifically related to task switching processes, we calculated the difference between fast vs. slow RT contrasts, subtracting the switch contrast from the non-switch. We found that nine out of the eleven ROIs demonstrated a significantly greater relationship with RT in the switch trials compared to non-switch trials at various points in time in an interval from 50ms – 500ms post switch cue (Figure 21). Of these nine regions, the right IPL was the first region to predict faster RTs at 64-72 ms post switch ($p < 0.05$). To understand the frequency components(s) contributing to these effects, we decomposed the data into its frequency components over time, following the

same contrast logic as the time domain analysis (Figure 22). In the right IPL, alpha/low beta band and gamma band activity (~10-20 Hz and ~40 Hz) was correlated with faster RTs on switch trials to a significantly greater extent than non-switch trials. A similar pattern of significance was observed in low beta band oscillations (~14-22 Hz) in the bilateral aIns and bilateral SPL. Additionally, gamma band oscillations (~40-50 Hz) in the left DLPFC and bilateral insula correlated with faster RTs on switch trials to a significantly greater extent than non-switch trials. Thus regions of the fronto-parietal network predicted trial-to-trial fluctuations in reaction times when task switching; however, the ACC did not, providing support for the notion that the ACC functions primarily as a conflict signal in the context of task switching.

We will be conducting follow up analyses in which we will enter trial by trial RTs into the deconvolution matrix to truly relate trial-to-trial fluctuations in activity to trial-to-trial RTs, rather than doing a median split.

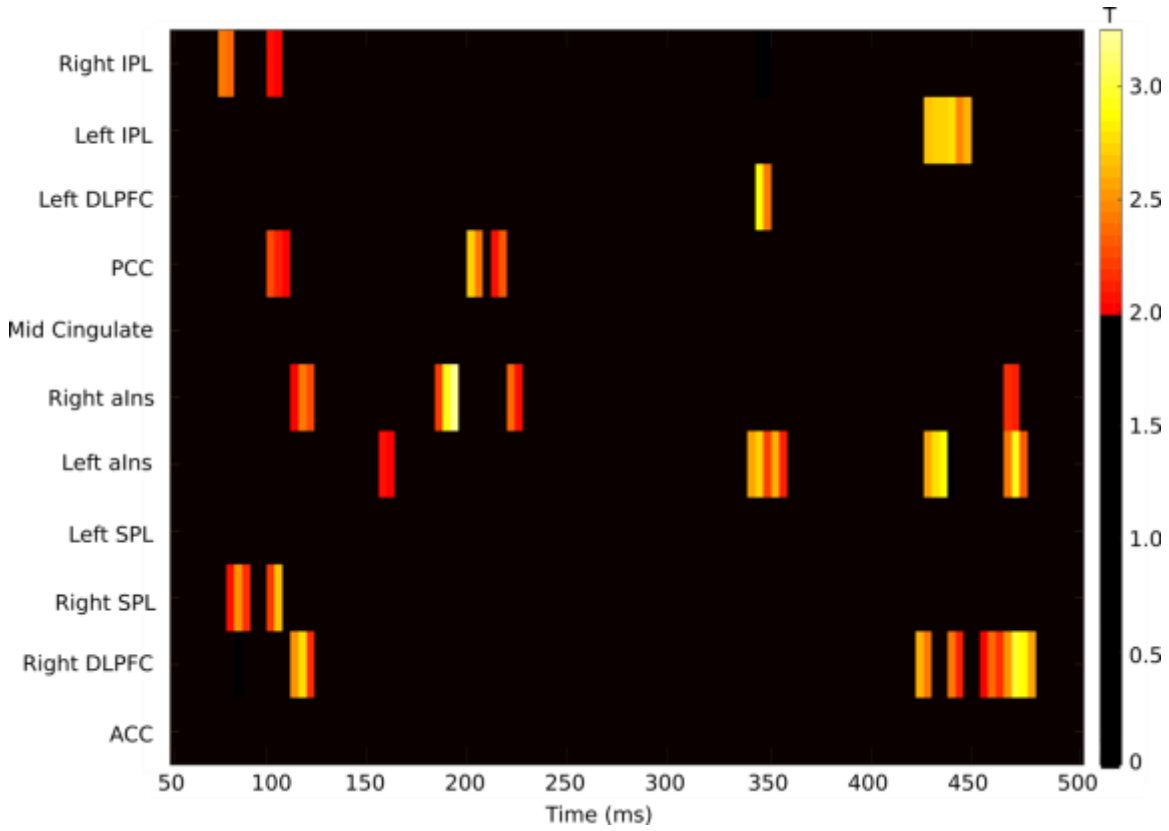

Figure 21. Regions displaying significantly more ability to predict RT in the switch vs. non-switch condition in the time-domain.

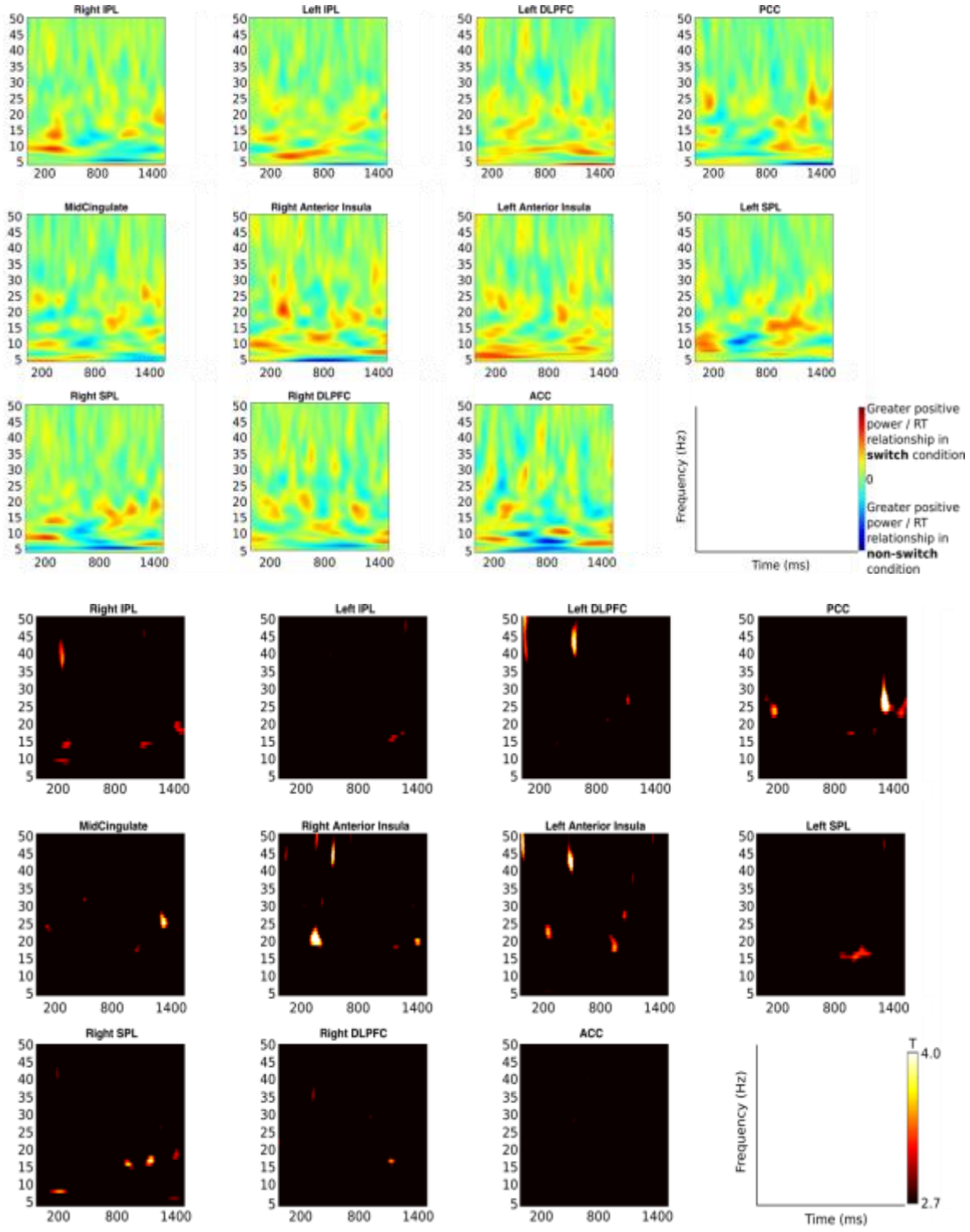

Figure 22. Regions displaying significantly more ability to predict RT in the switch vs. non-switch condition in the frequency domain as a function of time.

The top panel represents power as a function of frequency and time for each ROI. The bottom panel shows areas of the time/frequency shows the frequencies and time intervals in which there was a more significant relationship between power and RT. Note the lack of a relationship in the ACC.

4.3.6 Relationship between average power and average RT during task switching

Next, we asked whether power in any frequency band within each ROI predicted average RT. First, we regressed the difference in theta band power (switch – non-switch) against subject's switch cost (average RT on switch – non-switch trials), controlling for age. We found a positive linear relationship between the difference in ACC theta power and switch cost (t = 2.52, p = 0.01), indicating greater ACC activity in switch vs. non-switch trials results in a slowing of average RT. To further probe the locus of this effect, we regressed ACC theta band power on RT for switch and non-switch trials separately, controlling for age in both models. ACC theta band power demonstrated a significant positive relationship with RT in the switch condition (t = 2.96, p = 0.005) but not in the non-switch condition (t = 0.10, p = 0.91).

Alpha band oscillations (8-10 Hz) in left IPL, bilateral DLPFC, and right aIns followed a similar trajectory. Here, we found a positive linear relationship between the difference in alpha power and switch cost in the left IPL (t = 2.73, p = 0.009), left DLPFC (t = 2.58, p = 0.01), right DLPFC (t = 2.48, p = 0.02), and right aIns (t = 2.29, p = 0.03) indicating greater alpha band activity in the regions in switch vs. non-switch trials results in a slowing of RT, on average. For each of these ROIs, we then regressed alpha band power on RT for switch and non-switch trials separately, controlling for age in both models. Alpha band power demonstrated a significant

positive relationship with RT in the switch condition for the left IPL (t = -2.05, p = 0.04); left DLPFC (t = 2.12, p = 0.04), and right aIns (t = 2.29, p = 0.03) but not in the non-switch condition (all p > 0.05). The dissociation of effects by condition for these regions within these frequency bands indicates the behavioral relevance of these neural effects is specific to task switching rather than purely motor preparation or other computations not related to task switching.

4.3.7 Relationship between power and age during task switching

Given the increase in power observed in switch vs. non-switch trials and the predominance of theta band activity across several regions involved in task switching, we next wanted to determine which frequencies demonstrated a significant relationship with age. All reported intervals that exhibited a significant relationship with age were FDR corrected at p < 0.05. We observed a significant developmental decreases in power during switch trials within the theta band for the ACC (4-7 Hz; Figure 23A), MCC (6-8 Hz; Fig Figure 23B), right DLPFC (5-6Hz; Figure 23C), left DLPFC (5 Hz; Figure 23D), left IPL (7-8 Hz; Figure 23E), and left aIns (6-10 Hz; Figure 23F). Additional age-related decreases in power were observed within the gamma band in the left DLPFC (43-44 Hz) and the left IPL (37-38 Hz). For non-switch trials, the only developmental effect we observed was in the left aIns. Here, there was a significant increase in power across development in the interval from 12-13 Hz.

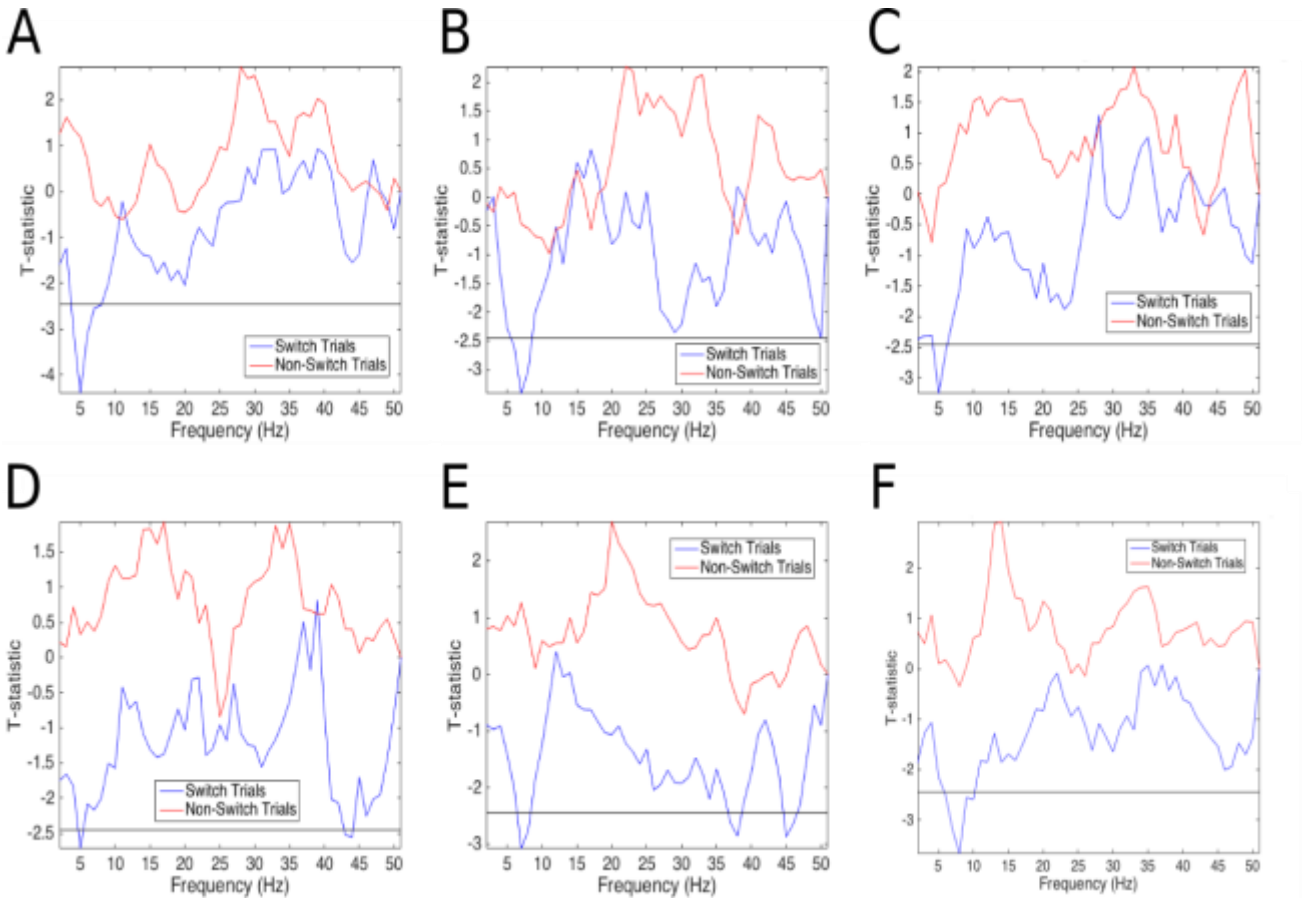

Figure 23. Changes in power across development in switch vs. non-switch trials.

Each plot demonstrates the T-statistic of the age regressor on power as a function of frequency. Blue traces represent switch trials, whereas red traces represent non-switch trials. Black horizontal line denotes significance threshold after correction for multiple comparisons. A = Anterior cingulate cortex; B = Mid cingulate cortex; C = Right dorsolateral prefrontal cortex; D = Left dorsolateral prefrontal cortex; E = Left inferior parietal lobe; F = Left anterior insula.

4.3.8 Interaction between power and age on RT during task switching

Because we observed both a relationship between theta/alpha power and RT during task switching across several regions, in addition to power and age, we ran a linear mixed effects

model, testing the interaction of normalized (switch minus non-switch) power and age on average normalized RTs (i.e., switch – non-switch RTs) for each region/frequency band pair separately. There was a weak interaction between ACC theta band power and age ($F_{(1,46)}$ = 4.25, t = -2.06, p = 0.05; Figure 24), such that greater ACC theta band power results in a slightly greater switch cost during adolescence than in adulthood (t = 1.97, p = .048, though ACC switch power still scales linearly with average RT in adults (t = 2.21, p = 0.03). There was also a significant interaction between right aIns alpha band power and age (F(1,46) = 4.94, t = -2.22 , p = 0.03; Figure 25). Similar to ACC theta band power, adolescents exhibiting high right aIns power incurred a significantly greater average switch cost than those exhibiting low right aIns alpha power (t = 2.14, p = 0.044); however, in contrast to ACC theta power, there was no relationship between right aIns power and switch cost in adults (t = -0.36, p = 0.71). No other region demonstrated a power/age interaction (all p > 0.05). In sum, adolescents demonstrated increased slow wave (theta/alpha) power when incurring a greater switch cost to a greater extent that adults within core regions of the brain's cingulo-opercular/salience network.

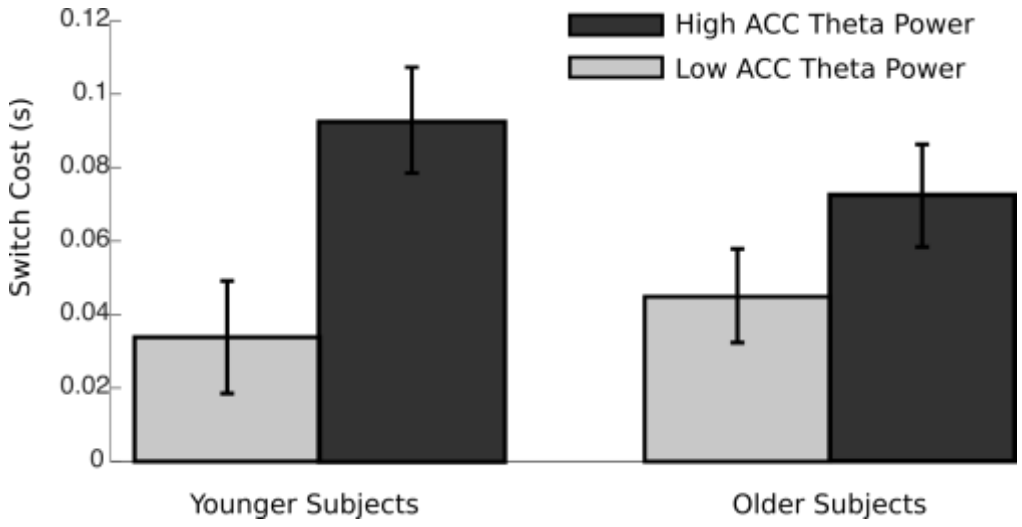

Figure 24. Interaction between ACC theta band power and age predicting average RT switch cost.

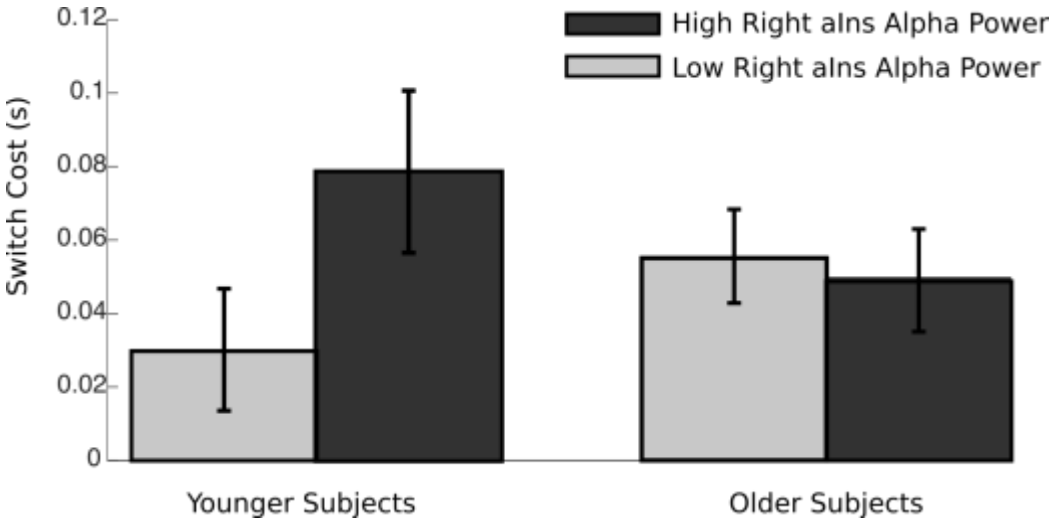

Figure 25. Interaction between right aIns alpha band power and age predicting average RT switch cost.

4.4 INTERIM DISCUSSION

We sought to characterize the spatiotemporal profile of task switching and its protracted development in adolescence and early adulthood. Our results provide evidence that: (1) task switching is characterized by a network of brain regions that comprise core regions of cognitive control networks, including the ACC, bilateral insula, bilateral DLPFC, and bilateral parietal association cortices; (2) theta band ACC scales linearly and positively with average reaction time but not trial-to-trial reaction time, indicating theta band oscillations in the ACC underlie conflict signaling arising from an exogenous cue switch signal; (3) a network of brain regions oscillating in the beta/gamma band, including the bilateral insula, IPL, DLPFC demonstrate greater activity preceding more rapid motor response during task switching at the single trial level (4) slower frequency power, specifically in the theta and alpha band (4-14 Hz) within the DLPFC, IPL and midline regions decrease into adulthood; (5) the relationship between ACC theta power and average RT is stronger during adolescence than in adulthood, suggesting adolescence require greater recruitment of ACC neurons to resolve conflict when switching between tasks[133,191,202]. These findings suggest that foundational aspects of oscillatory activity underlying task switching are present by adolescence. However, before adulthood it is more effortful to task switch requiring greater instantiation of cognitive control reflected in greater theta power through adolescence compared to adulthood. See gen discussion

4.4.1 Differential contributions of the ACC, DLPFC, and IPL in task switching

In this study, we found increases in the ACC in both switch and non-switch trials, with significantly greater activity in switch trials compared to non-switch trials in a window of time

from ~100-800 ms post switch cue presentation. This indicates that the ACC plays a key role in task switching specifically. The relationship between average ACC theta power and average RT, but the lack thereof at the single trial level, indicates that the ACC is not playing a role in the modulation of the motor response during task switching per se, but rather it is likely related to the average conflict/effort baseline and foundation of temporal coordination for subsequent adaptation[169,203]. As a follow-up to this, we subtracted average RTs from the pure block trials from average non-switch RTs from the mixed blocks (Appendix A.5, Figure 28). We then correlated this value with the average switch cost across subjects and did not observe a significant relationship. Given this finding, coupled with the early increase in ACC theta power, it is unlikely that the ACC is playing a direct regulatory/adaptive role in task switching. Rather, it appears the ACC is more likely functioning as to resolve conflict associated with task switching within a broader network of regions more directly related to the regulation of control (i.e., DLPFC and IPL), rather than being involved in the regulatory processes itself as proposed by other groups[204,205]. These data are consistent with recent theories of ACC functioning within the domain of cognitive control[133].

There is mounting evidence that the DLPFC is a critical region for the adaptation of behavior following conflict. The IPL was the first region temporally to contribute significantly to faster RTs on switch trials, over and above its contribution to RT in general (i.e., IPL/RT relationship in non-switch trials). This may be related to an early increase in attention that is related to the changing colored cue indicating the need to switch into a new task state.

The DLPFC/IPL and ACC are part of two largely parallel control networks[15], though anatomical evidence suggest reciprocal connections between these two regions do exist, but their connectivity strength is specific to the cytoarchitectonic regions[206]. The DLPFC and IPL are

hubs within the fronto-parietal network, while the ACC and aIns are core nodes of the cingulo-opercular/salience network[15]. The fronto-parietal network has been shown to be critical for task adaptation and task switching[10], while the cingulo-opercular network is more involved in the maintenance of control, including monitoring and updating. Thus, the fronto-parietal network often is associated with more transient control, while the cingulo-opercular network is associated with more stable forms of control. The rapid and transient increase in beta/gamma band oscillations in the DLPFC and IPL contributing to faster RTs on switch trials is in line with this interpretation of the functionality of the fronto-parietal network. Conversely, the lack of a trial-to-trial relationship between RT and ACC theta power (as well as alpha band oscillations in fronto-parietal regions) but the presence of a positive relationship on average, suggests that for a given individual, trial-to-trial variance in RT during task switching is more directly modulated by fronto-parietal activity in the beta/gamma frequency bands. Additionally, we found evidence that the aIns demonstrated predictive power in trial-to-trial fluctuations in RT during switch trials more significantly than non-switch trials may indicate this regions involvement as a switch board between these two control networks[53], which otherwise function in parallel.

4.4.2 Developmental decreases in theta/alpha power

Developmental decreases in relatively slower frequency power has been found both across many task states and in the resting state[170]. The age related decrease in theta and alpha oscillations within the ROIs surveyed may be indicative of greater need to instantiate control before adulthood, given these effects are not related directly to task adaptation (i.e., to trial to trial fluctuations in RT). This is supported by the result that adults demonstrated an increase in theta power when incurring a greater switch cost, thus greater difficulty results in greater theta power.

In fact, adults engage ACC at greater levels than adolescents when they commit inhibitory errors[113], further suggesting that greater ACC engagement supports cognitive control. This evidence indicates ACC theta band oscillations act to resolves conflict regardless of age. Thus, the foundational aspects of ACC functioning are online by adolescence. However, as one develops, ACC functioning becomes more refined, likely as a result of more successful implementation of conflict resolution as maturation occurs requiring less power to instantiate successful control in adulthood.

Alpha band oscillations are often prescribed an inhibitory role in brain functioning. Right aIns alpha band oscillations scaled positively with average RT, however, this effect was only observed during adolescence. Furthermore, we did not observe a significant decrease in alpha band oscillations within the right aIns. This result is in agreement with greater theta power reflecting increased effort when young requiring, in this instance, the significant engagement of inhibitory processes.

4.4.3 Summary

In this chapter we have shown that a wide network of regions underlying cognitive control demonstrated increased activity, most prominently in the slower frequency (i.e., theta/alpha) bands during the preparation to successfully switch tasks. Furthermore, these oscillations were related to increased RT on average during task switching, likely reflecting conflict resolving signals. We also showed the increased higher frequency oscillations (beta/gamma band) within the fronto-parietal network, namely the DLPFC and IPL, are related to faster RTs on switch trials, over and above their typical relationship during motor execution. However, we did not find a relationship between ACC and trial-to-trial fluctuations in RT, lending further support to

accounts of ACC function in control signaling, rather than regulation directly[133,191,202]. Lastly we showed the strength of theta oscillations within the ACC decreased with development, likely underscoring the notion that adults can resolve conflict successfully with less neural 'effort' than adolescents. We are currently examining to role of the phase of ACC theta oscillations in task switching and developmental trajectories in the phase of ACC theta oscillations.

5.0 GENERAL DISCUSSION

Components of cognitive control, including inhibitory control and cognitive flexibility, continue to improve through adolescence[13,69]. The experiments conceptualized and executed in this dissertation sought to characterize 1. the topology of developmental differences in component (i.e., network) interactions underlying the development of cognitive control; 2. the oscillatory contributions of these networks to the development of cognitive control, both in the resting-state and 3. while subjects performed a task probing cognitive flexibility.

First (Chapter 2), using fMRI we found that network organization of resting state networks remained stable throughout adolescence. That is, the same network topology was present from childhood to adulthood, suggesting that network organization may be a foundational aspect of higher-order cognitive functions. However, the correlation strength between the cingulo-opercular/salience network, which underlies that ability to sustain cognitive control[15,48], to other brain networks increased significantly through adolescence in tandem with improvements in cognitive control performance. These findings are important as they indicate that specific to the transition to adult level cognitive control is the ability for networks specific to sustaining cognitive control to impact networks that determine action, while other critical components of network dynamics are already online (network organization and integration between networks that support transient cognitive components and sensorimotor processes).

To probe the neural basis of developmental changes in interactions between networks, we next (Chapter 3) characterized age-related differences in resting state network oscillations and their association with impulsivity, a marker of cognitive control. Results indicated that coupling between network ROIs, defined by phase locking, were already online across most frequency ranges that have been associated with cognition (alpha and beta (10-30 Hz)), further supporting our findings from rsfMRI indicating that network organization is online by childhood. In contrast, we found age-related changes specific to the theta band (5-9 Hz), a frequency interval that is associated with the instantiation of cognitive control within midline frontal regions[169]. In line with this regional specificity of cortical theta band oscillations, we found age-related *decreases* in the strength of coupling between ROIs that was predominantly in frontal and midline regions. These regions comprise the default mode, frontoparietal, and salience networks, with the greatest decreases in coupling occurring within the salience network. Furthermore, theta band coupling between anterior frontal and temporal lobe regions mediated age-related decreases in impulsivity, such that less coupling was associated with less impulsivity.

Decreases in ACC theta phase coupling during rest may be an intrinsic marker for an increased ability for these regions to variably interact with disparate brain systems, enhancing the brain's flexibility of cognitive systems throughout development during the resting-state. Evidence is accumulating supporting the notion that the brain engages in multiple states[177,178], as rapidly as once every 100-200 ms[179]. Neural inflexibility during rest would not allow for the exploration of multiple network states along the brain's functional backbone, which is thought to be a primary function of resting state interactions[135,178]. Thus, decoupling of oscillations across brain networks may be the mechanism by which network flexibility enables dynamic network configuration enabling greater integration at rest.

Together, these findings suggest that crosstalk between ROI's that support the ability to instantiate and sustain cognitive control becomes less committed with age. We propose that perhaps an ease in the commitment of ROIs interacting with one another with age may support increased flexibility to more readily switch engagement with changing task demands into adulthood. We recognize that this finding initially appears at odds with our rsfMRI finding showing increases in integration between cingulo-opercular/salience networks and other networks. However, we propose that we may be characterizing different aspects of change in similar processes. BOLD time courses in rsfMRI may capture a general effectiveness of the ability for networks to collaborate, while the refined timescale of neural oscillations measured by MEG may show the variability in regional interactions that contribute to enhanced network integration. The fact that both approaches show age-related changes in the same cognitive domain of the ability to sustain cognitive control is compelling in highlighting that specialization is specific to this more metacognitive aspect of cognitive control, namely the ability to sustain a state of cognitive control. Future studies, which we are presently investigating, should probe the relationship between BOLD and MEG oscillations to better understand shared neural mechanisms.

Finally, given the robust developmental effects within the cingulo-opercular/salience network, both in this dissertation and in other developmental literature[90,98,99,113], we next wanted to probe the development of this network in the context of cognitive flexibility (i.e., transient control) by using a task approach (Chapter 4). Both of our resting state studies showed age-related changes involving core regions within the salience network (i.e., ACC and aIns, which are anatomical and functional hubs), which is involved in both sustained and transient aspects of cognitive control[15,50,186]. Thus, we hypothesized their engagement during task switching would

play an important role in development. Results showed that theta band oscillations, which play a central role in the instantiation of cognitive control[133,169], were related to increased RT on average (but not trial-to-trial) during task switching, likely reflecting conflict-resolution signals[191,202]. In line with our resting state MEG findings, we found evidence that the strength of theta oscillations within the ACC decreased with development. Importantly, this changes was observed in the context of no age-related differences in task switching performance. Together, these findings may reflect that adults can resolve conflict successfully with less neural 'effort' than adolescents can. Adult studies show that there are increases in theta oscillations with increasing cognitive load[207,208], supporting our notion that greater theta in adolescence may reflect greater cognitive effort. Thus, adolescents displaying greater theta band coupling at rest and concomitant increases in theta power during task suggest that neural processes related to theta in particular underlie improvements in cognitive control into adulthood. An important implication is that adolescents can show adult level performance and engage similar neural processes, indicating that base cognitive processes are online. However, they do not have ability to readily and flexibly engage them as well as adults, supporting the notion that adolescence is a period in the refinement in neural processes and interactions underlying cognitive control.

Development brings greater integration and potentially greater flexibility between the cingulo-opercular/salience network, supporting sustained cognitive control[15,147], and regions that underlie action output such as the somatomotor networks, resulting in the ability to generate quicker execution of successful cognitive control signals[133]. We also found that integration between the cingulo-opercular/salience network and regions involved in transient control (i.e., DLPFC and IPL) increased throughout adolescence (Chapter 2). Given our finding of the lack of a relationship between trial-to-trial ACC theta band activity and RT in a task switching

paradigm, the influence of ACC activity in the context of cognitive flexibility is likely mediated, at least partially, through other regulatory systems, such as the DLPFC, or more broadly, the fronto-parietal network[48,186]. One compelling possibility is that the conflict signal generated in the ACC is passed to the anterior insula, which then reorients brain networks to regulate behavior towards a successful goal state[55].

During adolescence important structural changes are occurring that may be associated with our results. In particular, the cingulum, a white matter tract that provides connectivity between frontal and posterior midline regions, continues to show increases in white matter integrity into adulthood [83,122,209]. Myelination is a primary contributor to white matter integrity and is known to speed up neural processing, as well as protecting the integrity of signaling[210]. Thus, increased myelination of the cingulum would afford greater connectivity of the salience network (i.e., ACC and aIns) supporting the ability to more effectively sustain a cognitive control state while being able to flexibly interact with other systems[210]. The transition to adult level cognition then would reflect increased flexibility of theta band oscillations during rest while requiring a weaker signal into adulthood to instantiate the required level of cognitive control.

5.1 CLOSING REMARKS

Together our studies identify that critical to the transition to adult level cognition is engagement of the salience network and its component regions. We found that it increases its interactions with other networks, supporting improvements in cognitive control. Increases in salience network integration at rest likely affords this network greater flexibility at rest and more effective

engagement of transient control systems needed to implement cognitive flexibility. The systems supporting transient components of cognitive control itself, such as the frontoparietal network are on line by childhood. Taken together, these results support the model that by adolescence, foundational aspects of cognitive control are available, but the ability to effectively engage them continues to improve into adulthood. This active strengthening of control processes through adolescence may be critical in the maturation of cognitive control systems that, once established, switch to a mode of flexible engagement supporting the ability to readily integrate information from cognitive and default networks underlying adult level cognition. A break in this active strengthening of cognitive control brain systems may contribute to abnormal maturation, such as in psychopathology.

APPENDIX A

A.1 FIGURES

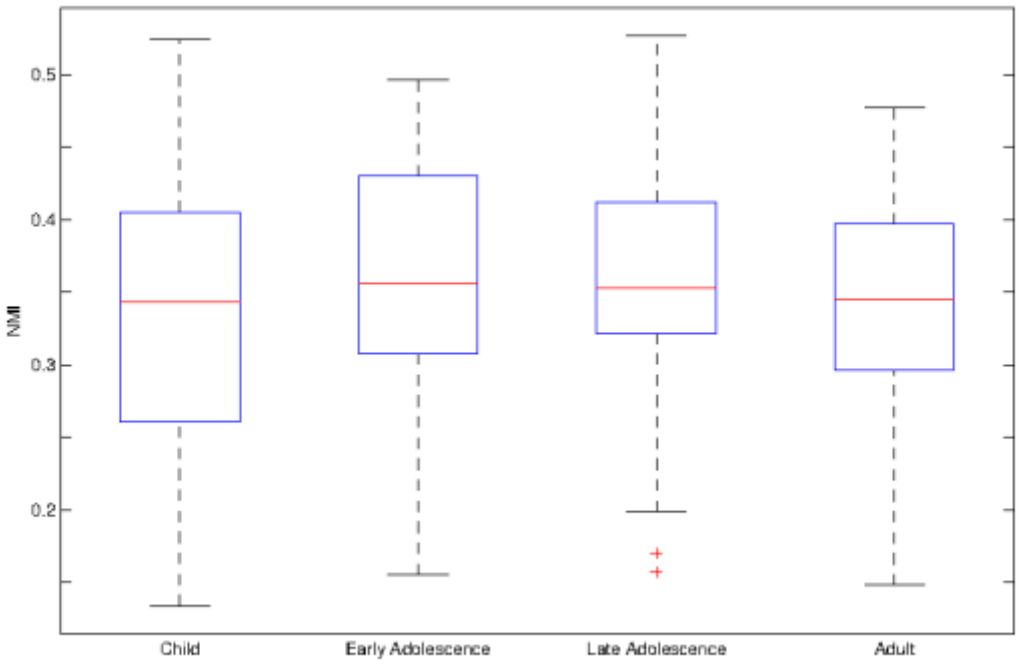

Figure 26. Normalized mutual information between individual subjects and adults.

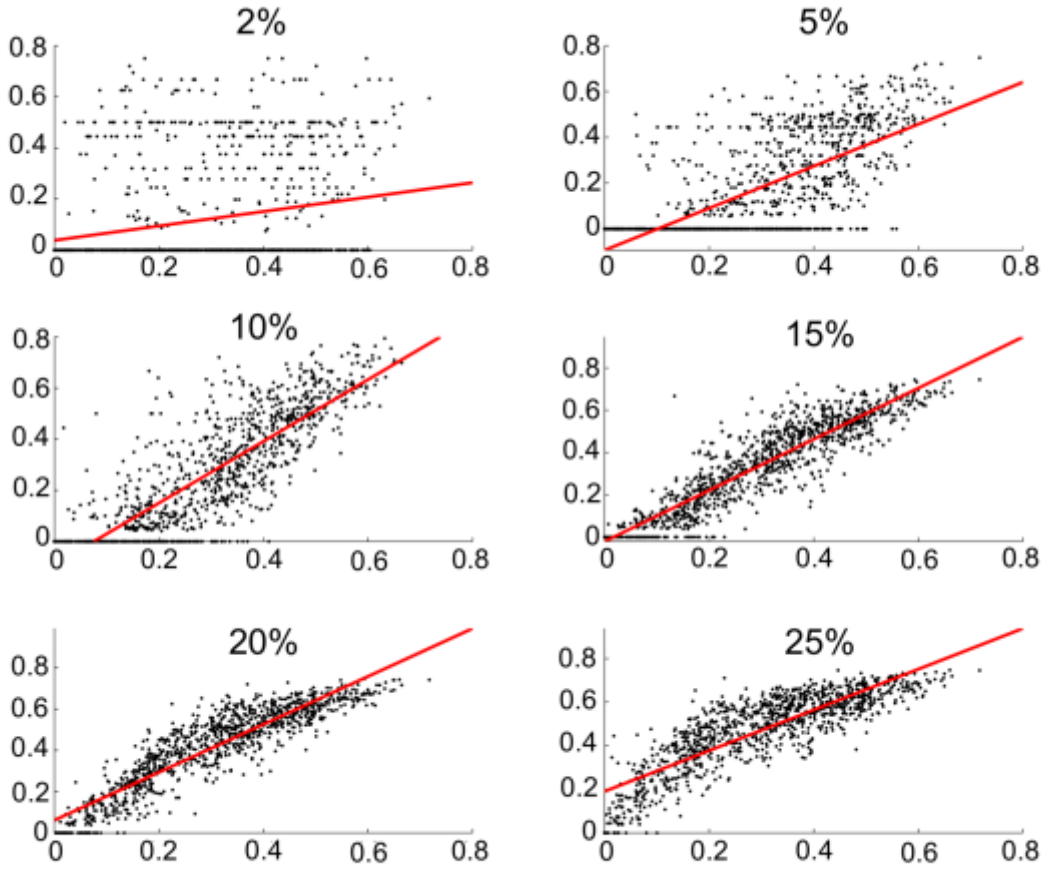

Figure 27. Participation coefficient is robust to network density.

Y-axis represents participation coefficient (PC) for the representative network density. X-axis represents mean PC across network densities.

A.2 TABLES

Network Density (%)	Adult vs. Child		Child vs. Early Adolescence		Early Adolescence vs. Late Adolescence		Late Adolescence vs. Adult	
	Observed	Null (mean)	Observed	Null (mean)	Observed	Null (mean)	Observed	Null (mean)
1	0.43	0.49	0.53	0.49	0.48	0.49	0.42	0.5
2	0.33	0.37	0.56	0.48	0.58	0.39	0.35	0.39
3	0.4	0.45	0.47	0.4	0.51	0.4	0.34	0.4
4	0.52	0.53	0.53	0.46	0.54	0.47	0.49	0.46
5	0.5	0.58	0.54	0.61	0.56	0.64	0.54	0.6
6	0.63	0.62	0.67	0.64	0.7	0.64	0.63	0.61
7	0.62	0.65	0.67	0.67	0.65	0.65	0.61	0.63
8	0.63	0.66	0.67	0.64	0.65	0.6	0.59	0.61
9	0.69	0.67	0.51	0.65	0.49	0.61	0.6	0.66
10	0.73	0.68	0.67	0.66	0.69	0.65	0.77	0.7
11	0.74	0.68	0.55	0.71	0.57	0.71	0.72	0.75
12	0.8	0.68	0.7	0.7	0.77	0.72	0.81	0.75
13	0.72	0.69	0.69	0.71	0.76	0.71	0.72	0.72
14	0.65	0.69	0.69	0.72	0.73	0.71	0.69	0.68
15	0.63	0.69	0.68	0.7	0.63	0.68	0.72	0.67
16	0.64	0.69	0.61	0.71	0.65	0.68	0.63	0.67
17	0.8	0.69	0.69	0.71	0.71	0.78	0.8	0.68
18	0.74	0.7	0.66	0.74	0.75	0.7	0.78	0.71
19	0.75	0.7	0.67	0.74	0.74	0.71	0.79	0.71
20	0.72	0.7	0.67	0.73	0.73	0.71	0.73	0.72
21	0.71	0.7	0.68	0.71	0.74	0.71	0.75	0.7
22	0.72	0.7	0.66	0.7	0.7	0.72	0.67	0.7
23	0.71	0.7	0.64	0.7	0.7	0.73	0.74	0.7
24	0.67	0.7	0.61	0.71	0.7	0.75	0.7	0.72
25	0.73	0.7	0.61	0.71	0.72	0.76	0.76	0.72

Table 4. Stable network organization is not dependent on network density

Contrast	ROI	Hemisphere	Network	Δ Degree	DM	SM	Vis	CO/S	FP	w/in	b/w
Childhood vs. Early Adolescence	Culmen	R	DM	2	0	0	2	0	0	0	2
	Precuneus	L	SM	2	1	-4	3	1	1	-5	7
	Postcentral G.	R	SM	1	-1	-5	4	1	2	-5	6
	Insula	R	CO/S	14	2	9	2	1	0	1	13
	Postcentral G.	L	SM	17	3	-1	11	3	2	-1	18
	Middle Occipital	L	VIS	16	6	5	0	5	0	0	16
	Lingual	R	VIS	12	1	8	1	0	2	1	11
	Parahippocampal G.	R	VIS	11	0	8	2	0	1	2	9
	Lingual	L	VIS	4	2	2	-1	0	1	-1	5
	Cuneus	L	VIS	23	3	8	6	3	3	6	17
	Lingual	L	VIS	5	2	1	1	0	1	1	4
	Middle Occipital	R	VIS	9	2	5	0	0	2	0	9
	Middle Occipital	L	VIS	9	3	4	0	0	2	0	9
	Cuneus	R	VIS	6	3	2	-2	0	3	-2	8
	Middle Occipital	L	VIS	8	2	3	2	0	1	2	6
	Anterior Cingulate	L	CO/S	-5	0	1	0	-6	0	-6	1
	Anterior Cingulate	L	CO/S	1	1	1	-1	-3	3	-3	4
	Thalamus	R	CO/S	-6	1	1	1	-8	-1	-8	2
	Thalamus	R	CO/S	1	-3	4	0	-5	-6	-5	6
	Thalamus	L	CO/S	0	2	1	2	-5	0	-5	5
	Lentiform	L	CO/S	12	2	6	1	3	0	3	9
	Lentiform	L	CO/S	21	6	7	0	3	5	3	18
	Lentiform	R	CO/S	2	0	4	0	-1	-1	-1	3
	Lentiform	R	CO/S	4	1	3	1	-1	0	-1	5
	Thalamus	R	CO/S	6	7	1	-1	-6	5	-6	12
	Declive	L	DM	12	0	6	-1	7	0	0	12
Early Adolescence vs. Late Adolescence	Orbital G.	R	DM	4	-1	0	0	5	0	-1	5
	Paracentral G.	L	SM	7	2	3	-1	0	3	3	4
	Postcentral G.	R	SM	12	-1	5	7	0	1	5	7
	Precentral G.	L	SM	10	0	4	6	0	0	4	6
	Precentral G.	L	SM	13	0	6	3	2	2	6	7
	Precentral G.	L	SM	16	0	11	6	-1	0	11	5
	Postcentral G.	L	SM	13	0	2	8	0	3	2	11
	Postcentral G.	L	SM	8	-1	2	5	0	2	2	6
	Inferior Parietal Lobe	R	SM	4	0	-1	0	2	3	-1	5
	Insula	R	CO/S	14	1	6	3	2	2	2	12
	Superior Temporal G.	R	SM	21	0	11	2	7	1	11	10
	Superior Temporal G.	R	SM	6	1	2	0	3	0	2	4
	Postcentral G.	L	SM	7	0	1	2	3	1	1	6
	Precentral G.	R	SM	2	-1	3	2	-3	0	-1	3
	Postcentral G.	R	SM	10	0	7	1	0	2	7	3
	Postcentral G.	L	SM	10	1	3	2	4	0	3	7
	Posterior Cingulate G.	L	DM	5	-1	0	1	4	1	-1	6
	Cuneus	L	VIS	15	2	11	1	0	1	1	14
	Precuneus	R	VIS	15	1	11	1	1	1	1	14
	Middle Occipital	L	VIS	7	2	2	0	1	2	0	7
Late Adolescence vs. Adulthood	Parahippocampal G.	L	DM	7	-2	3	3	0	3	-2	9
	Insula	R	SM	1	0	-3	1	3	0	-3	4
	Middle Temporal G.	L	DM	1	-5	3	3	-1	1	-5	6
	Angular G	L	DM	4	-1	2	1	1	1	-1	5
	Posterior Cingulate G.	L	DM	3	1	3	-1	0	0	1	2
	Superior Frontal G.	L	DM	2	-2	0	1	1	2	-2	4
	Medial Frontal G.	R	DM	8	4	1	1	2	1	4	4
	Medial Frontal G.	R	DM	5	0	0	0	4	1	0	5
	Medial Frontal G.	L	DM	4	1	1	0	2	0	1	3
	Medial Frontal G.	L	DM	2	0	-1	1	1	1	0	2
	Cuneus	L	VIS	5	3	1	-2	3	0	-2	7
	Lingual G.	L	VIS	8	5	2	-3	2	2	-3	11
	Lingual G.	R	VIS	6	1	1	1	2	1	1	5
	Lingual G.	R	VIS	3	1	0	-1	3	0	-1	4
	Inferior Parietal Lobe	L	FP	1	2	1	0	4	-6	-6	7
	Medial Frontal G.	L	CO/S	6	7	0	0	-6	5	-6	12
	Middle Frontal G.	L	FP	3	0	4	0	-1	0	0	3

Table 5. Regional increases in participation coefficient.

DM = default mode network; SM = somatomotor network; Vis = visual network; CO/S = cingulo-opercular/salience network; FP = fronto-parietal network; w/in = degree change in within-network connectivity; b/w = degree change in between-network connectivity. Each cell within each of these columns represents the change in degree.

A.3 WORKING MEMORY TASK

The spatial working memory task is modeled on the classic Sternberg working memory paradigm. Cue stimuli were yellow circles appearing in one of eight possible locations. Each trial began with fixation followed by a presentation of three frames (300ms each) showing one cue stimulus at a time in either the same location or three different locations. A blank grid was inserted between the frames for 200ms to decrease chunking and motion perception. A 1500ms (50% of trials), 3000ms (25% of trials), or 4500ms (25% of trials) delay period was used to minimize habituated preparatory responses.

Following the delay period, subjects made a button press to indicate whether a frame showing four circles located among eight possible locations had occurred in any of the previous cue locations (50% of trials), or were all in novel locations (50% of trials). A total of 144 high load trials and 144 low load trials were distributed across 12 runs, with the order randomized within runs. Inter-trial fixation intervals ranged between 1000 and 4500ms, with a short break between runs. The task was designed and run using E-Prime (Psychology Software Tools, Inc., Pittsburgh, PA).

A.4 TASK MEG DATA PREPROCESSING

MEG data were first manually inspected for flat or noisy channels that can arise due to sensor malfunction, and these channels were removed from further analysis. The maximum number of channels excluded within a single participant was 23. As we did with the resting-state data, we attenuated environmental noise using the MaxFilter software to apply temporal signal space separation (tSSS). If at any time during a trial the total displacement of MEG sensors relative to the head was greater than 5mm, the trial was rejected from all future analyses. Across all participants, only 38 total trials were dropped for head motion, with at most 4 trials dropped for head motion within a single participant.

The remaining preprocessing steps were applied using tools in the MNE Python package[211]. First, the data was band-pass filtered to the frequency range of interest (1-55Hz) using a 10-second overlap-add FIR filter. Cardiac, eye-blinks, and eye movement (saccade) artifacts are not identified by tSSS as they originate from the subject's body, so we used an independent components analysis (ICA) method to attenuate these artifacts, similar to the resting-state methods. The shapes of the automatically-detected artifactual components were checked visually to verify the selection of artifactual components, and the selection of components was then amended in the rare cases that the automatic procedure failed to identify components which showed clear EOG or ECG patterns. Finally, trials were screened for remaining sensor jumps, muscle artifacts, or saccade artifacts by checking for magnetometer amplitudes which exceeded $2.5*10^{-10}$ T or gradiometer amplitudes which exceeded $4*10^{-10}$ T/m; no further trials were rejected by these criteria.

During the experiment, trial event onset times were recorded into a digital stimulus channel through the E-Prime software. The event timings and codes from this channel were checked against E-Prime log files to remove spurious events which occurred in some runs due to software timing synchronization glitches. Based on this verified trial event data, trials with incorrect or omitted responses were removed, as we are interested only in trials during which working memory was successfully engaged. In addition, a total of 10 trials across all participants were rejected due to mismatches between stimulus channel event codes and timing reported by E-Prime, with at most 4 trials dropped from a single subject for this reason.

After preprocessing, we extracted the first 1500 ms of the maintenance period from the task and calculated the PLV between each of the 333 ROIs in the 5-9 Hz frequency range, mimicking the resting-state analysis. For each ROI pair, we then regressed the PLV onto age, controlling for subject head motion. Next, the beta weight from the age regressor was extracted from each model and beta weight matrices were constructed. As in the resting-state analysis, we summed down the columns of the matrix to get a summed beta weight representing the total linear age effect. We then regressed this value for ROI against the ROI's anatomical y-coordinate and did not observe any posterior-to-anterior effects (t = -0.02, p = 0.98).

A.5 ACC THETA BAND OSCILLATIONS ARE NOT ADAPTIVE

We asked whether or not the slowing of RT with greater ACC theta power was *adaptive* in that incurring a greater switch cost (higher RT on a switch trial relative to non-switch trials within the mix block) led to a dampening of cost in the mixed block (mix cost) (i.e., decrease in the difference between average RT on non-switch trials in the mix block and the average RT on trials in the pure block)[48]. Evidence for an adaptive role for a switch cost beyond the switch trial itself would manifest as a negative relationship between mix cost and switch cost.

We calculated the mixing cost and regressed individual subject's average switch cost onto mixing cost. We did not find support for this adaptive effect as there was no significant relationship between switch cost and mixing cost (r = -0.17, p = 0.26; Figure 28). In sum, the lack of an ACC/RT trial-to-trial relationship and lack of a switch cost/mixing cost effect provides strong evidence in favor of a control instantiation signal functioning to resolve conflict brought about by task switching via other regulatory regions within the switch trial itself.

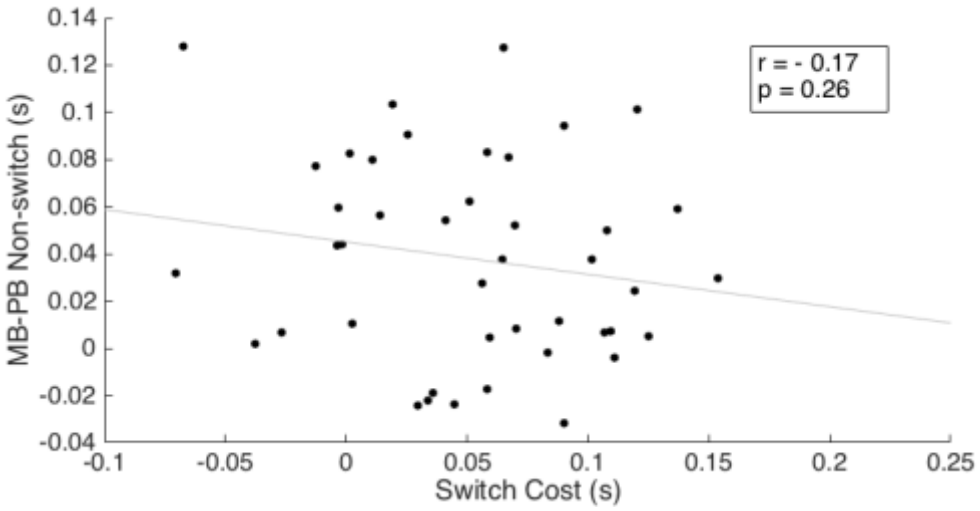

Figure 28. Mixing cost vs. switching cost.

The lack of evidence for a significant relationship between mixing cost and switch cost lends further support to the notion that increases in ACC theta band power prior to motor output are likely related solely to conflict related to task switching.

BIBLIOGRAPHY

1. Steinberg, L. A dual systems model of adolescent risk-taking. *Dev. Psychobiol.* **52,** 216–224 (2010).
2. Giedd, J. N. *et al.* Brain development during childhood and adolescence: a longitudinal MRI study. *Nat. Neurosci.* **2,** 861–863 (1999).
3. Gogtay, N. *et al.* Dynamic mapping of human cortical development during childhood through early adulthood. *Proc. Natl. Acad. Sci. U. S. A.* **101,** 8174–8179 (2004).
4. Shaw, P. *et al.* Neurodevelopmental trajectories of the human cerebral cortex. *J Neurosci* **28,** 3586–3594 (2008).
5. Yakovlev, P. I., Lecours, A. R. & Minkowski, A. in *Regional Development of the Brain in Early Life* 3–70 (Blackwell Scientific, 1967).
6. Dahl, R. E. Adolescent brain development: a period of vulnerabilities and opportunities. Keynote address. *Ann. N. Y. Acad. Sci.* **1021,** 1–22 (2004).
7. Paus, T., Keshavan, M. & Giedd, J. N. Why do many psychiatric disorders emerge during adolescence? *Nat Rev Neurosci* **9,** 947–957 (2008).
8. Gonzalez-Burgos, G. & Lewis, D. A. GABA neurons and the mechanisms of network oscillations: implications for understanding cortical dysfunction in schizophrenia. *Schizophr.Bull.* **34,** 944–961 (2008).

9. Braver, T. S. The variable nature of cognitive control: a dual mechanisms framework. *Trends Cogn. Sci.* **16,** 106–113 (2012).

10. Cole, M. W. *et al.* Multi-task connectivity reveals flexible hubs for adaptive task control. *Nat. Neurosci.* **16,** 1348–1355 (2013).

11. Luna, B., Garver, K. E., Urban, T. A., Lazar, N. A. & Sweeney, J. A. Maturation of cognitive processes from late childhood to adulthood. *Child Dev.* **75,** 1357–1372 (2004).

12. Velanova, K., Wheeler, M. E. & Luna, B. Maturational changes in anterior cingulate and frontoparietal recruitment support the development of error processing and inhibitory control. *Cereb. Cortex* **18,** 2505–2522 (2008).

13. Luna, B., Padmanabhan, A. & O'Hearn, K. What has fMRI told us about the development of cognitive control through adolescence? *Brain Cogn.* **72,** 101–13 (2010).

14. Biswal, B., Yetkin, F. Z., Haughton, V. M. & Hyde, J. S. Functional connectivity in the motor cortex of resting human brain using echo-planar MRI. *Magn. Reson. Med.* **34,** 537–541 (1995).

15. Dosenbach, N. U. F. *et al.* Distinct brain networks for adaptive and stable task control in humans. *Proc. Natl. Acad. Sci. U. S. A.* **104,** 11073–11078 (2007).

16. Raichle, M. E. *et al.* A default mode of brain function. *Proc. Natl. Acad. Sci. U. S. A.* **98,** 676–682 (2001).

17. Sporns, O., Tononi, G. & Kötter, R. The human connectome: A structural description of the human brain. *PLoS Comput. Biol.* **1,** e42 (2005).

18. Newman, M. E. J. Modularity and community structure in networks. *Proc. Natl. Acad. Sci.* **103,** 8577–8582 (2006).

19. Blondel, V. D., Guillaume, J.-L., Lambiotte, R. & Lefebvre, E. Fast unfolding of communities in large networks. *J. Stat. Mech. Theory Exp.* **2008,** P10008 (2008).

20. Gordon, E. M. *et al.* Generation and Evaluation of a Cortical Area Parcellation from Resting-State Correlations. *Cereb. Cortex N. Y. N 1991* (2014). doi:10.1093/cercor/bhu239

21. Power, J. D. *et al.* Functional network organization of the human brain. *Neuron* **72,** 665–678 (2011).

22. Yeo, B. T. *et al.* The Organization of the Human Cerebral Cortex Estimated By Functional Connectivity. *J. Neurophysiol.* (2011).

23. Guimerà, R. & Amaral, L. A. N. Cartography of complex networks: modules and universal roles. *J. Stat. Mech. Online* **2005,** nihpa35573 (2005).

24. Power, J. D., Schlaggar, B. L., Lessov-Schlaggar, C. N. & Petersen, S. E. Evidence for Hubs in Human Functional Brain Networks. *Neuron* **79,** 798–813 (2013).

25. Cole, M. W., Bassett, D. S., Power, J. D., Braver, T. S. & Petersen, S. E. Intrinsic and task-evoked network architectures of the human brain. *Neuron* **83,** 238–251 (2014).

26. Fransson, P. *et al.* Resting-state networks in the infant brain. *Proc.Natl.Acad.Sci.U.S.A* **104,** 15531–15536 (2007).

27. Thomason, M. E. *et al.* Cross-hemispheric functional connectivity in the human fetal brain. *Sci. Transl. Med.* **5,** 173ra24 (2013).

28. Doria, V. *et al.* Emergence of resting state networks in the preterm human brain. *Proc. Natl. Acad. Sci. U. S. A.* **107,** 20015–20020 (2010).

29. Gao, W. *et al.* Intersubject Variability of and Genetic Effects on the Brain's Functional Connectivity during Infancy. *J. Neurosci. Off. J. Soc. Neurosci.* **34,** 11288–11296 (2014).

30. Hwang, K., Hallquist, M. N. & Luna, B. The Development of Hub Architecture in the Human Functional Brain Network. (2012).

31. Fransson, P., Aden, U., Blennow, M. & Lagercrantz, H. The functional architecture of the infant brain as revealed by resting-state fMRI. *Cereb. Cortex N. Y. N 1991* **21,** 145–154 (2011).

32. Menon, V. Developmental pathways to functional brain networks: emerging principles. *Trends Cogn. Sci.* **17,** 627–640 (2013).

33. Grayson, D. S. *et al.* Structural and functional rich club organization of the brain in children and adults. *PloS One* **9,** e88297 (2014).

34. Cao, M. *et al.* Topological organization of the human brain functional connectome across the lifespan. *Dev. Cogn. Neurosci.* **7,** 76–93 (2014).

35. Simmonds, D., Hallquist, M. N., Asato, M. & Luna, B. Developmental Stages and Sex Differences of White Matter and Behavioral Development through Adolescence: A Longitudinal Diffusion Tensor Imaging (DTI) Study. *NeuroImage* (2013). doi:10.1016/j.neuroimage.2013.12.044

36. Hwang, K., Velanova, K. & Luna, B. Strengthening of Top-Down Frontal Cognitive Control Networks Underlying the Development of Inhibitory Control: A Functional Magnetic Resonance Imaging Effective Connectivity Study. *J. Neurosci.* **30,** 15535–15545 (2010).

37. Fair, D. A. *et al.* Development of distinct control networks through segregation and integration. *Proc. Natl. Acad. Sci. U. S. A.* **104,** 13507–13512 (2007).

38. Fair, D. A. *et al.* Functional brain networks develop from a 'local to distributed' organization. *PLoS.Comput.Biol.* **5,** e1000381 (2009).

39. Supekar, K., Musen, M. & Menon, V. Development of large-scale functional brain networks in children. *PLoS.Biol.* **7,** e1000157 (2009).

40. Power, J. D., Barnes, K. A., Snyder, A. Z., Schlaggar, B. L. & Petersen, S. E. Spurious but systematic correlations in functional connectivity MRI networks arise from subject motion. *NeuroImage* **59,** 2142–2154 (2012).

41. Hallquist, M. N., Hwang, K. & Luna, B. The nuisance of nuisance regression: Spectral misspecification in a common approach to resting-state fMRI preprocessing reintroduces noise and obscures functional connectivity. *NeuroImage* **82,** 208–225 (2013).

42. van den Heuvel, M. P. & Sporns, O. An anatomical substrate for integration among functional networks in human cortex. *J. Neurosci. Off. J. Soc. Neurosci.* **33,** 14489–14500 (2013).

43. Guimerà, R. & Amaral, L. A. N. Cartography of complex networks: modules and universal roles. *J. Stat. Mech. Online* **2005,** nihpa35573 (2005).

44. Hindriks, R. *et al.* Can sliding-window correlations reveal dynamic functional connectivity in resting-state fMRI? *NeuroImage* **127,** 242–256 (2016).

45. Hutchison, R. M. & Morton, J. B. Tracking the Brain's Functional Coupling Dynamics over Development. *J. Neurosci.* **35,** 6849–6859 (2015).

46. Marusak, H. A. *et al.* Dynamic functional connectivity of neurocognitive networks in children. *Hum. Brain Mapp.* **38,** 97–108 (2017).

47. McIntosh, A. R., Kovacevic, N. & Itier, R. J. Increased Brain Signal Variability Accompanies Lower Behavioral Variability in Development. *PLOS Comput. Biol.* **4,** e1000106 (2008).

48. Braver, T. S., Reynolds, J. R. & Donaldson, D. I. Neural mechanisms of transient and sustained cognitive control during task switching. *Neuron* **39,** 713–26 (2003).

49. Dosenbach, N. U. F., Fair, D. A., Cohen, A. L., Schlaggar, B. L. & Petersen, S. E. A dual-networks architecture of top-down control. *Trends Cogn. Sci.* **12,** 99–105 (2008).

50. Seeley, W. W. *et al.* Dissociable Intrinsic Connectivity Networks for Salience Processing and Executive Control. *J. Neurosci.* **27,** 2349–2356 (2007).

51. Craig, A. D. How do you feel — now? The anterior insula and human awareness. *Nat. Rev. Neurosci.* **10,** 59–70 (2009).

52. Shackman, A. J. *et al.* The integration of negative affect, pain and cognitive control in the cingulate cortex. *Nat. Rev. Neurosci.* **12,** 154–167 (2011).

53. Uddin, L. Q. Salience processing and insular cortical function and dysfunction. *Nat. Rev. Neurosci.* **16,** 55–61 (2015).

54. Sridharan, D., Levitin, D. J. & Menon, V. A critical role for the right fronto-insular cortex in switching between central-executive and default-mode networks. *Proc. Natl. Acad. Sci. U. S. A.* **105,** 12569–12574 (2008).

55. Uddin, L. Q., Supekar, K. S., Ryali, S. & Menon, V. Dynamic reconfiguration of structural and functional connectivity across core neurocognitive brain networks with development. *J. Neurosci. Off. J. Soc. Neurosci.* **31,** 18578–18589 (2011).

56. Buzsaki, G. *Rhythms of the brain*. (Oxford University Press, 2006).

57. Fries, P. A mechanism for cognitive dynamics: neuronal communication through neuronal coherence. *Trends Cogn Sci* **9,** 474–480 (2005).

58. Lachaux, J. P., Rodriguez, E., Martinerie, J. & Varela, F. J. Measuring phase synchrony in brain signals. *Hum. Brain Mapp.* **8,** 194–208 (1999).

59. Donner, T. H. & Siegel, M. A framework for local cortical oscillation patterns. *Trends Cogn Sci* **15,** 191–199 (2011).

60. von Stein, A. & Sarnthein, J. Different frequencies for different scales of cortical integration: from local gamma to long range alpha/theta synchronization. *Int. J. Psychophysiol.* **38,** 301–13 (2000).

61. Palva, S. & Palva, J. M. Functional roles of alpha-band phase synchronization in local and large-scale cortical networks. *Front. Psychol.* **2,** 204 (2011).

62. Palva, J. M., Monto, S., Kulashekhar, S. & Palva, S. Neuronal synchrony reveals working memory networks and predicts individual memory capacity. *Proc. Natl. Acad. Sci. U. S. A.* **107,** 7580–7585 (2010).

63. Uhlhaas, P. J. & Singer, W. The development of neural synchrony and large-scale cortical networks during adolescence: relevance for the pathophysiology of schizophrenia and neurodevelopmental hypothesis. *Schizophr. Bull.* **37,** 514–523 (2011).

64. Uhlhaas, P. J. *et al.* The development of neural synchrony reflects late maturation and restructuring of functional networks in humans. *Proc.Natl.Acad.Sci.U.S.A* **106,** 9866–9871 (2009).

65. Uhlhaas, P. J., Haenschel, C., Nikolic, D. & Singer, W. The role of oscillations and synchrony in cortical networks and their putative relevance for the pathophysiology of schizophrenia. *Schizophr.Bull.* **34,** 927–943 (2008).

66. Cohen, J. R., Gallen, C. L., Jacobs, E. G., Lee, T. G. & D'Esposito, M. Quantifying the reconfiguration of intrinsic networks during working memory. *PloS One* **9,** e106636 (2014).

67. Dwyer, D. B. *et al.* Large-scale brain network dynamics supporting adolescent cognitive control. *J. Neurosci. Off. J. Soc. Neurosci.* **34,** 14096–14107 (2014).

68. Satterthwaite, T. D. *et al.* Functional maturation of the executive system during adolescence. *J. Neurosci. Off. J. Soc. Neurosci.* **33,** 16249–16261 (2013).

69. Luna, B., Marek, S., Larsen, B., Tervo-Clemmens, B. & Chahal, R. An Integrative Model of the Maturation of Cognitive Control. *Annu. Rev. Neurosci.* **38,** 151-170 (2015).

70. Cocchi, L., Zalesky, A., Fornito, A. & Mattingley, J. B. Dynamic cooperation and competition between brain systems during cognitive control. *Trends Cogn. Sci.* **17,** 493–501 (2013).

71. Diamond, A. Executive functions. *Annu. Rev. Psychol.* **64,** 135–168 (2013).

72. Luna, B. & Sweeney, J. A. The emergence of collaborative brain function: FMRI studies of the development of response inhibition. *Ann. N. Y. Acad. Sci.* **1021,** 296–309 (2004).

73. Medaglia, J. D. *et al.* Flexible Traversal Through Diverse Brain States Underlies Executive Function in Normative Neurodevelopment. *ArXiv151008780 Q-Bio* (2015).

74. Monsell, S. Task switching. *Trends Cogn. Sci.* **7,** 134–140 (2003).

75. Rubia, K. *et al.* Progressive increase of frontostriatal brain activation from childhood to adulthood during event-related tasks of cognitive control. *Hum Brain Mapp* **27,** 973–993 (2006).

76. Christakou, A. *et al.* Sex-dependent age modulation of frontostriatal and temporo-parietal activation during cognitive control. *Neuroimage.* **48,** 223–236 (2009).

77. Badre, D. Defining an ontology of cognitive control requires attention to component interactions. *Top. Cogn. Sci.* **3,** 217–221 (2011).

78. Lenartowicz, A., Kalar, D. J., Congdon, E. & Poldrack, R. A. Towards an ontology of cognitive control. *Top. Cogn. Sci.* **2,** 678–692 (2010).

79. Sabb, F. W. *et al.* A collaborative knowledge base for cognitive phenomics. *Mol. Psychiatry* **13,** 350–360 (2008).

80. Diamond, A. in *The development and neural bases of higher cognitive functions* (Academy of Science Press, 1989).

81. Luna, B., Paulsen, D. J., Padmanabhan, A. & Geier, C. Cognitive Control and Motivation. *Curr. Dir. Psychol. Sci.* **22,** 94–100 (2013).

82. Petanjek, Z. *et al.* Extraordinary neoteny of synaptic spines in the human prefrontal cortex. *Proc. Natl. Acad. Sci.* **108,** 13281–13286 (2011).

83. Simmonds, D. J., Hallquist, M. N., Asato, M. & Luna, B. Developmental stages and sex differences of white matter and behavioral development through adolescence: a longitudinal diffusion tensor imaging (DTI) study. *NeuroImage* **92,** 356–368 (2014).

84. Luna, B. & Sweeney, J. A. The emergence of collaborative brain function: FMRI studies of the development of response inhibition. *Ann. N. Y. Acad. Sci.* **1021,** 296–309 (2004).

85. Whiteside, S. P. & Lynam, D. R. The Five Factor Model and impulsivity: using a structural model of personality to understand impulsivity. *Personal. Individ. Differ.* **30,** 669–689 (2001).

86. Menon, V. Developmental pathways to functional brain networks: emerging principles. *Trends Cogn. Sci.* **17,** 627–640 (2013).

87. Newman, M. E. J. *Networks: an introduction*. (Oxford University Press, 2010).

88. Fair, D. A. *et al.* Functional brain networks develop from a ‘local to distributed’ organization. *PLoS Comput. Biol.* **5,** e1000381 (2009).

89. Fransson, P., Aden, U., Blennow, M. & Lagercrantz, H. The functional architecture of the infant brain as revealed by resting-state fMRI. *Cereb. Cortex N. Y. N 1991* **21,** 145–154 (2011).

90. Kelly, A. M. C. *et al.* Development of anterior cingulate functional connectivity from late childhood to early adulthood. *Cereb. Cortex N. Y. N 1991* **19,** 640–657 (2009).

91. Power, J. D. *et al.* Methods to detect, characterize, and remove motion artifact in resting state fMRI. *NeuroImage* **84,** 320–341 (2014).

92. Hwang, K., Hallquist, M. N. & Luna, B. The Development of Hub Architecture in the Human Functional Brain Network. *Cereb. Cortex* bhs227 (2012). doi:10.1093/cercor/bhs227

93. Bullmore, E. & Sporns, O. Complex brain networks: graph theoretical analysis of structural and functional systems. *Nat. Rev. Neurosci.* **10,** 186–198 (2009).

94. Rubinov, M. & Sporns, O. Complex network measures of brain connectivity: uses and interpretations. *NeuroImage* **52,** 1059–1069 (2010).

95. Fischer, B., Biscaldi, M. & Gezeck, S. On the development of voluntary and reflexive components in human saccade generation. *Brain Res.* **754,** 285–297 (1997).

96. Klein, C. & Foerster, F. Development of prosaccade and antisaccade task performance in participants aged 6 to 26 years. *Psychophysiology* **38,** 179–189 (2001).

97. Levin, H. S. *et al.* Developmental changes in performance on tests of purported frontal lobe functioning. *Dev. Neuropsychol.* **7,** 377–395 (1991).

98. Rubia, K., Smith, A. B., Taylor, E. & Brammer, M. Linear age-correlated functional development of right inferior fronto-striato-cerebellar networks during response inhibition and anterior cingulate during error-related processes. *Hum. Brain Mapp.* **28,** 1163–1177 (2007).

99. Velanova, K., Wheeler, M. E. & Luna, B. Maturational Changes in Anterior Cingulate and Frontoparietal Recruitment Support the Development of Error Processing and Inhibitory Control. *Cereb. Cortex* **18,** 2505–2522 (2008).

100. Geier, C. F. & Luna, B. Developmental effects of incentives on response inhibition. *Child Dev.* **83,** 1262–1274 (2012).

101. Gitelman, D. R. ILAB: A program for postexperimental eye movement analysis. *Behav. Res. Methods Instrum. Comput.* **34,** 605–612 (2002).

102. Cox, R. W. AFNI: software for analysis and visualization of functional magnetic resonance neuroimages. *Comput. Biomed. Res.* **29,** 162–173 (1996).

103. Fischl, B. *et al.* Whole brain segmentation: automated labeling of neuroanatomical structures in the human brain. *Neuron* **33,** 341–355 (2002).

104. Patel, A. X. *et al.* A wavelet method for modeling and despiking motion artifacts from resting-state fMRI time series. *NeuroImage* (2014). doi:10.1016/j.neuroimage.2014.03.012

105. Cohen, A. L. *et al.* Defining functional areas in individual human brains using resting functional connectivity MRI. *NeuroImage* **41,** 45–57 (2008).

106. Nelson, S. M. *et al.* A Parcellation Scheme for Human Left Lateral Parietal Cortex. *Neuron* **67,** 156–170 (2010).

107. Sporns, O. Network attributes for segregation and integration in the human brain. *Curr. Opin. Neurobiol.* **23,** 162–171 (2013).

108. Lancichinetti, A. & Fortunato, S. Community detection algorithms: a comparative analysis. *Phys. Rev. E* **80,** (2009).

109. Rouder, J. N., Speckman, P. L., Sun, D., Morey, R. D. & Iverson, G. Bayesian t tests for accepting and rejecting the null hypothesis. *Psychon. Bull. Rev.* **16,** 225–237 (2009).

110. Xia, M., Wang, J. & He, Y. BrainNet Viewer: a network visualization tool for human brain connectomics. *PloS One* **8,** e68910 (2013).

111. Luna, B. *et al.* Maturation of widely distributed brain function subserves cognitive development. *NeuroImage* **13,** 786–793 (2001).

112. Munoz, D. P., Broughton, J. R., Goldring, J. E. & Armstrong, I. T. Age-related performance of human subjects on saccadic eye movement tasks. *Exp. Brain Res.* **121,** 391–400 (1998).

113. Ordaz, S. J., Foran, W., Velanova, K. & Luna, B. Longitudinal growth curves of brain function underlying inhibitory control through adolescence. *J. Neurosci. Off. J. Soc. Neurosci.* **33,** 18109–18124 (2013).

114. Klein, C., Foerster, F., Hartnegg, K. & Fischer, B. Lifespan development of pro- and anti-saccades: multiple regression models for point estimates. *Dev. Brain Res.* **160,** 113–123 (2005).

115. Eenshuistra, R. M., Ridderinkhof, K. R. & van der Molen, M. W. Age-related changes in antisaccade task performance: inhibitory control or working-memory engagement? *Brain Cogn.* **56,** 177–188 (2004).

116. Alahyane, N., Brien, D. C., Coe, B. C., Stroman, P. W. & Munoz, D. P. Developmental improvements in voluntary control of behavior: effect of preparation in the fronto-parietal network? *NeuroImage* **98,** 103–117 (2014).

117. Fukushima, J., Hatta, T. & Fukushima, K. Development of voluntary control of saccadic eye movements. I. Age-related changes in normal children. *Brain Dev.* **22,** 173–180 (2000).

118. Hwang, K., Ghuman, A. S., Manoach, D. S., Jones, S. R. & Luna, B. Cortical neurodynamics of inhibitory control. *J. Neurosci. Off. J. Soc. Neurosci.* **34,** 9551–9561 (2014).

119. Van Dijk, K. R., Sabuncu, M. R. & Buckner, R. L. The influence of head motion on intrinsic functional connectivity MRI. *Neuroimage.* **59,** 431–438 (2012).

120. Satterthwaite, T. D. *et al.* An improved framework for confound regression and filtering for control of motion artifact in the preprocessing of resting-state functional connectivity data. *NeuroImage* **64,** 240–256 (2013).

121. Hagmann, P. *et al.* White matter maturation reshapes structural connectivity in the late developing human brain. *Proc. Natl. Acad. Sci.* **107,** 19067–19072 (2010).

122. Lebel, C. *et al.* Diffusion tensor imaging of white matter tract evolution over the lifespan. *NeuroImage* **60,** 340–352 (2012).

123. Fair, D. A. *et al.* Distinct neural signatures detected for ADHD subtypes after controlling for micro-movements in resting state functional connectivity MRI data. *Front. Syst. Neurosci.* **6,** 80 (2012).

124. Nelson, S. M. *et al.* Role of the anterior insula in task-level control and focal attention. *Brain Struct. Funct.* **214,** 669–680 (2010).

125. Paus, T. Primate anterior cingulate cortex: where motor control, drive and cognition interface. *Nat. Rev. Neurosci.* **2,** 417–424 (2001).

126. Craig, A. D. B. Significance of the insula for the evolution of human awareness of feelings from the body. *Ann. N. Y. Acad. Sci.* **1225,** 72–82 (2011).

127. Menon, V. & Uddin, L. Q. Saliency, switching, attention and control: a network model of insula function. *Brain Struct. Funct.* **214,** 655–667 (2010).

128. Menon, V. Large-scale brain networks and psychopathology: a unifying triple network model. *Trends Cogn. Sci.* **15,** 483–506 (2011).

129. Uddin, L. Q. & Menon, V. The anterior insula in autism: under-connected and under-examined. *Neurosci. Biobehav. Rev.* **33,** 1198–1203 (2009).

130. Lebel, C., Walker, L., Leemans, A., Phillips, L. & Beaulieu, C. Microstructural maturation of the human brain from childhood to adulthood. *NeuroImage* **140,** 1044–1055 (2008).

131. Larsen, B. & Luna, B. In vivo evidence of neurophysiological maturation of the human adolescent striatum. *Dev. Cogn. Neurosci.* **12C,** 74–85 (2014).

132. Luciana, M. & Collins, P. F. Incentive Motivation, Cognitive Control, and the Adolescent Brain: Is It Time for a Paradigm Shift? *Child Dev. Perspect.* **6,** 392–399 (2012).

133. Shenhav, A., Botvinick, M. M. & Cohen, J. D. The expected value of control: An integrative theory of anterior cingulate cortex function. *Neuron* **79,** 217–240 (2013).

134. Raichle, M. E. Two views of brain function. *Trends Cogn. Sci.* **14,** 180–190 (2010).

135. Deco, G., Jirsa, V. K. & McIntosh, A. R. Emerging concepts for the dynamical organization of resting-state activity in the brain. *Nat Rev Neurosci* **12,** 43–56 (2011).

136. He, B. J., Snyder, A. Z., Zempel, J. M., Smyth, M. D. & Raichle, M. E. Electrophysiological correlates of the brain's intrinsic large-scale functional architecture. *Proc.Natl.Acad.Sci.U.S.A* **105,** 16039–16044 (2008).

137. Vincent, J. L. *et al.* Intrinsic functional architecture in the anaesthetized monkey brain. *Nature* **447,** 83–86 (2007).

138. Van Dijk, K. R. *et al.* Intrinsic functional connectivity as a tool for human connectomics: theory, properties, and optimization. *J. Neurophysiol.* **103,** 297–321 (2010).

139. Bi, G. & Poo, M. Distributed synaptic modification in neural networks induced by patterned stimulation. *Nature* **401,** 792–796 (1999).

140. Power, J. D., Fair, D. A., Schlaggar, B. L. & Petersen, S. E. The development of Human Functional Brain Networks. *Neuron* **67,** 735–748 (2010).

141. Honey, C. J., Kotter, R., Breakspear, M. & Sporns, O. Network structure of cerebral cortex shapes functional connectivity on multiple time scales. *Proc. Natl. Acad. Sci. U. S. A.* **104,** 10240–10245 (2007).

142. Birn, R. M. *et al.* The effect of scan length on the reliability of resting-state fMRI connectivity estimates. *NeuroImage* **83,** 550–558 (2013).

143. Galvan, A., Hare, T., Voss, H., Glover, G. & Casey, B. J. Risk-taking and the adolescent brain: who is at risk? *Dev. Sci.* **10,** F8–F14 (2007).

144. Ordaz, S. J., Foran, W., Velanova, K. & Luna, B. Longitudinal growth curves of brain function underlying inhibitory control through adolescence. *J. Neurosci.* **33,** 18109–18124 (2013).

145. Crone, E. A., Zanolie, K., Van, L. L., Westenberg, P. M. & Rombouts, S. A. Neural mechanisms supporting flexible performance adjustment during development. *Cogn Affect.* **8,** 165–177 (2008).

146. Hwang, K., Velanova, K. & Luna, B. Strengthening of top-down frontal cognitive control networks underlying the development of inhibitory control: A functional magnetic resonance imaging effective connectivity study. *J. Neurosci.* **30,** 15535–15545 (2010).

147. Marek, S., Hwang, K., Foran, W., Hallquist, M. N. & Luna, B. The Contribution of Network Organization and Integration to the Development of Cognitive Control. *PLoS Biol* **13,** e1002328 (2015).

148. Di Martino, A. *et al.* Unraveling the miswired connectome: a developmental perspective. *Neuron* **83,** 1335–1353 (2014).

149. Gasser, T., Verleger, R., Bächer, P. & Sroka, L. Development of the EEG of school-age children and adolescents. I. Analysis of band power. *Electroencephalogr. Clin. Neurophysiol.* **69,** 91–99 (1988).

150. Matousek, M. & Petersén, I. Automatic evaluation of EEG background activity by means of age-dependent EEG quotients. *Electroencephalogr. Clin. Neurophysiol.* **35,** 603–612 (1973).

151. Boord, P. R., Rennie, C. J. & Williams, L. M. Integrating 'brain' and 'body' measures: correlations between EEG and metabolic changes over the human lifespan. *J Integr Neurosci* **6,** 205–218 (2007).

152. Whitford, T. J. *et al.* Brain maturation in adolescence: concurrent changes in neuroanatomy and neurophysiology. *HumBrain Mapp* **28,** 228–237 (2007).

153. Gasser, T., Jennen-Steinmetz, C., Sroka, L., Verleger, R. & Möcks, J. Development of the EEG of school-age children and adolescents. II. Topography. *Electroencephalogr. Clin. Neurophysiol.* **69,** 100–109 (1988).

154. Thatcher, R. W., North, D. M. & Biver, C. J. Development of cortical connections as measured by EEG coherence and phase delays. *HumBrain Mapp* **29,** 1400–1415 (2008).

155. Buchmann, A. *et al.* EEG sleep slow-wave activity as a mirror of cortical maturation. *Cereb. Cortex N. Y. N 1991* **21,** 607–615 (2011).

156. Ghuman, A. S., McDaniel, J. R. & Martin, A. A wavelet-based method for measuring the oscillatory dynamics of resting-state functional connectivity in MEG. *NeuroImage* **56,** 69–77 (2011).

157. Fries, P. A mechanism for cognitive dynamics: neuronal communication through neuronal coherence. *Trends Cogn. Sci.* **9,** 474–80 (2005).

158. Taulu, S., Kajola, M. & Simola, J. Suppression of interference and artifacts by the Signal Space Separation Method. *Brain Topogr.* **16,** 269–75 (2004).

159. Taulu, S. & Hari, R. Removal of magnetoencephalographic artifacts with temporal signal-space separation: demonstration with single-trial auditory-evoked responses. *HumBrain Mapp* **30,** 1524–1534 (2009).

160. Gonzalez-Moreno, A. *et al.* Signal-to-noise ratio of the MEG signal after preprocessing. *J. Neurosci. Methods* **222,** 56–61 (2014).

161. Nenonen, J. *et al.* Validation of head movement correction and spatiotemporal signal space separation in magnetoencephalography. *Clin. Neurophysiol.* **123,** 2180–91 (2012).

162. Dale, A. M., Fischl, B. & Sereno, M. I. Cortical Surface-Based Analysis: I. Segmentation and Surface Reconstruction. *NeuroImage* **9,** 179–194 (1999).

163. Fischl, B., Sereno, M. I. & Dale, A. M. Cortical surface-based analysis. II: Inflation, flattening, and a surface-based coordinate system. *Neuroimage* **9,** 195–207 (1999).

164. Benjamini, Y. & Hochberg, Y. Controlling the False Discovery Rate: A Practical and Powerful Approach to Multiple Testing. *J. R. Stat. Soc. B Methodol.* **57,** 289–300 (1995).

165. Lynam, D. R., Smith, G. T., Whiteside, S. P. & Cyders, M. A. The UPPS-P: Assessing five personality pathways to impulsive behavior. *West Lafayette Purdue Univ.* (2006).

166. Zalesky, A., Fornito, A. & Bullmore, E. T. Network-based statistic: identifying differences in brain networks. *NeuroImage* **53,** 1197–1207 (2010).

167. Tingley, D., Yamamoto, T., Hirose, K., Keele, L. & Imai, K. Mediation: R package for causal mediation analysis. (2014).

168. Crews, F. T. & Boettiger, C. A. Impulsivity, Frontal Lobes and Risk for Addiction. *Pharmacol. Biochem. Behav.* **93,** 237–247 (2009).

169. Cavanagh, J. F. & Frank, M. J. Frontal theta as a mechanism for cognitive control. *Trends Cogn. Sci.* **18,** 414–421 (2014).

170. Segalowitz, S. J., Santesso, D. L. & Jetha, M. K. Electrophysiological changes during adolescence: a review. *Brain Cogn.* **72,** 86–100 (2010).

171. Thatcher, R. W., North, D. M. & Biver, C. J. Development of cortical connections as measured by EEG coherence and phase delays. *Hum. Brain Mapp.* **29,** 1400–1415 (2008).

172. Augustine, J. R. Circuitry and functional aspects of the insular lobe in primates including humans. *Brain Res. Rev.* **22,** 229–244 (1996).

173. Bechara, A., Damasio, A. R., Damasio, H. & Anderson, S. W. Insensitivity to future consequences following damage to human prefrontal cortex. *Cognition* **50,** 7–15 (1994).

174. Berlin, H. A., Rolls, E. T. & Kischka, U. Impulsivity, time perception, emotion and reinforcement sensitivity in patients with orbitofrontal cortex lesions. *Brain J. Neurol.* **127,** 1108–1126 (2004).

175. Hillebrand, A. *et al.* Direction of information flow in large-scale resting-state networks is frequency-dependent. *Proc. Natl. Acad. Sci.* **113,** 3867–3872 (2016).

176. McIntosh, A. R., Kovacevic, N. & Itier, R. J. Increased Brain Signal Variability Accompanies Lower Behavioral Variability in Development. *PLoS Comput. Biol.* **4,** (2008).

177. Handwerker, D. A., Roopchansingh, V., Gonzalez-Castillo, J. & Bandettini, P. A. Periodic changes in fMRI connectivity. *NeuroImage* **63,** 1712–1719 (2012).

178. Allen, E. A. *et al.* Tracking whole-brain connectivity dynamics in the resting state. *Cereb. Cortex N. Y. N 1991* **24,** 663–676 (2014).

179. Baker, A. P. *et al.* Fast transient networks in spontaneous human brain activity. *eLife* **3,** (2014).

180. Marusak, H. A. *et al.* Dynamic functional connectivity of neurocognitive networks in children. *Hum. Brain Mapp.* (2016). doi:10.1002/hbm.23346

181. Garrett, D. D., Kovacevic, N., McIntosh, A. R. & Grady, C. L. Blood oxygen level-dependent signal variability is more than just noise. *J. Neurosci. Off. J. Soc. Neurosci.* **30,** 4914–4921 (2010).

182. Garrett, D. D. *et al.* Moment-to-moment brain signal variability: a next frontier in human brain mapping? *Neurosci. Biobehav. Rev.* **37,** 610–624 (2013).

183. Muthukumaraswamy, S. D. & Singh, K. D. A cautionary note on the interpretation of phase-locking estimates with concurrent changes in power. *Clin. Neurophysiol. Off. J. Int. Fed. Clin. Neurophysiol.* **122,** 2324–2325 (2011).

184. Dajani, D. R. & Uddin, L. Q. Demystifying cognitive flexibility: Implications for clinical and developmental neuroscience. *Trends Neurosci.* **38,** 571–578 (2015).

185. Womelsdorf, T., Johnston, K., Vinck, M. & Everling, S. Theta-activity in anterior cingulate cortex predicts task rules and their adjustments following errors. *Proc. Natl. Acad. Sci. U. S. A.* **107,** 5248–5253 (2010).

186. Dosenbach, N. U. F. *et al.* A core system for the implementation of task sets. *Neuron* **50,** 799–812 (2006).

187. Cole, M. W. & Schneider, W. The cognitive control network: Integrated cortical regions with dissociable functions. *Neuroimage.* **37,** 343–360 (2007).

188. Barceló, F., Periáñez, J. A. & Knight, R. T. Think differently: a brain orienting response to task novelty. *Neuroreport* **13,** 1887–1892 (2002).

189. Cunillera, T. *et al.* Brain oscillatory activity associated with task switching and feedback processing. *Cogn. Affect. Behav. Neurosci.* **12,** 16–33 (2012).

190. Barcelo, F., Escera, C., Corral, M. J. & Periáñez, J. A. Task switching and novelty processing activate a common neural network for cognitive control. *J. Cogn. Neurosci.* **18,** 1734–1748 (2006).

191. Botvinick, M., Nystrom, L. E., Fissell, K., Carter, C. S. & Cohen, J. D. Conflict monitoring versus selection-for-action in anterior cingulate cortex. *Nature* **402,** 179–181 (1999).

192. Cavanagh, J. F., Zambrano-Vazquez, L. & Allen, J. J. B. Theta lingua franca: a common mid-frontal substrate for action monitoring processes. *Psychophysiology* **49,** 220–238 (2012).

193. Nigbur, R., Ivanova, G. & Stürmer, B. Theta power as a marker for cognitive interference. *Clin. Neurophysiol. Off. J. Int. Fed. Clin. Neurophysiol.* **122,** 2185–2194 (2011).

194. Scherbaum, S. & Dshemuchadse, M. Higher response time increases theta energy, conflict increases response time. *Clin. Neurophysiol. Off. J. Int. Fed. Clin. Neurophysiol.* **124,** 1477–1479 (2013).

195. Cohen, M. X. & Nigbur, R. Reply to 'Higher response time increases theta energy, conflict increases response time'. *Clin. Neurophysiol. Off. J. Int. Fed. Clin. Neurophysiol.* **124,** 1479–1481 (2013).

196. Voytek, B. *et al.* Oscillatory dynamics coordinating human frontal networks in support of goal maintenance. *Nat. Neurosci.* **18,** 1318–1324 (2015).

197. Clayton, M. S., Yeung, N. & Cohen Kadosh, R. The roles of cortical oscillations in sustained attention. *Trends Cogn. Sci.* **19,** 188–195 (2015).

198. Tadel, F., Baillet, S., Mosher, J. C., Pantazis, D. & Leahy, R. M. Brainstorm: A User-Friendly Application for MEG/EEG Analysis. *Comput. Intell. Neurosci.* **2011,** e879716 (2011).

199. Leahy, R. M., Mosher, J. C., Spencer, M. E., Huang, M. X. & Lewine, J. D. A study of dipole localization accuracy for MEG and EEG using a human skull phantom. *Electroencephalogr. Clin. Neurophysiol.* **107,** 159–173 (1998).

200. Huang, M. X., Mosher, J. C. & Leahy, R. M. A sensor-weighted overlapping-sphere head model and exhaustive head model comparison for MEG. *Phys. Med. Biol.* **44,** 423–440 (1999).

201. Van Veen, B. D., van Drongelen, W., Yuchtman, M. & Suzuki, A. Localization of brain electrical activity via linearly constrained minimum variance spatial filtering. *IEEE Trans. Biomed. Eng.* **44,** 867–880 (1997).

202. Ridderinkhof, K. R., Ullsperger, M., Crone, E. A. & Nieuwenhuis, S. The role of the medial frontal cortex in cognitive control. *Science* **306,** 443–447 (2004).

203. Womelsdorf, T. & Fries, P. The role of neuronal synchronization in selective attention. *Curr. Opin. Neurobiol.* **17,** 154–60 (2007).

204. Boschin, E. A., Brkic, M. M., Simons, J. S. & Buckley, M. J. Distinct Roles for the Anterior Cingulate and Dorsolateral Prefrontal Cortices During Conflict Between Abstract Rules. *Cereb. Cortex* **27,** 34–45 (2017).

205. Mansouri, F. A., Buckley, M. J. & Tanaka, K. Mnemonic function of the dorsolateral prefrontal cortex in conflict-induced behavioral adjustment. *Science* **318,** 987–990 (2007).

206. Neural Basis of Motivational and Cognitive Control - 9780262016438_sch_0001.pdf. Available at: https://mitpress.mit.edu/sites/default/files/titles/content/9780262016438_sch_0001.pdf. (Accessed: 12th March 2017)

207. Gevins, A., Smith, M. E., McEvoy, L. & Yu, D. High-resolution EEG mapping of cortical activation related to working memory: effects of task difficulty, type of processing, and practice. *Cereb. Cortex* **7,** 374–385 (1997).

208. Jensen, O. & Tesche, C. D. Frontal theta activity in humans increases with memory load in a working memory task. *Eur. J. Neurosci.* **15,** 1395–1399 (2002).

209. Asato, M. R., Terwilliger, R., Woo, J. & Luna, B. White matter development in adolescence: a DTI study. *Cereb. Cortex* **20,** 2122–31 (2010).

210. Chevalier, N. *et al.* Myelination Is Associated with Processing Speed in Early Childhood: Preliminary Insights. *PLoS ONE* **10,** (2015).

211. Gramfort, A. *et al.* MEG and EEG data analysis with MNE-Python. *Front. Neurosci.* **7,** 267 (2013).